

Regenerative Action of the Wall on the Heat Transfer for Directly and Indirectly Heated Rotary Kilns

**Dissertation
zur Erlangung des akademischen Grades**

**Doktoringenieur
(Dr. –Ing)**

von Sri Silvia Agustini, M.Sc.

Geboren am 17.08.1975 in Medan, Indonesien

**Genehmigt durch die Fakultät für Verfahrens- und Systemtechnik
der Otto-von-Guericke-Universität Magdeburg**

Promotionskommission: Prof. Dr. –Ing. Jürgen Schmidt (Vorsitzender)

Prof. Dr. –Ing. Eckehard Specht (Betreuer)

Prof. Dr. –Ing. Evangelos Tsotsas (Gutachter)

eingereicht am 9. Juni 2006

Promotionskolloquium am 10. Juli 2006

Acknowledgments

First of all, I would like to thank God for leading my way up to now, irrespective of all the difficulties that were encountered. Also, my husband and children for their motivation and trust during the difficult moments.

My sincere thanks to Prof. Dr. –Ing. E. Specht, promoter of my thesis for his technical suggestions, the discussions and for all the support during my work. I would like to thanks also Prof. Dr. –Ing. E. Tsotsas for the co-operation and disposition as a referee, and to all the persons that contributed to the culmination of this work.

ZUSAMMENFASSUNG

Der Wärmeübergang eines Drehrohrofens ist einmalig im Vergleich zu anderen geometrischen Formen, weil er Wärme sowohl unter der Lagerung als auch darüber überträgt. Die Wärme wird an das Feststoffbett auf zwei Wegen übertragen: über die freie Oberfläche des Bettes (direkter Wärmestrom) und über die bedeckte untere Oberfläche des Bettes (regenerativer Wärmestrom). Einige Studien über letzteren Mechanismus der Wärmeübertragung wurden in der Literatur zitiert. Jedoch wurden diese Arbeiten numerisch gelöst, wegen des zweidimensionalen Problems, das die Wärmeleitung in radialer und Umfang Richtung betrachtet. Deshalb basiert diese Studie auf einer einfachen analytischen Herangehensweise, um die Aufgabe in einem direkten und indirekt beheizten Drehrohrofen zu lösen. In direkt beheizten Drehrohröfen gibt das heiße Gas, das in den Ofen eingeleitet wird, Wärme direkt zur freien Ofenwandoberfläche und zur freien Bettoberfläche ab. Bei Rotation des Ofens wird die in der Ofenwand gespeicherte Wärme wieder zum Feststoffbett übertragen. Bei indirekt beheizten Öfen ist die Wärmequelle ein heißes Gas oder Dampf. Die Wärme wird an die äußere Schicht der Ofenwand abgegeben und diese Wärme wird über den Umfang des Ofens verteilt. Der Wärmeübergangsmechanismus zum Feststoffbett ist zweigeteilt: in Wärmestrahlung von der freien Wandoberfläche zu der freien Oberfläche des Stoffbettes und in Wärmeleitung von der bedeckten Wand zum Feststoffbett.

Um den gesamten Wärmeübertragungsmechanismus im direkt beheizten Drehrohrofen zu analysieren, wurde ein analytisches eindimensionales Modell entwickelt, mit dem der Einfluss der verschiedenen Parameter auf die regenerative Wärmeübertragung durch die Wand festgestellt werden kann. Grundlage dieses Modells ist die Einführung einer thermisch aktiven Schicht charakterisiert durch eine unendliche Wärmeleitfähigkeit in radialer Richtung. Die Dicke der Schicht wird durch die Eindringtiefe in den halbunendlicher Körper bestimmt. Die betrachteten Parameter sind: Ofendurchmesser, Drehzahl, Füllungsgrad, Stoffwerte der Wand und der Wärmeaustausch zwischen Gas-Wand sowie Wand-Feststoffbett. Später wird das Modell mit den zweidimensionalen numerischen Ergebnissen mit einer Fehlerquote von weniger als 5% verifiziert. Ein neuer Parameter konnte vom analytischen Modell abgeleitet werden. Er heißt Wärmetransportkoeffizient ($\alpha_T = \pi \cdot \sqrt{\lambda \cdot \rho \cdot c \cdot n}$) und kann den Einfluss der Wand auf einfache Weise beschreiben. Mit diesem neuen Koeffizienten kann der regenerative Wärmeübergangskoeffizient als Serie von drei Widerständen beschrieben

werden ($\alpha_{WS}, \alpha_{GW}, \alpha_T$). Es wurden Experimente mit einem Versuchsdrehrohrofen durchgeführt. Die Temperaturschwankung der inneren Wand stimmt mit dem in dieser Arbeit verwendeten Modell überein. Das Temperaturniveau hängt vom Verhältnis der Wärmeübergangskoeffizienten ab, so dass Temperaturmessungen der Wand behilflich sind bei der Analyse des Wärmeübergangsmechanismus.

Zum Schluss wurde ein analytisches Modell für einen indirekt beheizten Drehrohrofen entwickelt um den Beitrag der Ofenwand zum gesamten Wärmeübergang zum Feststoffbett zu analysieren. Das Modell wurde für einen elektrischen Heizer und Gas oder Dampf als Wärmequelle entwickelt. Es wurden die gleichen Parameter wie die der Simulation des direkt beheizten Drehrohrofens benutzt. Das Modell zeigt die Verteilung des Wärmeübergangs von der offenen Wandoberfläche und der bedeckten Wandoberfläche zum Feststoffbett. In diesem Modell kann der Einfluss der Wand wieder beschrieben werden mit Hilfe des Wärmetransportkoeffizient, jedoch in einer anderen Definition ($\alpha_n = \rho \cdot c \cdot n \cdot s$).

ABSTRACT

The heat transfer in a rotary kiln is unique compared to other geometries because it transfers the heat under the load as well as on the top. The heat is transferred to the solid bed in two paths: across the exposed surface of the solid bed (direct heat flow) and the covered surface of the bed (regenerative heat flow). Some studies about the latter heat transfer mechanism have been cited in the literature. However, the works have to be solved numerically because of the 2-dimensional problem which considers the thermal conduction in radial and circumference direction. Therefore, this study has established an analytical solution in a simple manner to accomplish the task in directly and indirectly heated rotary kilns. In directly heated rotary kilns the hot gas introduced into the kiln is transferred directly to the exposed kiln wall surface and to the exposed bed surface. As the kiln rotates the heat, which is stored in the kiln wall, is transferred again to the solid bed. In indirectly heated rotary kilns the heat source is from the hot gas or the steam. The heat is given to the outer shell of the kiln wall and that this heat is distributed over the circumference of the kiln. The heat transfer mechanism to the solid bed is divided into two parts: the radiation heat flow from the exposed wall surface to the exposed bed surface and the conduction heat flow from the covered wall to the solid bed.

To examine the overall heat transfer mechanism in directly heated rotary kiln an analytical one-dimensional model has been developed to determine the impact of the different kiln variables on the regenerative heat transfer by the wall. The basis of this model is to introduce a lumped capacity layer with infinite conductivity in radial direction. The thickness of this layer is determined from the heat penetration in a semi-infinite body. The parameters considered are: kiln diameter, rotational speed, filling degree, material properties of the wall, and gas-to-wall as well as wall-to-solid heat transfer. Latter on the model is verified with the two-dimensional numerical results with an error of less than $\pm 5\%$. A new parameter could be derivated from the analytical model which is named as heat transportation coefficient ($\alpha_T = \pi \cdot \sqrt{\lambda \cdot \rho \cdot c \cdot n}$) which can describe the influence of the wall in a simple manner. With this new coefficient the regenerative heat transfer coefficient can be described as a series of three resistances: the heat transfer coefficient gas-to-wall (α_{GW}), the heat transportation coefficient (α_T), and the heat transfer coefficient wall-to-solid (α_{WS}). Experiments were carried out in a pilot plant kiln. The fluctuation of the inner wall temperature is in accordance with the model in this work. The temperature level depends on the ratio of the heat transfer

coefficients, thus the measurements of the wall temperature help to analyze the heat transfer mechanism.

Finally, in indirectly heated rotary kiln an analytical model has been developed to estimate the contribution of the kiln wall to the overall heat transfer to the solid bed. The model was developed for electrical heater and gas or steam as heat sources, respectively. The same parameters as the simulation for the directly heated rotary kiln are used. The model shows the distribution of the heat transfer from the exposed wall surface and from the covered wall surface to the solid bed. In this model, the influence of the wall could be described again using a heat transportation coefficient but using other definition ($\alpha_n = \rho \cdot c \cdot n \cdot s$).

Nomenclature

Latin symbols

A	-	Heat resistance ratio
A	m	Area per unit length
a	m^2/s	Thermal Diffusivity
Bi	-	Biot number
b	mm	Effective depth of penetration in the solid bed
c	J/kgK	Thermal heat capacity
D	m	Diameter
De	m	Equivalent diameter
d	m	Wall layer thickness
F	-	Surface area
f	-	Filling degree
G	$\text{kg}/\text{m}^2 \text{ s}$	Gas mass flux
Gr	-	Grashoff number
H	W/m	Enthalpy flow
h	mm	Mean thickness of gas film
L	m	Kiln length
Nu	-	Nusselt number
n	rpm	Rotational speed
Pe	-	Peclet number
Pr	-	Prandlt number
\dot{Q}	W/m	Heat transfer per unit length of kiln
\dot{q}	W/m^2	Heat flux
R	m	Radius

R	-	Resistance
Re	-	Reynold number
r	m	Radial coordinate
St	-	Stanton number
s	m	Lumped capacity layer
s	m	Wall thickness
T	K	Absolute temperature
t	s	Time
u	m/s	Velocity
w	m/s	Tangential velocity
x	rad	Circumferential coordinate
Z	-	Axial coordinate along kiln length

Greek Symbols

α	W/m ² K	Heat transfer coefficient
β	rad	Central angle of solid bed
χ	mm	Gas film thickness
δ	m	Particle roughness
δ	m	Thickness at the contact point
ε	rad	Half central angle of sectional solid bed
ε	-	Emmissivity
ε	-	Surface porosity between particles
φ	degree	Circumferential coordinate
λ	W/mK	Thermal heat conductivity
π	-	Constant (3.14)

ρ	kg/m ³	Density
σ	W/m ² K ⁴	Stefan's Boltzman Constant (5.67e-8)
τ	s	Contact time between solid and covered wall
ω	1/s	Rotary frequency

Superscript

<i>ad</i>	Advection
<i>cd</i>	Conduction

Subscript

<i>B</i>	Solid bed
<i>c</i>	Critical
<i>D</i>	Diameter
<i>D</i>	Direct
<i>eff</i>	Effective
<i>el</i>	Electric
<i>G</i>	Gas
<i>G,0</i>	Initial wall temperature in contact with gas
<i>G0</i>	Convective outer wall
<i>GS</i>	Gas to solid
<i>GW</i>	Gas to wall
<i>g</i>	Gas
<i>i</i>	Inner
<i>k</i>	Bulk
<i>L</i>	Loss
<i>lam</i>	Laminar

lc	Lumped capacity layer
m	Material
n	Transportation
0	Outer
$0G$	Shell wall in contact with gas at covered wall region
$0S$	Shell wall in contact with gas at uncovered wall region
p	Particle
R	Regenerative
rad	Radiation
sb	Bed surface
S	Solid bed
$S,0$	Initial wall temperature in contact with solid
φ	Circumference coordinate
T	Transportation
$turb$	Turbulent
u	Gas layer
ω	Velocity
W	Wall
W,G	Exposed wall
WP	Wall to particle
WS	Wall to solid
1	Surface 1
2	Surface 2

Table of Contents

1	Introduction	1
1.1	Background	1
1.2	Scope of the work	4
2	Literature review	5
2.1	Covered wall-bed heat transfer	5
2.1.1	Conduction heat transfer coefficient	5
2.1.2	Regenerative heat transfer	18
2.2	Convection in the freeboard gas	21
2.2.1	Convection between the gas and wall	21
2.2.2	Convection between gas and solid bed	25
2.2.3	Convection to the outer shell	29
2.3	Radiation in the freeboard gas	30
2.3.1	Radiative heat transfer	30
2.3.2	Linearization of radiation	32
3	Regenerative action of the kiln wall in a directly heated rotary kiln	34
3.1	Introduction	34
3.2	Numerical method	35
3.2.1	Description of the Model	35
3.2.2	Temperature distribution	39
3.2.3	Heat flow	42
3.3	Analytical solution	43
3.3.1	Temperature distribution	43
3.3.2	Heat flow	48
3.3.3	Thin lumped capacity layer	50
3.3.4	Comparison of analytical and numerical results	54
3.3.5	Comparison of regenerative and direct heat flows	60
4	Regenerative action of the wall in an indirectly heated rotary kiln	65
4.1	Electrical heating	65
4.1.1	Description of the model	65
4.1.2	Temperature distribution	69
4.1.3	Heat flow	80
4.2	Gas heating	84
4.2.1	Model Description	85

4.2.2	Temperature distribution	88
4.2.3	Heat flow	98
4.2.4	Overall heat transfer coefficient	100
4.2.5	Simplified resistance network	104
5	Experimental investigation of the temperature distribution in the kiln	111
5.1	Experimental apparatus and measuring technique	111
5.2	Experimental work	113
5.3	Results and discussion	115
5.4	Comparison of extended model with experimental results	119
5.4.1	Temperature distribution	119
5.4.2	Gas and solid mass flow	122
6	Conclusion	124
	REFERENCES	126
	APPENDIX	132

1 Introduction

1.1 Background

Rotary kilns are widely fixtures of the chemical, metallurgical and pharmaceutical process industries. They are capable of operating at high burning zone temperature, for example: burning of cement clinker (2000°C) [Peray and Waddell 1972], calcinations of aluminium oxide, coke (1300°C) [Manitius, A., et al. 1974, Bui, R.T., et al. 1995], lime burning (1200°C) [Georgallis 2004], calcinations of petroleum coke (1100°C) [Martins et al. 2001]. Other application of the rotary kilns are the thermal treatment of waste material [Rovaglio et al. 1998, Silcox and Persing 1990, Ikuo 2001], the gasification of waste tires or wood to obtain activated carbon [San Miguel et al. 2001, Ortiz et al. 2005], and the thermal desorption of contaminated soils [Cundy and Cook 1995, Wilbrand 1997, Wocaldo 1994, Rensch 2001].

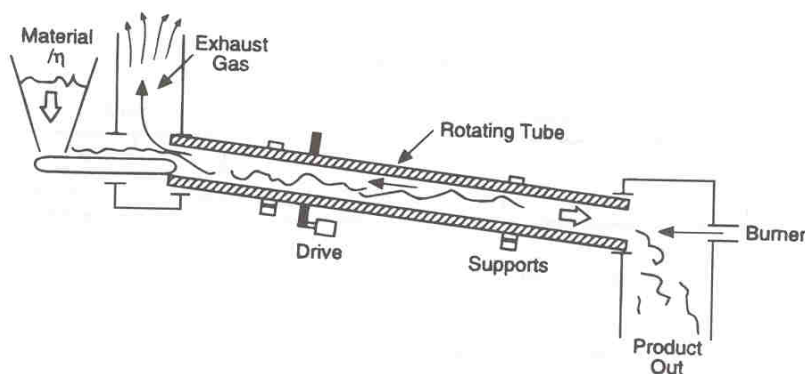


Figure 1-1. A direct heated rotary kiln [Baukal 2000]

As shown in Figure 1-1, rotary kilns are typically cylindrical, refractory-lined vessels. The raw materials are often granular in composition so that they can easily flow through the kiln. They are fed in at the higher end and exit at the lower end of the kiln. This geometry is normally characterized by a single burner located in or near the center of one end of the kiln and firing parallel to the axis of the kiln. In counter-current kilns, the material is fed in on the opposite end of the burner and in co-current kilns, the material inlet and the burner are at the same end. However, industrial kilns are normally operated counter current. Large kilns can be up to 6 m in diameter and 160 m in length [Baukal 2000].

The heat transfer in a rotary kiln is unique compared to other furnaces because it involves not only the gas and the moving bed of solids, but also the rotating kiln wall. The heat transfer steps are shown in Figure 1-2.

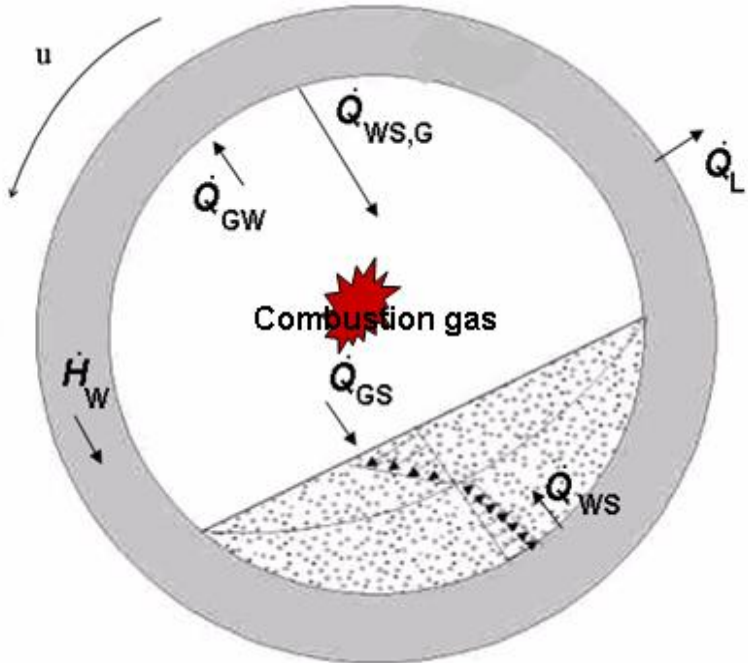


Figure 1-2. Heat flow paths in a rotary kiln

The heat is transferred to the solid burden in two paths: across the exposed surface of the solid bed (direct heat flow) and the covered lower surface of the bed (regenerative heat flow). The mechanisms of the heat transfer to the two surfaces of the bed are very different. The exposed solid bed surface receives heat directly by radiation and convection from the freeboard gas (\dot{Q}_{GS}), whereas on the covered solid surface heat flows by conduction from the wall to the solid (\dot{Q}_{WS}). This latter heat transfer path is part of the regenerative heat transfer of the kiln wall. During the rotation, the wall receives thermal energy via radiation and convection from the hot combustion gas (\dot{Q}_{GW}). A part of this energy is stored in the kiln wall and transported back as enthalpy flow (\dot{H}_W) to the covered solid surface. However, owing to the high temperatures attained in the freeboard gas, radiation is the dominant heat transfer mechanism [Gorog 1989]. The other part of the heat which is radiated to the wall is reflected exclusively back to the solid bed ($\dot{Q}_{WS,G}$). For high temperature processes and high emissivity of the gas, the radiation heat transfer from wall to solid is neglected [Siegel and Howell

2002]. In addition, the solids typically tumble inside the kiln, which constantly exposes new material to the heat source. Tumbling of the solid and heating from below help to increase the efficiency of this process.

In the design or modeling of rotary kilns, four important aspects should be considered from the process engineering point of view: heat transfer, flow of material through the kiln, gas-solid mass transfer, and reaction kinetics. Heat transfer is the most important out of these aspects because in many practical cases heat transfer limits the performance of the rotary kiln [Barr et al. 1989].

Numerous heat transfer models for rotary kilns are available in the literature [Sass 1967, Pearce 1973, Gardeike 1978, Goshdastidar et al. 1996, Bui and Perron 1993]. The heat transfer model from these previous works has to be solved numerically because of the 2-dimensional problem which considers the thermal heat conduction in radial and circumferential direction. Therefore, it is difficult to see the effect of the influencing parameters and to transfer the result to different kiln geometry. The study from Queck 2002 in the same research group had tried to solve the problem by introducing the fictitious layer in the wall. However, the study has some deficiencies in terms of the investigated parametric zones of the pilot kiln, the interpretation of the results and to many influencing parameters which has to be considered. Therefore, in this study a new model is introduced for the regenerative heat transfer that has a one-dimensional analytical solution. This can provide a very clear description not only of the regenerative heat transfer but also of its ratio to the direct heat transfer.

Rotary kilns can also be heated externally either with electric heat flux or the outer wall that is indirectly heated by the high temperature flow as its heat source see Figure 1-3. The externally heated kiln is often adopted as a pyrolyzer or gasifier of a special kind of waste [Schulz et al. 1993, Li, et al. 1999, Androutsopoulos et al. 2003]. Used also as an indirect rotary dryer for organic material [Wang et al. 1993, Canales, et al. 2001, Vega et al. 2000]. However, most of these studies are not focused on the heat transfer in the kiln. No study has yet been made available to predict the temperature distribution on the kiln wall and the impact of the parameters to the overall heat transfer.

1.2 Scope of the work

1. A sophisticated heat transfer model was developed to contribute a better understanding of the regenerative heat transfer of the kiln wall, which enabled the simple calculation of the temperature distribution on the kiln wall, the net rate of energy input to the bed material and unique to this study is introducing the heat transportation coefficient which described the influence of the wall in a simple manner.
2. A series of heat transfer trials were carried out using the laboratory pilot kiln facility, which enabled the comparison with those of the recent study.
3. To investigate the heat transfer phenomenon in the externally heated rotary kiln and the impact of the parameters to the overall heat transfer.

2 Literature review

It is pointed out in the opening discussion that in rotary kilns energy from the freeboard gas is transferred to the kiln wall and the solid bed by both radiative and convective heat transfer. The wall received the heat and transferred it back to the solid bed as the kiln rotate. The subsequent distribution of this energy is of vital importance to the satisfactory operation of the kiln. Therefore the radiative and convective exchange among the exposed wall and bed surfaces as well as the conductive exchange between the covered wall and the solid bed must be characterized. This in turn depends on many parameters those are different for each kiln and bed material. Before moving on to a brief examination of the fairly extensive studies pertaining to the regenerative action of the wall, it is appropriate to first review the literature relating to the heat transfer mechanism which influences the regenerative heat transfer and to investigate a range of values based on the previous studies.

2.1 Covered wall-bed heat transfer

2.1.1 Conduction heat transfer coefficient

Heat transfer coefficient by conduction is employed to calculate the covered wall and solid bed exchange. This heat transfer includes both the heat transfer coefficient of the bed surface to the bulk solids and that of the wall surface to the bed surface. Estimation of this coefficient has generally been studied either by pure guess work or by adopting some type of surface renewal or penetration model. Typical guess-estimated values for wall-solid heat transfer coefficient were made by Gorog et al. (1982) in the range of 50-100 W/m^2K and by Agustini et al. (2005) in the range of 50-500 W/m^2K .

The earlier investigation on this heat transfer was by Watchers and Kramers (1964) using heating sand of unspecified size in a rotating copper drum of 0.152 m ID x 0.475 m A heat balance for a circumferential element consisting of particles adjacent to the wall yields

$$\frac{\partial T}{\partial t} = a_B \frac{\partial^2 T}{\partial x^2} \quad (2-1)$$

where a_b is the heat diffusivity of particles, m^2/s .

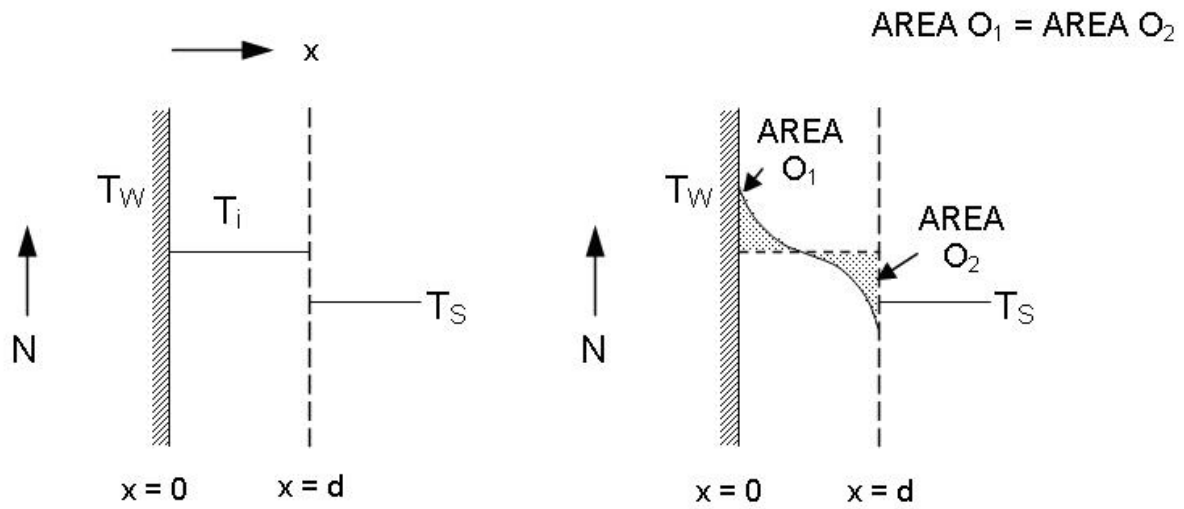


Figure 2-1. Penetration model for Bed-to-Wall heat transfer (after Watchers and Kramers, 1964)

The initial boundary condition is illustrated in Figure 2-1, assuming the average temperature of the wall layer was constant during the time of contact. Their experiments indicate that at higher speed ($n > 10rpm$) the heat transfer coefficients reduces by a factor of 3 with respect to that obtained from a simple penetration model

$$\alpha_{WS} = \frac{2 \cdot \lambda_B}{3 \cdot \sqrt{\pi \cdot a_B \cdot t_c}} \quad (2-2)$$

At relatively lower speed ($n < 10rpm$), it is gradually changed according to

$$\alpha_{WS} = \left[\frac{\sqrt{\pi \cdot a_B \cdot t_c} + d' \sqrt{\pi}}{2 \cdot \lambda_B} \right]^{-1} \quad (2-3)$$

The wall layer thickness, d' , was obtained by extrapolating the experimental data from the above equation

$$d' = 1.12 \times 10^{-3} \sqrt{\beta} \quad (2-4)$$

The values of d' were 1.8 mm and 1.5 mm with $\beta = 2.53$ and $\beta = 1.83 \text{ radians}$, respectively in their experiments. However, the dependence of d' in equation above on b , the central angle of the solids bed, can not be physically explained.

Other simplified model was applied by Wes et al. (1976) in a drum of industrial scale drum of $9.0 \text{ m ID} \times 0.6 \text{ m}$. The initial boundary condition is illustrated in Figure 2-2.

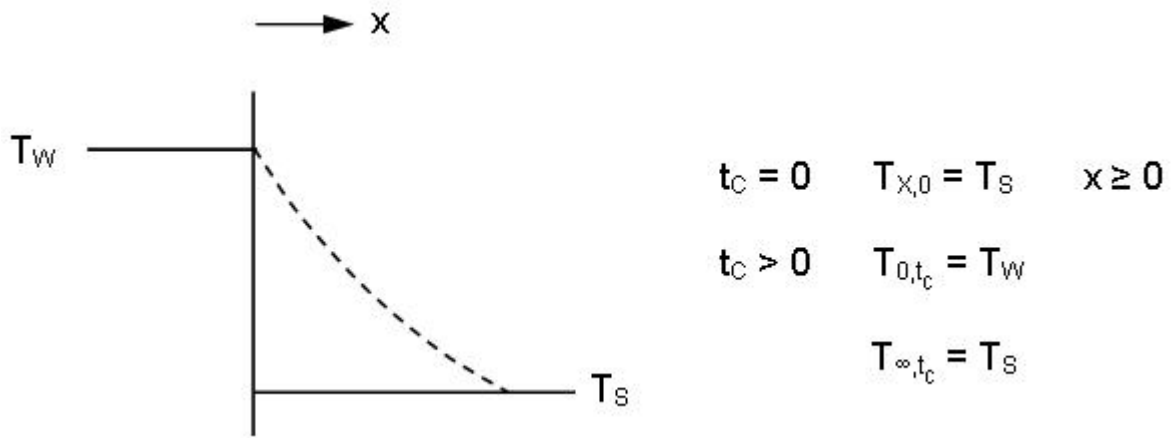


Figure 2-2. Boundary condition assumed for covered wall-bed heat transfer (after Wes et al. 1976)

The wall temperature was measured at 4.57 m from the entrance by thermocouple placed flush with the wall. Since the drum was heated by steam, the wall temperature was taken to be constant along the drum length. Potato starch or yellow dextrin with particle size of $15\text{-}100 \mu\text{m}$ and filling degree between 11 and 23% were used. The rotation speed was predetermined at $1.6\text{-}6.5 \text{ rpm}$. The experiment results were in accordance with the following equation, which is derived from the equation

$$\alpha_{WS} = \frac{2 \cdot \lambda_B}{\sqrt{\pi \cdot a_B \cdot t_c}} \quad (2-5)$$

Values of about $250 \text{ W/m}^2\text{K}$ were found for a rotational speed of 6 rpm .

In the work of Lemberg et al. (1977), a laboratory rotary kiln was used in his work in the size of 60 cm length, 25 cm diameter and wall thickness of 3 mm . They introduced two regions at the contact between the bulk and the wall (see Figure 2-3).

In region 1, the heat transfer occurs between the plane surface of the wall and the bulk perpendicular to this surface along x . And in region 2, he introduced a thin gas layer between

the bulk and the wall which causes a temperature jump at $x = 0$. They used the following set of initial and boundary conditions illustrated in Figure 2-4

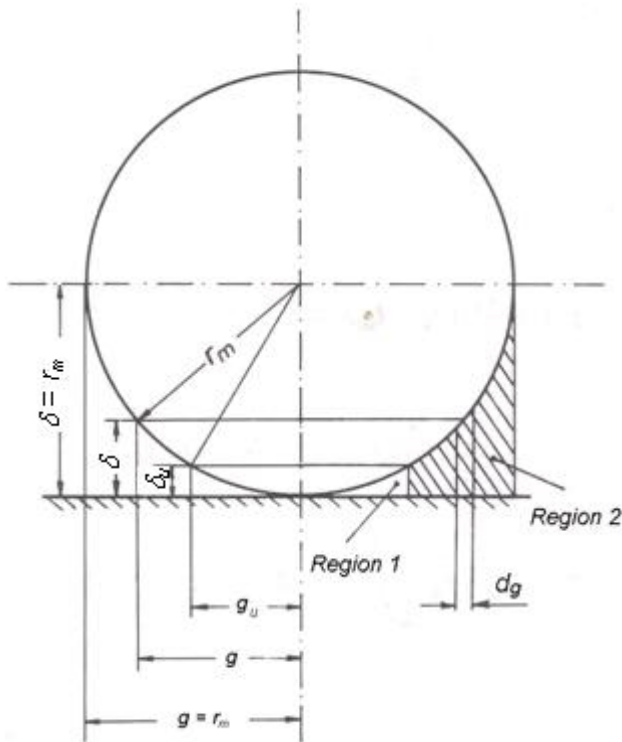


Figure 2-3. Two-region penetration model for wall-bed heat transfer (after Lehmborg et al. 1977)

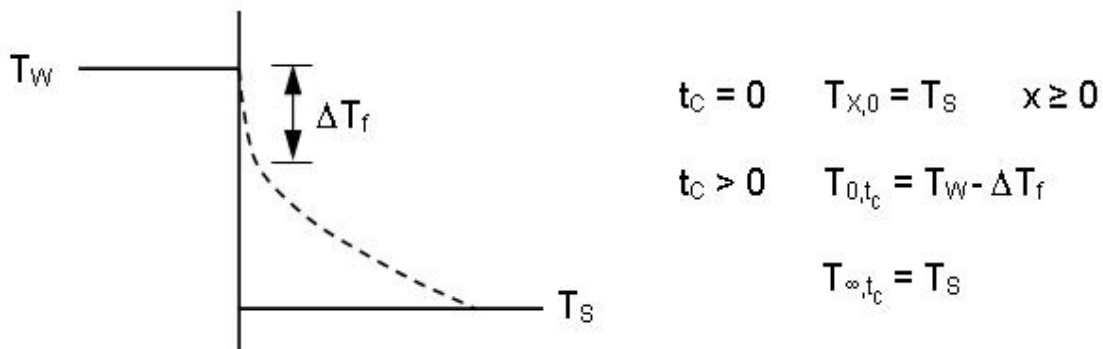


Figure 2-4. Boundary condition assumed for covered wall-bed heat transfer (after Lehmborg et al. 1977)

$T = T_W = \text{constant}$, for $x = 0$ for every t for region 1

$T = T_i = \text{constant}$, for $t = 0$ and every x for region 1 and 2

$$\left(\frac{\partial T}{\partial x} \right)_{x=0} = -\alpha_{eff} \cdot (T_W - T_{x=0}) \text{ for region 2}$$

The overall wall-bed heat transfer coefficient across the two regions

$$\alpha_{eff} = \frac{1}{\frac{1}{\alpha_{WS}} + \frac{1}{\alpha_G}} \quad (2-6)$$

where the heat transfer coefficient between the wall and bulk

$$\alpha_{WS} = \frac{b_e}{\sqrt{\tau_k}} \cdot \left[\frac{2}{\sqrt{\pi}} - \frac{1}{h \cdot \sqrt{a_B \cdot \tau_k}} + \frac{1}{h \cdot \sqrt{a_B \cdot \tau_k}} e^{h^2 \cdot a_B \cdot \tau_k} \cdot \text{erfc} \left(h \cdot \sqrt{a_B \cdot \tau_k} \right) \right] \quad (2-7)$$

and the heat transfer coefficient between the bulk and the thin gas layer

$$\alpha_G = h \cdot (1 - \varepsilon) \cdot \frac{(r_m - \delta_u)}{r_m^2} \quad (2-8)$$

$$h = 2 \cdot \lambda_G \cdot \frac{r_m}{(r_m - \delta_u)^2} \cdot \left[\ln \left(\frac{r_m}{\delta_u} \right) - 1 + \frac{\delta_u}{r_m} \right] \quad (2-9)$$

where $b_B = \sqrt{\lambda_B \cdot c_B \cdot \rho_B}$ is the effective depth of penetration in the solid bed, τ_k is the contact time between solid and covered wall, $a_B = \lambda_B / (c_B \cdot \rho_B)$ is the effective thermal diffusivities, r_m is the mean particle size, δ_u is the thin gas layer and ε is the surface porosity between particles.

By adjusting the values of h and δ_u , Equation (2-7) was reported in good agreement with their own experimental data using Quartz sand (mean particle sizes 157, 323, 794 and 1038 μm) and sodium carbonate (soda), with mean particle size 137 μm . He reported the value of heat transfer coefficient between wall and solid around 40-400 W/m^2K for a short contact time ($1/\tau_c = 2s^{-1}$). The mean thickness of the gas film ($1/h$) increases with increasing particle size. The parameters, h and δ_u were determined experimentally, therefore Equations (2-7) and (2-9) are not readily used for design purpose.

Recently Li et al. (2005) used the data from Lemberg 1975 to verify the validity of the heat transfer model in their paper. The principle mechanism of heat transfer of covered wall and solid bed model is described in Figure 2-5.

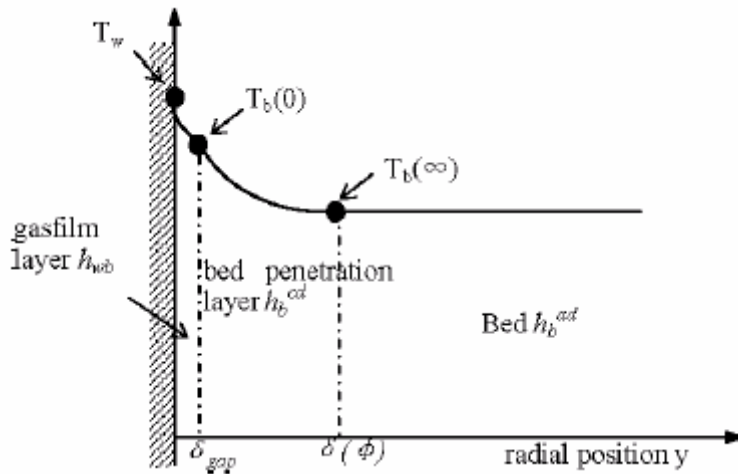


Figure 2-5. Mechanism of heat transfer between wall-solid (after Li et al.)

The total heat transfer coefficient is controlled by three heat resistance:

$\frac{1}{\alpha_{WB}}$, contact resistance caused by gas film between the covered wall and bed surface

$\frac{1}{\alpha_B^{cd}}$, thermal resistance due to unsteady state heat conduction from the bed surface to the solid bed, the temperature reduces from $T_b(0)$ to $T_b(\infty)$.

$\frac{1}{\alpha_B^{ad}}$, thermal resistance due to advection heat transfer within bulk solid, which can be approximated to zero.

Regression analysis of extended penetration theory led to the following equation

$$\alpha_{WS} = \frac{1}{\frac{1}{\alpha_{WB}} + \frac{1}{\alpha_B^{cd}} + \frac{1}{\alpha_B^{ad}}} = \left(\frac{St \cdot d_p}{\lambda_g} + \frac{1}{2\sqrt{\frac{n \cdot (\rho \cdot \lambda \cdot c)_B}{\varepsilon}}} \right) \quad (2-10)$$

A dimensionless terms of Eq. (2-10)

$$Nu_d = \frac{l}{\aleph + \frac{\sqrt{\pi}}{2} \cdot \sqrt{\frac{l}{Pe_d}}} \quad (2-11)$$

where $Nu_d = \alpha_{WS} \cdot \frac{d_p}{\lambda_g}$, $Pe_d = \left(\frac{d_p}{\lambda_g}\right)^2 \frac{(\rho \cdot \lambda \cdot c)_B}{t_c}$, $t_c = \frac{\varepsilon}{\pi \cdot n}$. Gas film thickness:

$\aleph = 0.085$, filling angle is ε .

Figure 2-6 shows the comparison between extended penetration theory and the experiment results of Lemberg 1977. In the study a range for α_{WS} between 40 to 400 W/m^2K was employed.

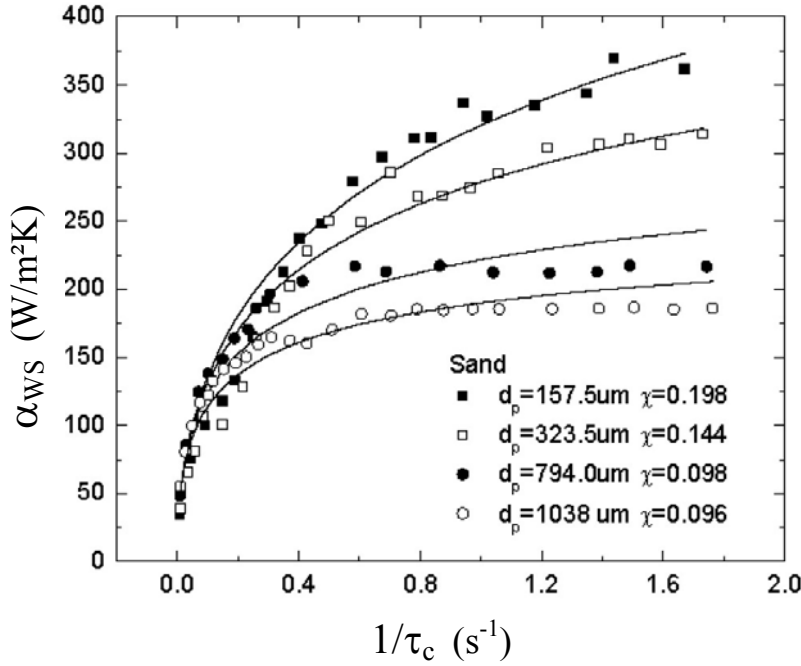


Figure 2-6. Comparison between extended model from Li et al. and experimental results from Lemberg et al. (after Li 2005)

The simple penetration model was proposed by Tscheng, S.H. (1979). It leads to the following dimensionless equation.

$$\frac{\alpha_{WS} \cdot L_{WS}}{\lambda_B} = 11.6 \cdot \left[\frac{n \cdot R^2 \cdot 2\varepsilon}{a_B} \right]^{0.3} \quad (2-12)$$

Where n is the rotational speed of the kiln, R is the inner radius, L_{WS} is the length of the contact part wall-solid, ε is the filling angle of the solid, and a_B is the thermal diffusivity of the bed.

$$a_B = \frac{\lambda_B}{\rho_S \cdot c_S} \quad (2-13)$$

The thermal properties of the wall have a significant influence to the heat transfer coefficient between wall and solid. However, the influence of the wall material is not considered. The effective thermal conductivity (λ_B) for sand is predicted from Figure 2-7

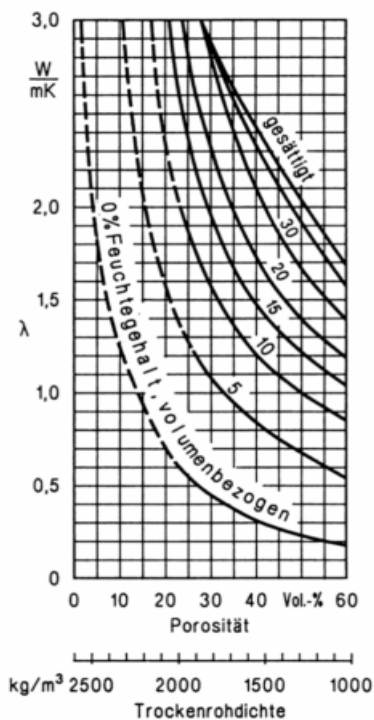


Figure 2-7. Effective thermal conductivity for Sand (VDI 1997)

Equation 2-12 is accordance with the investigations of 3 different authors (Wachters & Kramers, Wes et al., and Lemberg et al.) as shown in Figure 2.8.

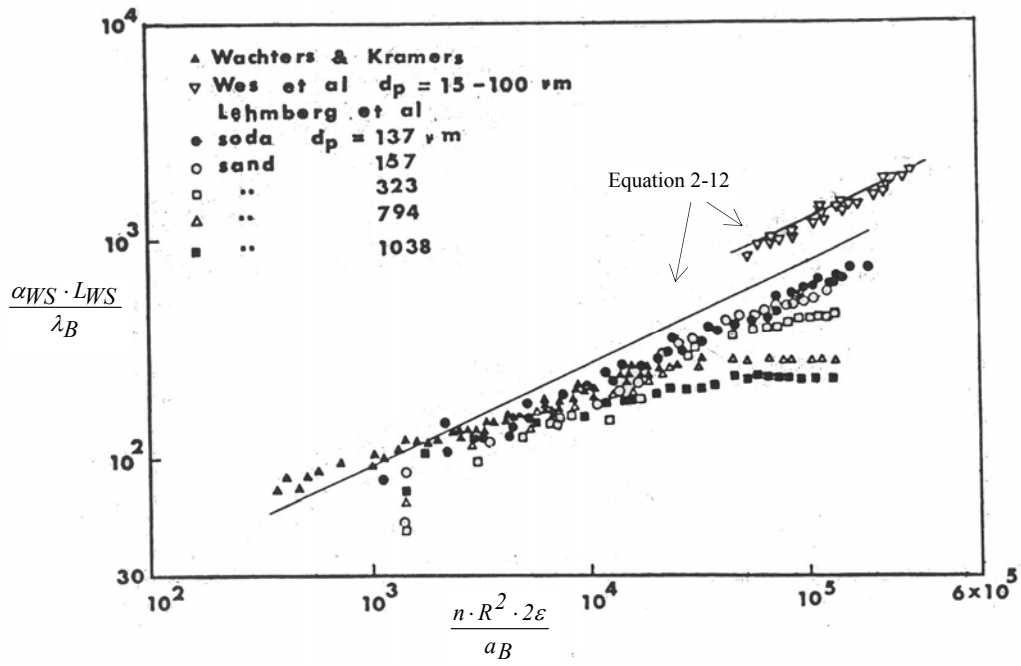


Figure 2-8. Correlation of simplified model from Tscheng S.H. and experiment results (after Tscheng 1979)

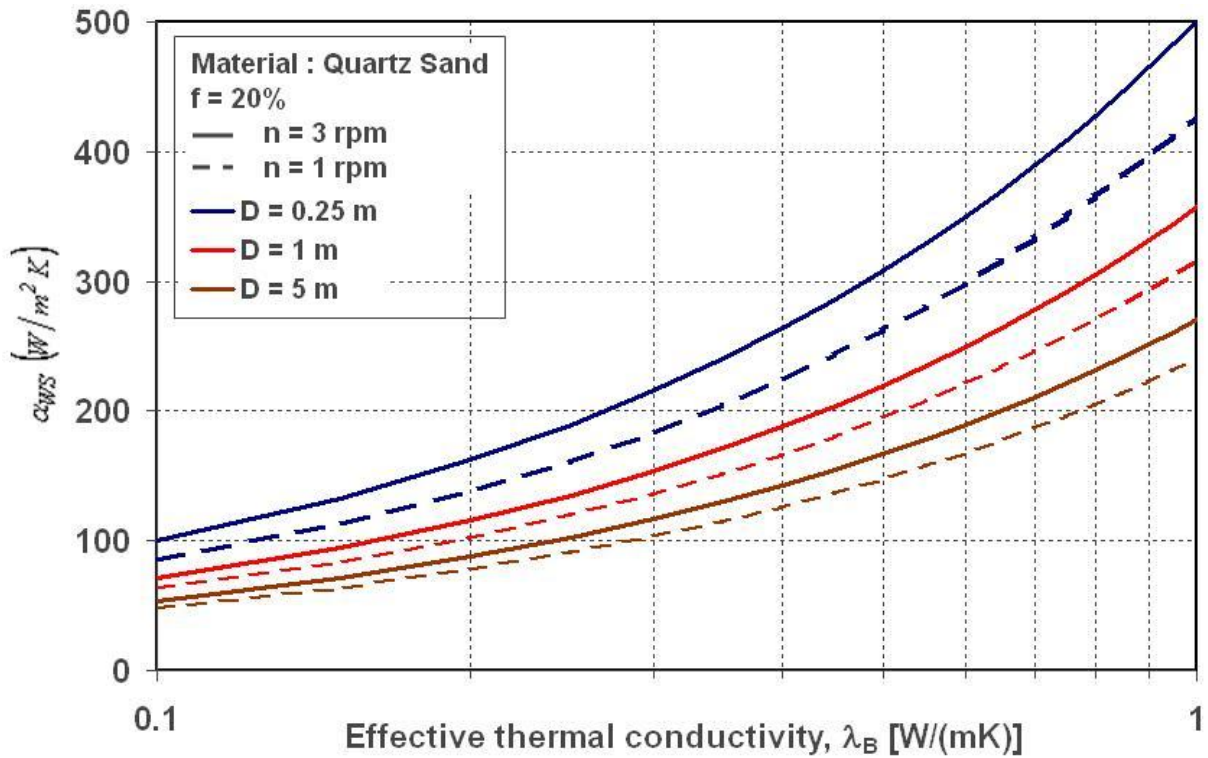


Figure 2-9. Effective thermal conductivity for sand

The influence of the effective heat conductivity on the heat transfer coefficient wall to solid after Eq. 2-12 is represented in Figure 2-9. The material Quartz Sand (SiO_2) (see chapter 5, experimental investigation) is used with filling degree 20% and rotational speed $n = 3 \text{ min}^{-1}$.

The effective thermal conductivity is increasing as the kiln diameter decreases. This phenomenon influences the heat transfer coefficient wall-solid. The range of this coefficient according to Figure 2.9 leads to α_{WS} between 50 to 500 W/m^2K .

Patison et al. (2000) used also this correlation to calculate the heat transfer in a rotary coal pyrolysis kiln. To calculate the effective conductivity of the charge, a correlation of Zehner and Schlünder (1972) is used. The value taken for the study was $\alpha_{WS} = 350 \text{ W/m}^2K$. This value had been used also by Barr (1986) in his calculation using pilot kiln trial with 0.4 m ID and prototype kiln model with 4 m ID.

Silcox et al.(1990) used this expression to calculate the heat transfer in rotary kiln for solid hazardous waste. He reported the heat transfer between wall and solid lies between 60-400 W/m^2K , which is shown in Table 2-1. The material was sand with filling degree 10% and rotation speed 3 rpm.

ε_f [W/m^2K]	T_{exit} [K]	α_{GS} [W/m^2K]	T_{exit} [K]	α_{WS} [W/m^2K]	T_{exit} [K]
0.1	696	27	783	61	751
0.2	748	54	760	123	783
0.3	783	216	711	246	818
0.4	807			392	843

Table 2-1. Heat transfer coefficient between wall-solid for contaminated soil (after Silcox et al. 1990)

Schlünder and Tsotsas (1988) introduce a penetration model of the heat transfer between bulk materials and heating surfaces. This model considers the mechanism of the contact heat transfer between wall and the first particle layer as shown in Figure 2-10 with shading as well as the drop of temperature within the solid bed material.

For a given heat flux \dot{q} , exists a temperature drop between the wall temperature T_w and the middle temperature T_θ . The temperature jump at the wall arises due to the contact resistance between wall and the first particle layer. Between this temperatures difference a contact resistance $1/\alpha_S$ is defined. A further temperature gradient takes place within the solid material and is computed by a penetration coefficient. A contact resistance in this range is defined as $1/\alpha_B$.

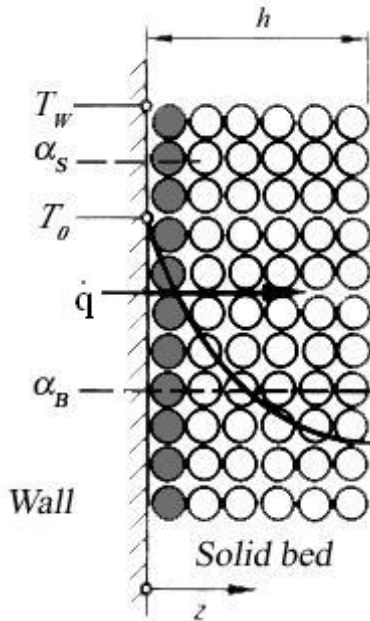


Figure 2-10. Temperature profile in a packed bed heated from the surface of an immersed body (after VDI 1997)

Thus, the total penetration model for a heat transfer coefficient wall to solid bed is given as

$$\frac{1}{\alpha_{WS}} = \frac{1}{\alpha_S} + \frac{1}{\alpha_B} \quad (2-14)$$

where α_S and α_B are the heat transfer coefficient between the wall to the first particle layer and the heat penetration coefficient in the solid bed, respectively. The first heat transfer coefficient represented as shadings in Figure 2-10 is applied from the correlation

$$\alpha_S = \varphi \cdot \alpha_{WP} + (1 - \varphi) \frac{2 \cdot \lambda_G / d}{\sqrt{2 + (2 \cdot l + 2 \cdot \delta) / d}} + \alpha_{rad} \quad (2-15)$$

with surface ratio of the heating surface $\varphi = 0.8$

For a small temperature difference between two surfaces

$$\alpha_{rad} = 4 \cdot \sigma \cdot \frac{l}{\frac{l}{\varepsilon_W} + \frac{l}{\varepsilon_B} - l} \cdot T_W^3 \quad (2-16)$$

The heat transfer coefficient between wall and a single particle

$$\alpha_{WP} = \frac{4\lambda_G}{D} \left[\left(1 + \frac{2(l+\delta)}{D} \right) \ln \left(1 + \frac{D}{2(l+\delta)} \right) - 1 \right] \quad (2-17)$$

The heat transfer coefficient for a single particle in dependence of the pressure is presented in Figure 2-11 for smooth $\delta = 0$ and rough particles ($\delta = 2$ and $10 \mu\text{m}$). This case was measured for a particle diameter 2 mm, thermal conductivity 0.0275 W/mK and thermal capacity 1008 J/kgK .

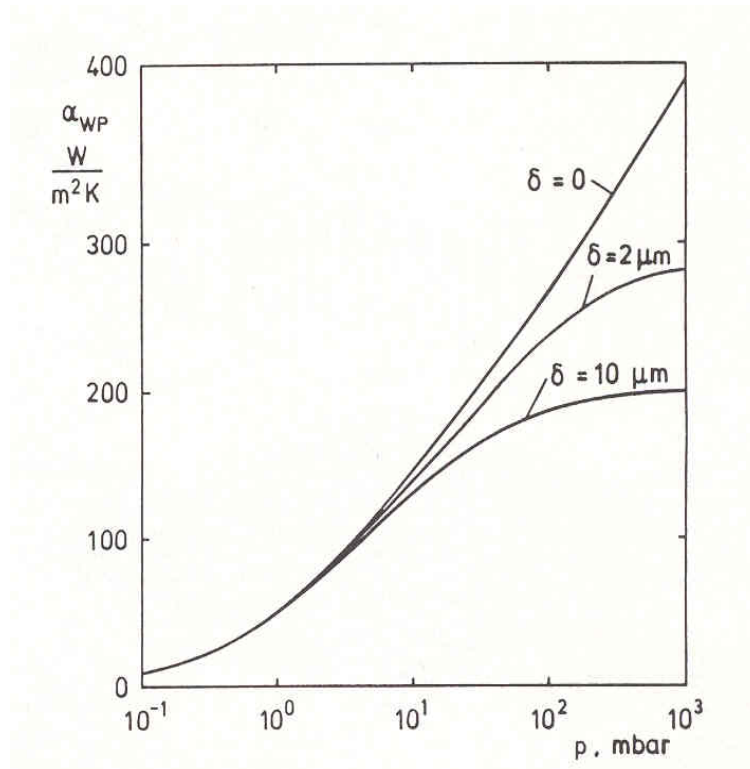


Figure 2-11. Heat transfer coefficient for single particle from kiln wall for different particle surface roughness (after Schlünder and Tsotsas 1988)

For a low pressure $l + \delta \approx l$. Where δ is the roughness of particle and l is the modified free path length of the gas and γ are the accommodation coefficient of the gas

$$l = 2 \cdot \Omega \cdot \frac{2 - \gamma}{\gamma} \quad (2-18)$$

$$\frac{l}{\gamma} = 10^{0.6 \cdot \frac{\frac{1000}{T} + 1}{2.8}} + 1 \quad (2-19)$$

The free path length is defined as

$$\Omega = \Omega_0 \cdot \frac{P_0}{P} \cdot \frac{T}{T_0} \quad (2-20)$$

where T is the absolute Temperature, P_0 and T_0 for air are 1 bar and 373 K, respectively. The initial accommodation coefficient $\Omega_0 = 0.0654 \cdot 10^{-6} m$.

The heat penetration coefficient α_B is defined as follows

$$\alpha_B = \frac{2}{\sqrt{\pi}} \cdot \frac{\sqrt{(\rho \cdot \lambda \cdot c)_B}}{\sqrt{t}} \quad (2-21)$$

The fictitious contact time t can be calculated from this correlation

$$t = t_{mix} \cdot N_{mix} \quad (2-22)$$

$$t_{mix} = \frac{l}{n} \quad (2-23)$$

where n is the rotational speed of the kiln and N_{mix} is the Dimensionless mixing quality number. For typical rotary kiln according to (Wocaldo 1994) N_{mix} is equal to 2. The influence of the effective heat conductivity on the heat transfer coefficient wall to solid after Eq. 2-14 for material Quartz Sand (SiO_2) is represented in Figure 2-12.

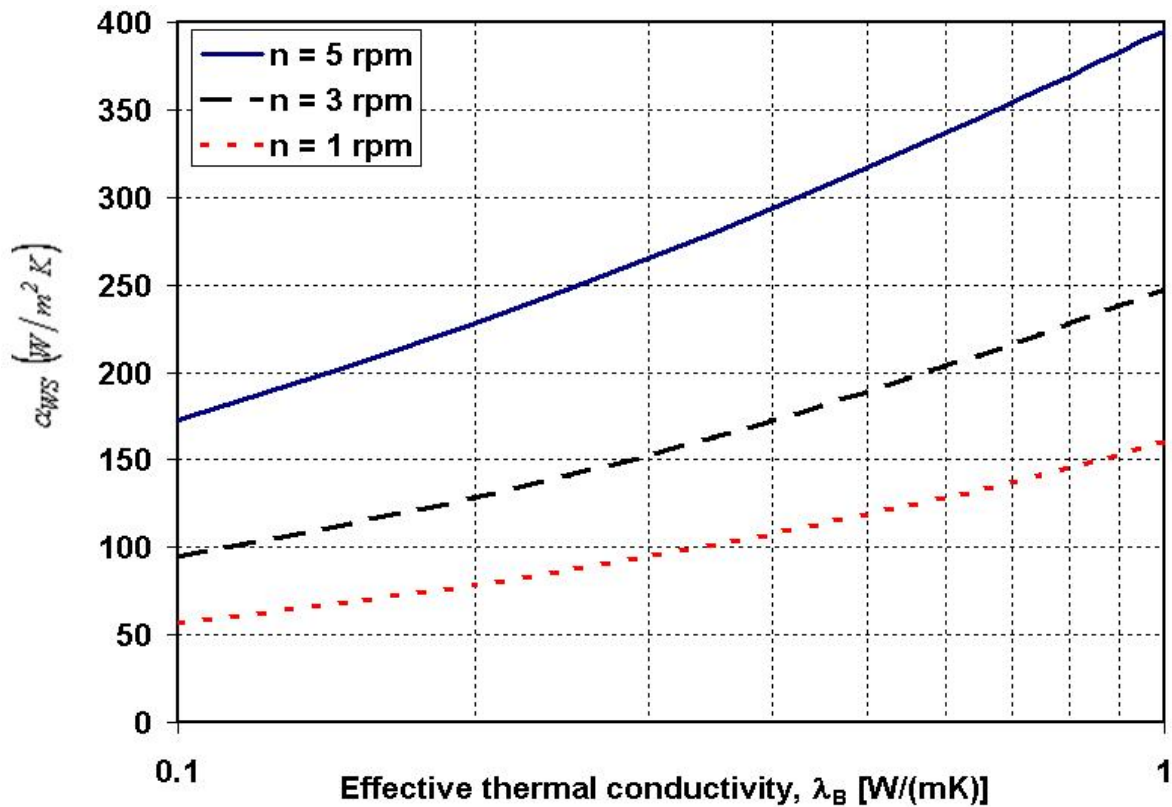


Figure 2-12. Heat transfer coefficient for single particle from kiln wall for different particle surface roughness (after Schlünder and Tsotsas 1988)

The calculation of the contact heat transfer requires knowledge of numerous parameters, and the approach is difficult to apply in practice. Therefore, it is appropriate to have a range of values of this heat transfer coefficient in order to determine the impact parameter influencing the heat transfer in the rotary kiln. Thus, based on the above studies, the suitable values for typical rotary kiln are in the range of 50 to 500 W/m^2K .

2.1.2 Regenerative heat transfer

Previous studies to predict the regenerative heat flow of the kiln wall were relatively crude. The earlier attempt was reported by Brimacombe and Watkinson (1978). They reported that only small fluctuations of the temperature exist on the inner wall and are negligible in the middle of the refractory wall as shown in Figure 2-13. There was no analytical solution to predict the fluctuations of the wall temperature.

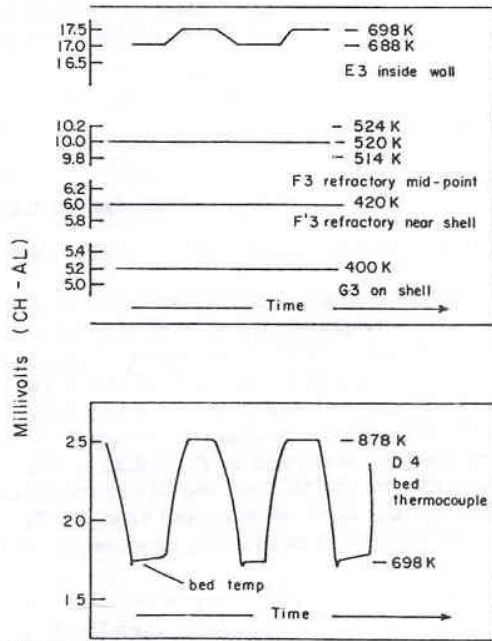


Figure 2-13. Typical wall and bed thermocouple traces (after Brimacombe and Watkinson 1978)

Barr et al. (1989) extended the experiment by inserting thermocouples at several depths in the kiln wall Figure 2-14.

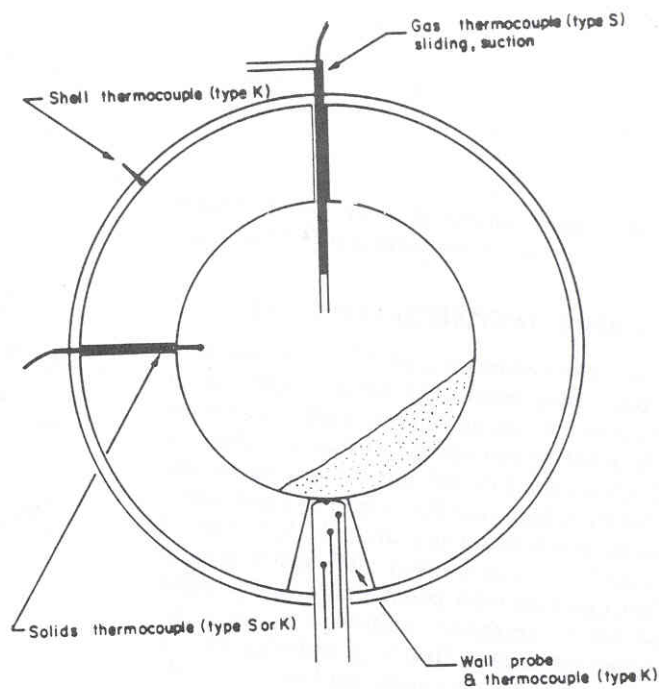
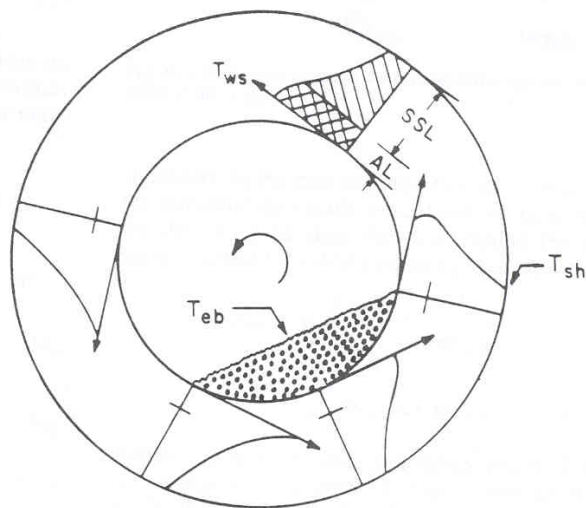


Figure 2-14. Thermocouple installations at a cross-section of the pilot kiln (after Barr et al. 1989)

The result indicates that the kiln wall is divided into two regions, a thin active layer at the inner surface which undergoes a regular cyclic temperature change as the wall rotates, and a steady state layer which is not involved in the heat exchange Figure 2-15.

The results of their study indicate that during the kiln rotation, the region of the active layer rarely exceeds a depth of 15 mm and the cyclic temperature on the inner surface of the kiln wall lies in the range of 30 to 90 K. Unfortunately, the calculations for the wall active layer and the heat flux in the wall active layer had to be solved numerically. Thus, it is difficult to see the impact of the influencing parameters and to scale up results.



AL Wall active layer
SSL Wall steady state layer

Figure 2-15. The active and steady-state layer in the refractory wall (after Barr et al. 1989)

Gardeik and Jeschar (1979) studied a one-dimensional heat flow model which was developed by applying an infinite large thermal conductivity coefficient of the kiln wall. A set of dimensionless equations to predict the fluctuation of the wall temperatures depending on the Stanton number and filling degree were investigated. These equations could only be solved numerically. Therefore parameters influencing the regenerative heat flow are not much discussed. The whole thickness of the kiln wall was used to solve the problem and no prediction of wall active layer was found. Substantially, the impact of the regenerative heat flow relative to the other heat transfer steps were not described clearly.

Gorog et al. (1982) developed a two dimensional, finite difference method to predict the variation of the inside kiln wall temperature. The heat transfer between the covered wall and the bed was calculated using the analogy of an electrical circuit. The results of his study indicate that during the kiln rotation, the region of the active layer rarely exceeds a depth of 15 mm and the cyclic temperature on the inner surface of the kiln wall lies in the range of 30 to 90 K. However, the thickness of the active layer and the heat transfer model has to be solved numerically.

Since none of the models proposed in the literature could satisfactorily represent a simplified approach to predict the regenerative heat transfer in the rotary kiln, an attempt was made in this work to accomplish this task. This correlation is discussed in Chapter 3.

2.2 Convection in the freeboard gas

2.2.1 Convection between the gas and wall

The convective heat transfer includes two paths in the rotary kiln: heat transfer between the freeboard gas and the wall (α_{GW}) and heat transfer between the freeboard gas and the solid bed (α_{GS}). At low temperature, convection is the dominant energy transport process but at moderate or high temperature its importance is certainly less.

Several equations have been studied to predict the correlation of convective heat transfer coefficient to the kiln wall in rotary kilns. Earlier studies, Sass (1967), Riffaud et al. (1972), Wingfield et al. (1974), applied pipe flow correlations for gas to wall convection

$$\alpha_{GW} = 0.0981(G_g)^{0.67} \quad (2-24)$$

where G_g is the gas mass flux $kg/hr m^2$ (cross section kiln). The value of 10 W/m^2K is reported. For development of turbulent flow in a pipe Kreith and Black suggested the following equation

$$\alpha_{WS} = 0.036 \frac{\lambda_g}{D} Re^{0.8} Pr^{0.33} \left(\frac{D}{L}\right)^{0.055} \quad (2-25)$$

for a cylinder with $10 < L/D < 400$. This correlation was chosen by Gorog et al.(1982) to calculate the convection in a 3.5 m ID x 135 m long rotary kiln with $Re = 2.5 \cdot 10^5$. The results of Eq. (2-19) yield a heat transfer coefficient of about 12 W/m^2K . In their theoretical study a range of 10 to 30 W/m^2K was employed.

Watkinson and Brimacombe (1978) carried out a series of experiments using a 0.406m ID pilot kiln firing natural gas. The calculated analysis of the experiment data lead to

$$Nu_{GW} = 1.26 \left(Re_D Pr \frac{D}{2L} \right)^{0.43} \quad (2-26)$$

It is found that for the range of temperature higher than 700 K the convection heat transfer accounts for around 10%. At $Re_D = 2 \cdot 10^5$, representative of the pilot kiln, the values lie around 2-3 W/m^2K . The gas radiation was increased with the kiln size, due to the increase of beam lengths.

Wes et al. (1976) reported that a value of 4-5 W/m^2K exist at $Re_D = 2.5 \times 10^5$ in his experiment using air in an empty metal drum with flights. By doubling the air flow and Re enhanced the heat transfer coefficient by only 4%.

Tscheng and Watkinson (1979) carried out an extensive series of experiments in a 0.191 m x 2.44 m kiln using heated air to eliminate gas radiation. The parameter of the experiments was the rotational speed, gas flow rate, and filling degree. The correlation used to verify the analysis was

$$Nu_{GW} = 1.54 \cdot Re_D^{0.575} Re_\omega^{-0.292} \quad (2-27)$$

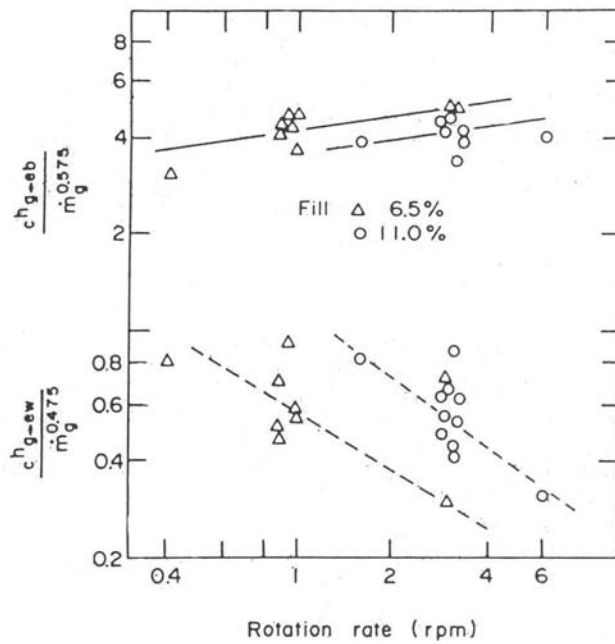


Figure 2-16. Effect of rotational speed on convective heat transfer coefficient (after Tscheng and Watkinson 1979)

The rotational speed has a slightly positive effect on α_{GS} , as shown in Fig. 2-16. This expression is valid in the range of $1600 < Re_D < 7800$ and $20 < Re_\omega < 800$. They reported a value of $2-9 \text{ W/m}^2\text{K}$ for the pilot kiln type.

Barr PV (1986) conducted a series of experiments using pilot rotary kiln $0.406 \text{ m} \times 5.5 \text{ m}$. He reported the range of convective coefficient around $1.5 - 15 \text{ W/m}^2\text{K}$ with the same range of Re_D as Tscheng (1979). The correlation over a flat plate was used

$$Nu_{GW} = 0.029 \cdot Re_D^{0.8} Pr^{0.33} \quad (2-28)$$

The scatters results are shown in Figure 2-17, which can be attributed to the fact that the kiln wall boundary layer is fully turbulent. The experiment were carried out using various material (Fine sand, coarse sand, petroleum coke, and limestone). The rotation speed was maintained at 1.5 rpm and the filling degree was held approximately constant ($\sim 12\%$), as was the kiln slope.

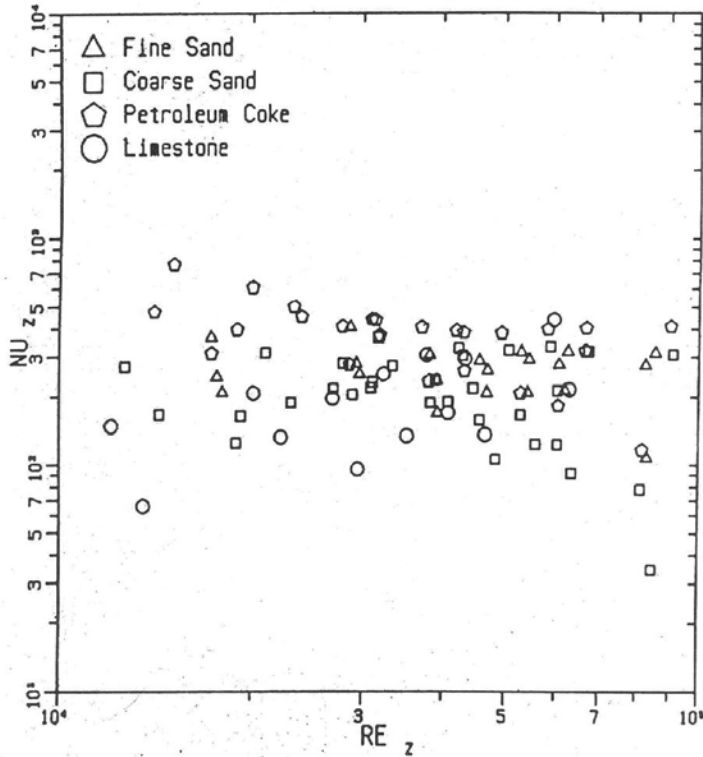


Figure 2-17. Convection to the exposed wall surface (after Barr 1989)

According to (VDI 1997), the convective heat transfer from gas to wall/gas to solid is calculated from the correlation below

$$Nu_{GW} = \frac{\zeta / 8 \cdot (Re - 1000) \cdot Pr}{1 + 12.7 \cdot \sqrt{\zeta / 8 \cdot (Pr^{2/3} - 1)}} \cdot \left[1 + \left(\frac{D_h}{L} \right)^{2/3} \right] \quad (2-29)$$

The friction factor, ζ , is determined from the correlation

$$\zeta = (1.82 \cdot \log_{10}(Re) - 1.64)^{-2} \quad (2-30)$$

Within the range of $0.5 < Pr < 1.5$, the correlation can be simplified as follows

$$Nu_{GW} = 0.0214 \cdot (Re^{0.8} - 100) \cdot Pr^{0.4} \cdot \left[1 + \left(\frac{D_h}{L} \right)^{2/3} \right] \quad (2-31)$$

2.2.2 Convection between gas and solid bed

The convective heat transfer coefficient between gas and exposed bed surface is considerably less important than to the exposed wall. Some investigators (Riffaud 1972, Sass 1967) have used Equation 2-24 for gas to wall convection to calculate heat flow from gas to solid bed. This coefficient is independent of the rotation speed, particle size, and inclination of the kiln. Other empirical equations for turbulent convection in a non-rotating tube

$$\alpha_{GS} = \alpha_{GW} = 0.023 \frac{\lambda_g}{D} Re^{0.8} Pr^{0.4} \quad (2-32)$$

were used for gas-wall and gas-solid convection in modeling iron ore reduction (Wingfield, 1974), alumina kiln (Manitius, 1974), and the non-reacting zone of a cement kiln (Ghoshdastidar, 1996).

Friedman and Marshall (1949) carried out several experiment trials in a rotary kiln heat exchanger using air and sand with and without internal flights. Values of $19 < \alpha_{GS} < 35 \text{ W/m}^2\text{K}$ were reported for kiln without flights independent on Re_D . There were no significant influence of particle size and rotation speed (3-20 rpm) on the coefficient. This condition might be expected if the bed surface played a limiting role in the heat transfer process.

In VDI 1997, the same correlation is used for heat transfer coefficient between gas and wall as well as gas and solid according to Eq. 2-29.

Wes et al. (1976) was the first who corrected this assumption. The results are given in Figure 2-18. They claimed that there should be a kind of penetration mechanism for the heat transfer to the flowing particles because of the rotational speed. This work showed that $\alpha_{GS} \approx (5 \sim 10) \cdot \alpha_{GW}$ for a rotary kiln with low flights. Thus, the assumption that $\alpha_{GS} = \alpha_{GW}$ is still questioned.

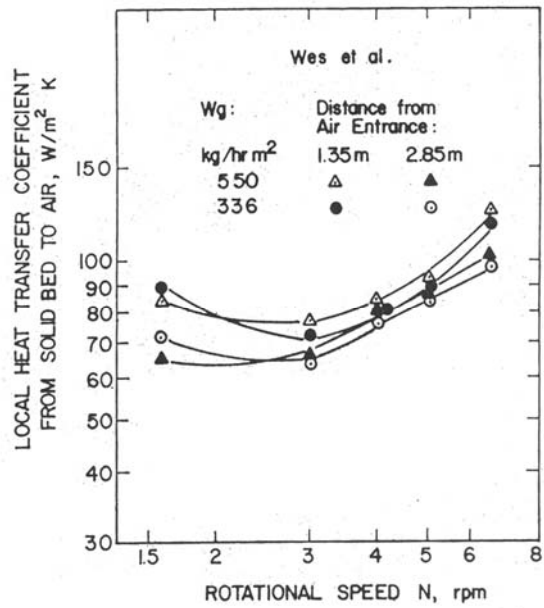


Figure 2-18. Convective heat transfer coefficient from freeboard gas to solid bed (after Wes et al. 1976)

The experimental study reported by Tscheng and Watkinson (1979) is the most thorough to date relating to the subject. The correlation

$$Nu_{GS} = \alpha_{GS} \cdot \frac{D_e}{\lambda_g} = 0.46 \cdot Re_{\infty}^{0.535} \cdot Re_{\omega}^{0.104} \cdot f^{-0.341} \quad (2-33)$$

where

$$Re_{\infty} = \frac{U_{\infty} \cdot D_e}{\nu} \quad (2-34)$$

$$Re_{\omega} = \frac{\omega \cdot D_e^2}{\nu} \quad (2-35)$$

where D_e is the equivalent diameter as a function of filling degree f . This correlation was obtained by regression analysis and the results are plotted in Figure 2-19. As it was the case of

the exposed wall, Eq. (2-33) implies a declining role for convection to the solid bed with increase in kiln diameter.

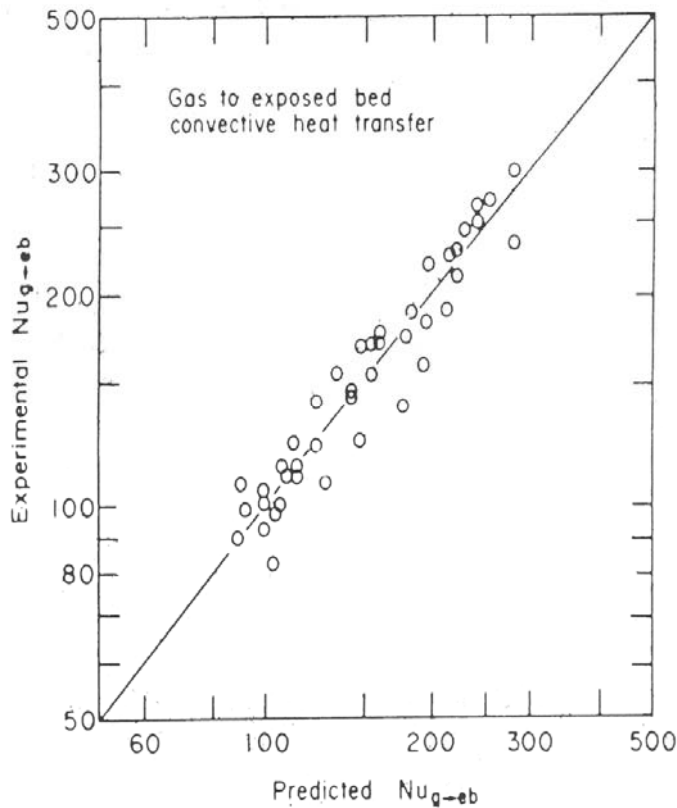


Figure 2-19. Predicted vs experimental values of freeboard gas to solid bed (after Tscheng 1979)

The results indicated that $\alpha_{GS} = 10 \cdot \alpha_{GW}$ as shown in Figure 2-20 for various gas flow rate. As shown previously in Fig. 2-18, this coefficient has a weak function of rotation speed. This condition might be expected because of the assumption that there was no temperature gradient in the solid bed.

Gorog et al. (1982) reported values in the range of 50 to 100 W/m^2K and recommended following equation for the kiln gas in contact with the solid bed

$$\alpha_{GS} = 0.4 \cdot (G_g)^{0.62} \tag{2-36}$$

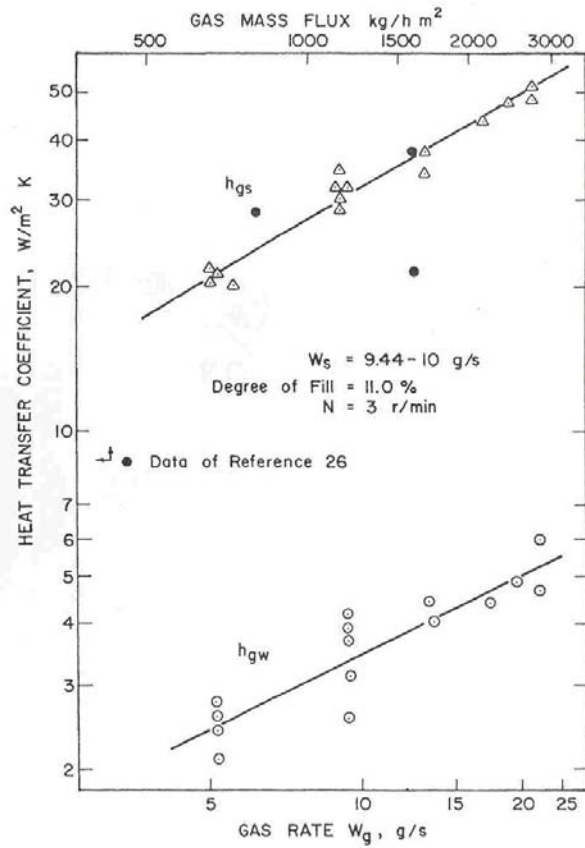


Figure 2-20. Effect of gas flowrate on convective heat transfer coefficient (after Tscheng 1979)

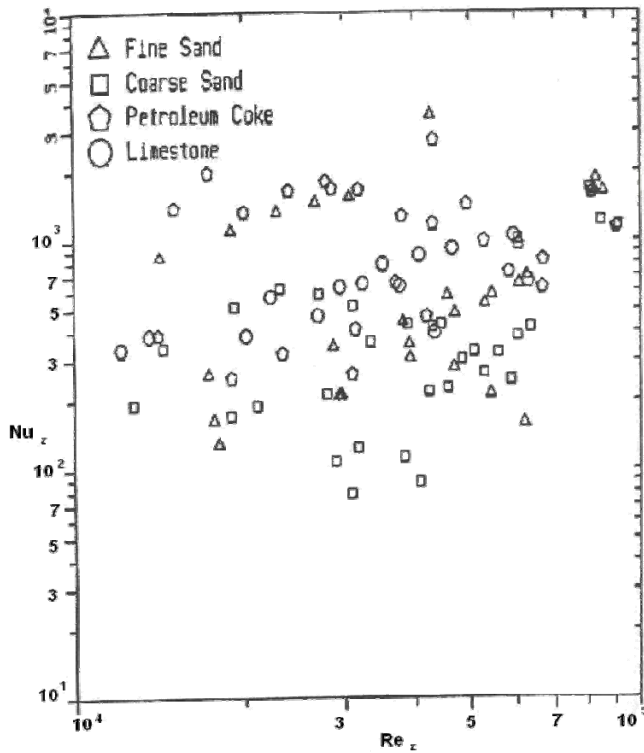


Figure 2-21. Convection to the solid bed surface (after Barr et al. 1989)

Barr et al. (1989) performed an extensive experimental study in a pilot kiln as used by Brimacombe and Watkinson (1978). The rotational speed of all the experimental studies was maintained at 1.5 *rpm* except for the last trials which were at a rotational speed of 1 *rpm*. Unfortunately, these rotational speeds were too low for the industrial rotary kiln. They concluded that the α_{GS} was slightly higher than α_{GW} . The mean value of $Nu_z \sim 480$ (Figure 2-21) is only about two times higher than the mean value for $Nu_z \sim 200$ (Figure 2-17), i.e. $\alpha_{GS} \sim 2 \cdot \alpha_{GW}$. However, in view of the large amount of scatter exhibited by the current data, the results must be viewed with caution.

Although exact values of convective coefficients remain elusive, appropriate values are sufficient to examine the relative importance of gas-convection versus gas-radiation. Barr (1986) emphasized that in the pilot kiln, convection to the exposed wall will be comparable to gas radiation only at low emitting gas concentrations or relatively low gas temperature. However, the convection to the solid bed is significant and accounted for about 20% of the total gas to bed surface heat transfer even at stoichiometric gas mixture and temperatures of 1000 K. For industrial rotary kiln, the role of convection is reduced to a very minor one due to the combined effects of longer emitting gas path lengths (high beam length). Thus, based on the above studies suitable ratios for heat transfer coefficient gas-solid, which incorporates radiation and convection, is in the range of $\alpha_{GS} \sim (2-10) \cdot \alpha_{GW}$.

2.2.3 Convection to the outer shell

Another convective heat transfer occurs at the outer kiln wall, which can be by natural convection or by forced convection when there is a wind. The empirical equations are given in VDI wärmeatlas (1997), in the case of natural convection in laminar flow the heat transfer coefficient is evaluated as

$$Nu_0 = 0.4 \cdot (Gr \cdot Pr)^{0.25} \quad (2-37)$$

and in the case of forced convection, condition between laminar and turbulent flow

$$Nu_0 = 0.3 + \sqrt{Nu_{lam}^2 + Nu_{turb}^2} \quad (2-38)$$

where

$$Nu_{lam} = 0.664 \cdot \sqrt{Re} \cdot \sqrt[3]{Pr} \quad (2-39)$$

$$Nu_{turb} = \frac{0.037 \cdot Re^{0.8} \cdot Pr}{1 + 2.443 \cdot Re^{-0.1} (Pr^{2/3} - 1)} \quad (2-40)$$

These equations gave a value of $\alpha_0 = 0.26 \text{ W/m}^2\text{K}$ for natural convection and $3 \leq \alpha_0 \leq 40 \text{ W/m}^2\text{K}$ for forced convection. Gardeik and Ludwig (1980) proposed a mean value of the heat transfer coefficient due to free and force convection and radiation on the external kiln wall. The mean value for convection is $8 \text{ W/m}^2\text{K}$ and for radiation $15 \text{ W/m}^2\text{K}$ for an external kiln wall temperature of 300°C with no air velocity.

2.3 Radiation in the freeboard gas

2.3.1 Radiative heat transfer

The radiative heat transfer is significant since most of the furnaces operate in high gas temperatures. Thus, a model for the radiative heat transfer among the gas, exposed wall, and bed surface is important for any kiln model. It is difficult to directly simulate the radiation in a rotary kiln. In general, radiative is negligible at gas temperature less than $300\text{-}400^\circ\text{C}$, but it is comparable to the convective heat transfer at temperature $700\text{-}900^\circ\text{C}$, and dominant at temperature greater than 1000°C (Gorog 1981, 1982). An accurate knowledge of the gas emissivity is difficult since it depends on various parameters e.g. kiln diameter (mean beam length), concentration of combustion gas, dust, and soot (emissivity of the gas), emissivity of the wall, etc., and it is different for each kiln. The emissivity of the gas in the rotary kiln depends on the absorbent concentration such as H_2O , CO_2 , CO , and CH_4 , and the present of dust. In the case of a $\text{H}_2\text{O}+\text{CO}_2$ mixture, the emissivity of the gas can be calculated from (VDI, 1997)

$$\varepsilon_g = \varepsilon_{CO_2} + \varepsilon_{H_2O} + \Delta\varepsilon \quad (2-41)$$

where the emissivities of each component are calculated from their partial pressure, corrected by the coefficients $\Delta\varepsilon$. The contribution of gases other than CO₂ and H₂O in the rotary kiln is small, due to their low concentrations. The contribution of dust is also important due to the ash from the fuel such as coal, the ash from the materials that break due to the kiln rotation or the breakage of the larger particles with increasing temperature.

Among the models for radiation in rotary kilns proposed in the literature, Gorog et al. (1981) and Barr et al. (1986) gave a detailed description of the heat transfer between the gas, solid and wall by employing the n-zone method. Most of the equations proposed are from VDI wärmeatlas (1997)

$$\dot{Q}_{GW} = \varepsilon_{GW} \cdot A_{W,G} \cdot \sigma \cdot (T_G^4 - T_{W,G}^4) \quad \text{with} \quad A_{W,G} = D_i \left(\pi - \frac{\varepsilon}{2} \right) \quad (2-42)$$

$$\dot{Q}_{GS} = \varepsilon_{GS} \cdot A_S \cdot \sigma \cdot (T_G^4 - T_S^4) \quad \text{with} \quad A_S = D_i \cdot \sin\left(\frac{\varepsilon}{2}\right) \quad (2-43)$$

$$\dot{Q}_{WS} = \varepsilon_{WS} \cdot A_S \cdot \sigma \cdot (T_{W,G}^4 - T_S^4) \quad (2-44)$$

where \dot{Q} is the radiative flux per unit length of the kiln, σ is the Stefan's Boltzman constant, A is the area per unit length, $T_G, T_S, T_{W,G}$ are the temperatures of the gas, solid, and the uncovered inner wall, respectively; and the coefficients $\varepsilon_{GW}, \varepsilon_{GS}, \varepsilon_{WS}$ are the emissivities of gas-to-wall, gas-to-solid, and wall-to-solid, respectively. The last coefficients are the radiation heat transfer coefficients which are depend on the view factor of the kiln, emissivities of gas, solid, and wall. The last coefficients depend on the view factors of the kiln, which is rather complicated. Recent investigators have attempted to solved this problem; Guruz and Bac (1981) using the Monte-Carlo method, Jenkins and Moles (1981) using the Zone method from a large enclosed flame, Jeschar et al. (1990) using exchange of two infinite parallel plate. The assumption that kiln enclosure is an infinite parallel plate, is not quite suitable for rotary kiln because the circumferential wall of the rotary kiln is approximately a concave shape. Thus, a

part of the radiant energy leaving the kiln wall will strike itself directly ($F_{ii} \neq 0$). Of all radiation models available, the Zone method is the accurate for calculating radiative heat transfer in fired heaters. Originally, it had been proposed by Hottel and Cohen (1958) for cuboids systems and was later extended to axisymmetrical cylindrical systems by Hottel and Sarofim (1965). Gorog et al. (1981) estimated the radiant heat transfer using exchange integral in multiple zone models. The prediction of total radiative exchange amongst the freeboard gas, kiln wall, and solids based on a real-gas radiative model, and comparison to simpler gray-gas models. The results proposed radiative heat transfer and modified view factor amongst the zone; however, the equations were so complicated and had to be evaluated using multiple integration. Recently, Murty (1993) proposed a non-stochastic type of Monte-Carlo method for calculation of direct exchange factor (view factor) of a rotary kiln. However, these calculations had to be evaluated in multiple integration using numerical techniques of Monte-Carlo method.

2.3.2 Linearization of radiation

The high freeboard gas temperatures of most rotary kilns ensure that radiative heat transfer is significant. The temperature of the combustion gas in the kiln is reduced in radial direction, thus the effect of convection should also be considered. Therefore, it is necessary to take into consideration both radiation and convection to the total heat transferred from the gas to the wall or to the solid bed. When the surface of body 1 is completely surrounded by a gray body 2 with a much larger surface area (the case in the rotary kiln), the rate of radiation heat transfer is given by (F.A. Schmidt et al. 1995)

$$\dot{Q} = \frac{\sigma \cdot (T_1^4 - T_2^4)}{\left[\frac{1 - \varepsilon_1}{\varepsilon_1 \cdot A_1} + \frac{1}{A_1 \cdot F_{1,2}} \right]} = \sigma \cdot \varepsilon_1 \cdot A_1 \cdot (T_1^4 - T_2^4) \quad (2-45)$$

Surface 1 represents freeboard gas and surface 2 represents solid bed or kiln wall. A radiation heat transfer coefficient, α_{rad} , can be introduced and the equation can be linearized (F.A. Schmidt et al. 1995, K.F. Wong 2002)

$$\begin{aligned}\dot{Q} &= \sigma \cdot \varepsilon_I \cdot A_I \cdot (T_G^2 + T_W^2) \cdot (T_G + T_W) \cdot (T_G - T_W) \\ &= \alpha_{rad} \cdot A_I \cdot (T_G - T_W)\end{aligned}\tag{2-46}$$

where

$$\alpha_{rad} = \varepsilon_{eff} \cdot \sigma \cdot T_G^3 \left[1 + \frac{T_W}{T_G} + \left(\frac{T_W}{T_G} \right)^2 + \left(\frac{T_W}{T_G} \right)^3 \right]\tag{2-47}$$

The total heat flux is

$$\dot{q} = (\alpha_{conv} + \alpha_{rad}) \cdot (T_G - T_W)\tag{2-48}$$

3 Regenerative action of the kiln wall in a directly heated rotary kiln

3.1 Introduction

The purpose of the work described in this chapter is to develop a fundamental understanding of the regenerative action of the wall relative to the overall heat transfer to the solid bed. Regenerative heat transfer has generally received inadequate attention. A detailed mathematical model has been developed which takes into account all of the heat-transfer steps which is previously described and shown schematically in Figure 1-2. However, these studies have neglected the influence of the regenerative heat by the wall. In additions, some previous attempts to predict the regenerative heat transfer is solved only numerically [Sass, A., 1967, Manitius, A.1974, Watkinson, A.P.and Brimacombe, J.K., 1978,]. Therefore, it is difficult to see the impact of the influencing parameters and to transfer the results to different kilns. Toward this goal, the model developed in this chapter, is used to explore the regenerative action of the kiln wall by introducing a simplified analytical model which has a small deviation with the numerical model. In the recent work of Queck 2002, the idea to predict the regenerative heat transfer by use of a fictitious layer thickness of the wall was introduced. The measurement of temperatures within the solid bed was investigated by inserting thermocouples into the bed at different depths. However, the measurements were performed only at two axial positions of the pilot kiln and the analytical model to solve this problem has some deficiencies. Therefore, an additional research is necessary to interpret the results. In addition, a simplified model also developed in this chapter to predict the inside wall temperature by introducing a thin lumped capacity layer, and also introducing a new parameter of heat transportation coefficient due to the rotating kiln wall. An advantage of this analytical solution is the implementation in complex simulation models of processes without the necessity to solve numerically the two-dimensional Fourier equation for the regenerative heat flow.

3.2 Numerical method

3.2.1 Description of the Model

For the computation of the stationary temperature distribution in the rotary kiln wall the Fourier-Kirchhoff differential equation is used in polar coordinates

$$c \cdot \rho \cdot w_{\varphi} \cdot \frac{1}{r} \cdot \frac{\partial T}{\partial \varphi} = \frac{\lambda}{r} \cdot \frac{\partial}{\partial r} \left(r \cdot \frac{\partial T}{\partial r} \right) + \frac{\lambda}{r^2} \cdot \frac{\partial^2 T}{\partial \varphi^2} \quad (3-1)$$

where φ is the angle of the circumference and r the radial coordinate according to Figure 3-1 for a cross-section of the rotary kiln. The length of the rotary kiln is long enough in comparison to its diameter; therefore the axial thermal conduction along the kiln can be neglected (3rd dimension: Z). Thus, it reduces to a 2-Dimensional problems depending on radial direction (r) and circumferential direction (φ).

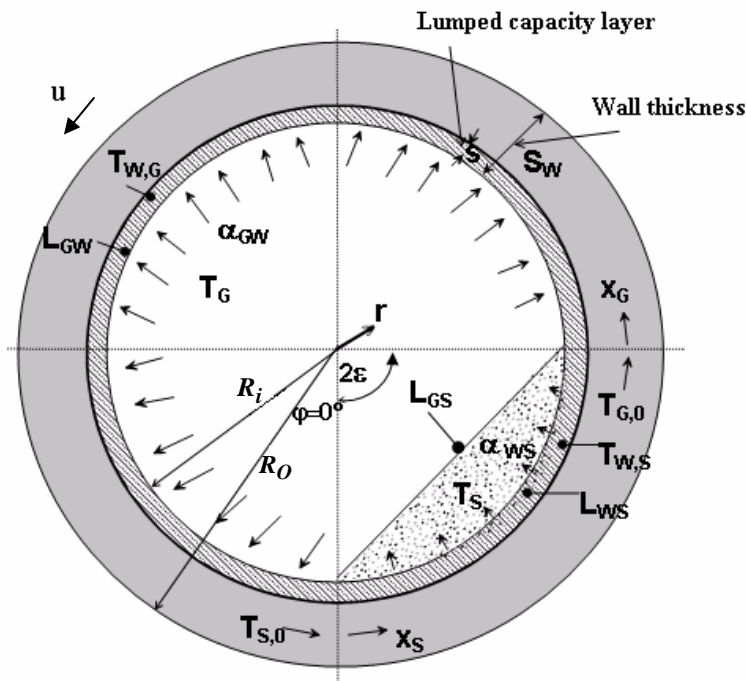


Figure 3-1. Symbols used for modeling heat transfer

The tangential velocity w_φ is replaced by the rotational frequency ω

$$w_\varphi = \omega \cdot r \quad (3-2)$$

This rotational frequency which is proportional to the rotational speed is used later as a parameter. The material properties are assumed to be constant because the temperature differences are relatively small across the kiln wall. Two boundary conditions in r and φ directions are needed. On the inner surface of the kiln wall the boundary condition in r -direction differs between the gas and the solid side.

The heat transfer on the internal kiln wall in contact with the solid is provided by

$$-\lambda \frac{\partial T}{\partial r} \Big|_{r=R_i} = \alpha_{WS} \cdot (T_{r=R_i} - T_S) \quad 0 \leq \varphi \leq 2\pi \quad (3-3)$$

where $T_{r=R_i}$ is the inner surface temperature of the kiln wall. The mean temperature of the solid bed (T_S) is assumed to be constant during the rotation. In reality, the temperature within the solid bed is distributed due to the mixing of the bed resulting from rotations but the temperature gradient is relatively small [Dhanjal, S.K. et al. 2004]. The bed movement depends on different forms of transport motion as explained by Mellman and Specht, 2001. For the description of the transverse solid motion, please refer to Liu et al., 2004. For the purpose of this study, it is not important to know the exact movement and the temperature distribution in the solid bed. A constant mean solid temperature is an appropriate simplification to provide a good approximation.

The heat transfer coefficient wall-to-solid (α_{WS}), as explained in Chapter 2, depends on many parameters such as kiln operating conditions (filling degree f and rotational speed n), material properties, the contact time and the length of the covered wall in circumference (L_{WS}). Therefore, this coefficient is taken as a parameter of the calculation. For example, the following expression is presented to compute this coefficient [Tscheng, S.H. and Watkinson, A.P., 1979]

$$\alpha_{WS} = 11.6 \cdot \left[\frac{n \cdot R_i^2 \cdot 2\varepsilon}{\lambda_B \cdot \rho_B \cdot c_B} \right]^{0.3} \cdot \frac{\lambda_B}{D} \quad (3-4)$$

where λ_{eB} , ρ_B and c_B are the effective thermal conductivity, the density and the heat capacity of the solid bed, respectively. From this equation the range of the values of the heat transfer coefficient can be clearly estimated. As mentioned previously in chapter 2, α_{WS} values is approximately in the range of 50- 500 $W/m^2 K$.

The heat transfer in the contact region of gas-wall is mainly transferred by radiation [Gorog, J.P., 1981]. But later for comparison with the analytical model, a linearization of this heat transfer is required. Therefore, in this region the heat transfer is described by the law of convection

$$-\lambda \left. \frac{\partial T}{\partial r} \right|_{r=R_i} = \alpha_{GW} \cdot (T_{r=R_i} - T_G) \quad (3-5)$$

$$2\varepsilon \leq \varphi \leq 2\pi$$

where T_G is the gas temperature which is assumed as constant throughout the cross section.

The heat transfer coefficient α_{GW} is given as

$$\alpha_{GW} = \varepsilon_{eff} \cdot \sigma \cdot T_G^3 \left[1 + \frac{T_W}{T_G} + \left(\frac{T_W}{T_G} \right)^2 + \left(\frac{T_W}{T_G} \right)^3 \right] \quad (3-6)$$

The fluctuation of the wall temperature T_W is less than 15% of the temperature difference between gas and wall, e.g. less than 70 K if the $T_G - T_S$ is about 500 K. An example will be shown later. Therefore, this temperature is assumed as constant with a mean value of $T_{r=R_i}$ in circumferential direction.

The effective emissivity ε_{eff} depends on many parameters, e.g. kiln diameter (mean beam length), concentration of combustion gas, dust, and soot (emissivity of the gas), emissivity of the wall, etc., and it is different for each kiln. Therefore, this heat transfer coefficient is again taken as a parameter. The range of its value is estimated as follows. For a high value of the combustion gas temperature of $2000^{\circ}C$ and $\varepsilon_{eff} = 0.5$, the maximum value of α_{GW} is approximately $1000 W/m^2K$. For a low value of combustion gas temperature of $1000^{\circ}C$ and $\varepsilon_{eff} = 0.35$, the value is approximately $200 W/m^2K$. The values are varied within this range.

The boundary condition on the external kiln wall is given as

$$-\lambda \frac{\partial T}{\partial r} \Big|_{r=R_0} = \dot{q}_L \quad (3-7)$$

$$0 \leq \varphi \leq 2\pi$$

The heat loss is approximated by the stationary heat conduction through the wall (Gorog, J.P., 1982)

$$\dot{q}_L = 2 \cdot \pi \cdot R_0 \cdot \alpha_0 \cdot (T_{W0} - T_0) \quad (3-8)$$

where α_0 is the mean value of the heat transfer coefficient due to free and force convection and radiation on the external kiln wall. This coefficient is determined in the study of Gardeik and Ludwig 1980, the mean value for convection is $8 W/m^2K$ and for radiation $15 W/m^2K$ for an external kiln wall temperature of $300^{\circ}C$ and no air velocity. Typical values of the heat loss lie between $2700 W/m^2$ and $4000 W/m^2$. The amount of the heat loss does not affect the regenerative heat transport by the wall which can be seen later.

Due to the closed ring, the following boundary conditions for the angular direction are valid

$$T(\varphi = 0^{\circ}) \approx T(\varphi = 360^{\circ}) \quad (3-9)$$

and

$$\frac{\partial T}{\partial \varphi}(\varphi = 0^\circ) = \frac{\partial T}{\partial \varphi}(\varphi = 360^\circ) \quad (3-10)$$

The differential equation (Eq. 3-1) was solved by the means of an implicit Finite Element Method (FEM) under ANSYS version 6.1. The segmental geometric configuration with cylindrical faces and the structure grid with four nodes were chosen. Five thousand cells were used for the meshing of the segmental geometry of the cylindrical kiln. The faces were divided into 360 grids along the circumferential direction and 15 grids along the radial direction. Using more cells will not lead to any remarkable changes in temperature and will give less than 0.5% deviation in heat flow. The standard element type plane 55 for two dimensional thermal solids is used for the ANSYS calculations. This element type can be used as a plane element or as an axisymmetric ring element with a two-dimensional thermal conduction capability.

3.2.2 Temperature distribution

The fluctuation on the internal surface temperature of the kiln wall is presented in Figure 3-2 as a dimensionless form along the circumference. For this example, a typical refractory material with values of $\rho = 2100 \text{ kg/m}^3$, $c = 1040 \text{ J/kgK}$, $\lambda = 2 \text{ W/mK}$ is used. The rotational speed varies within a range of 0.5 -10 rpm. A lab-scale kiln for the experimental work with 0.4 m ID and the filling degree 10% is used. Wall-to-solid and gas-to-wall heat transfer coefficients have the same value of $100 \text{ W/m}^2\text{K}$. This figure shows that the rotational speed has low influence, for example for kiln speed 1 rpm the fluctuation of the temperature only 2%. The fluctuation of the kiln wall temperature decreases as the kiln speed increases. The kiln wall is alternately cooled and heated during each revolution by the hot gas and the cold solid respectively. In addition, for a very low kiln speed the fluctuation is increased.

The fluctuation of the kiln wall temperature can be clearly seen in Figure 3-3. In this case the parameter is the ratio of heat transfer coefficient wall-solid to heat transfer coefficient gas-wall. The kiln wall stores heat as it rotates on the gas side and gives the heat back to the solid bed as the kiln wall touches the solid. As the contact heat transfer wall-solid increases, the temperature of the kiln wall decreases toward the temperature of the solid bed. Vice versa, for a higher radiation on the gas side, the kiln wall temperature increases.

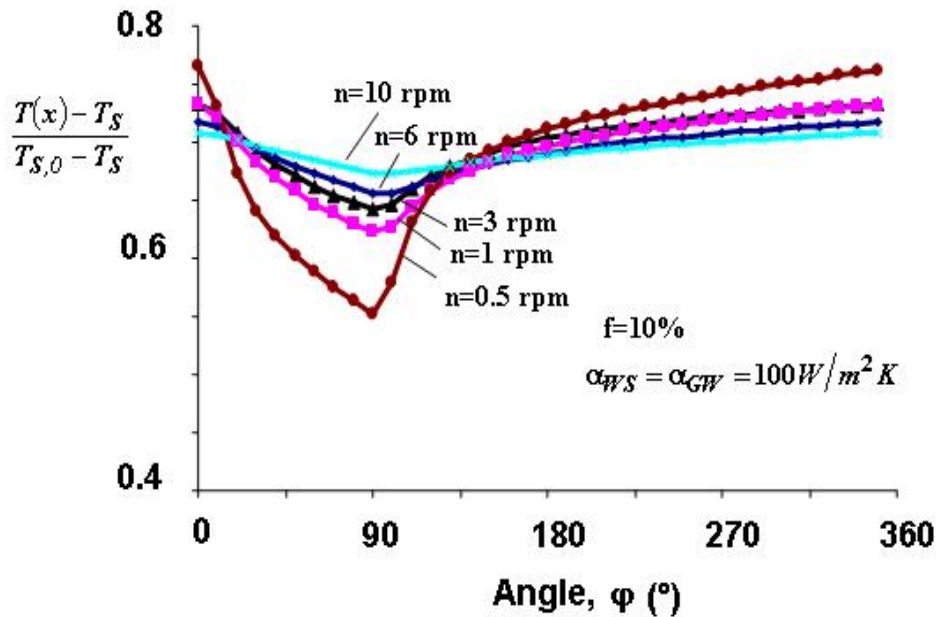


Figure 3-2. Surface temperature on the kiln wall for various rotational speeds

Typical radial wall temperature profiles are plotted in Figure 3-4 and Figure 3-5. The temperatures are set to be constant for the gas at 1000°C and the solid at 500°C . Four different circumferential positions are presented in a small figure above the curve. $T_{S,0}$ is the initial point of the inner surface wall temperature in contact with the solid, and $T_{G,0}$ is the point in contact with the gas. These two points are the maximum fluctuation temperatures of the internal surface kiln wall. The range where the curves of the solid side and gas side overlap is known as the penetration depth. This penetration depth is much smaller than the wall thickness which is typical in the range of 300 mm . After this range, the temperature gradient is determined by the heat loss. Back to Figure 3-4, for example a typical rotary kiln is considered with a filling degree of 10% and a rotation speed of 3 rpm . The circumferential inner wall temperature fluctuation is around 70 K and the penetration depth in the wall is around 10 mm . A similar penetration depth and fluctuation temperature is also reported by Gorog et al., 1982. The penetration depth depends on the contact time between the solid and the rotating wall. Thus, for a lower rotation speed and higher filling degree, the range of the predicted penetration depth is increased as shown in Figure 3-5 for a rotary kiln with a filling degree of 20% and a rotation speed of 1.5 rpm . On the other hand, the penetration depth is independent of the kiln diameter, which will be explained later in the analytical model.

Therefore, the kiln diameter will not affect the range of the penetration depth. Experimental work conducted by Barr et al. 1989 and Queck 2002 supports this behavior.

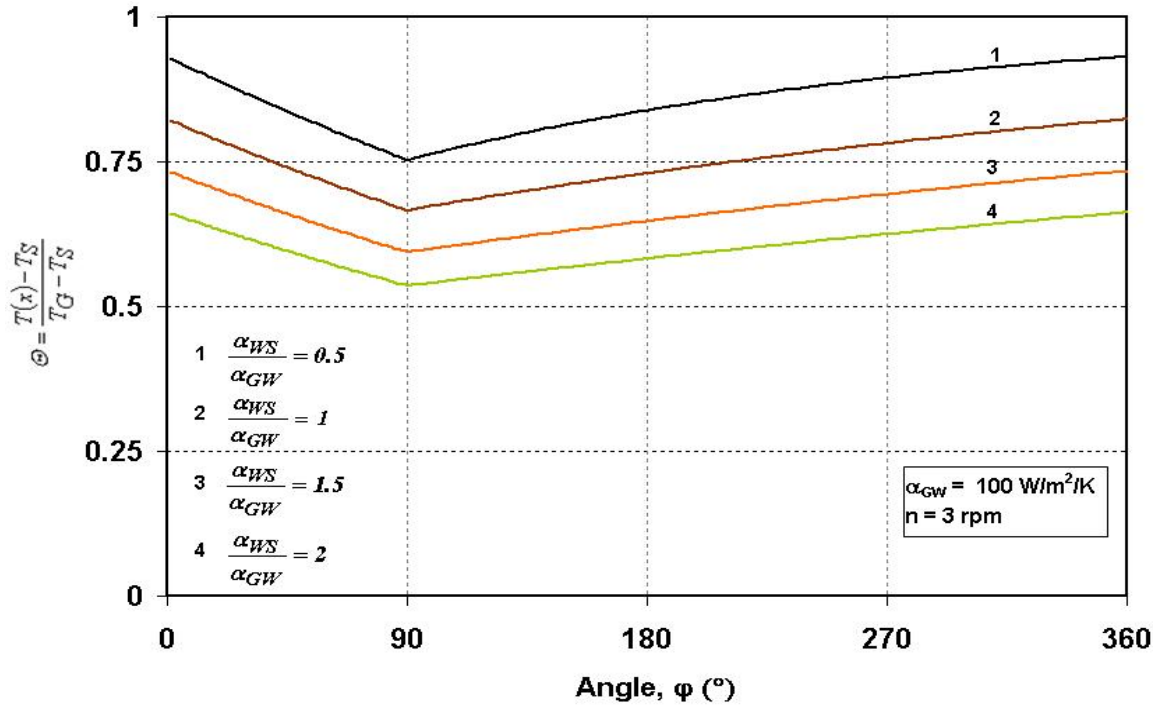


Figure 3-3. Dimensionless temperature in the circumferential direction

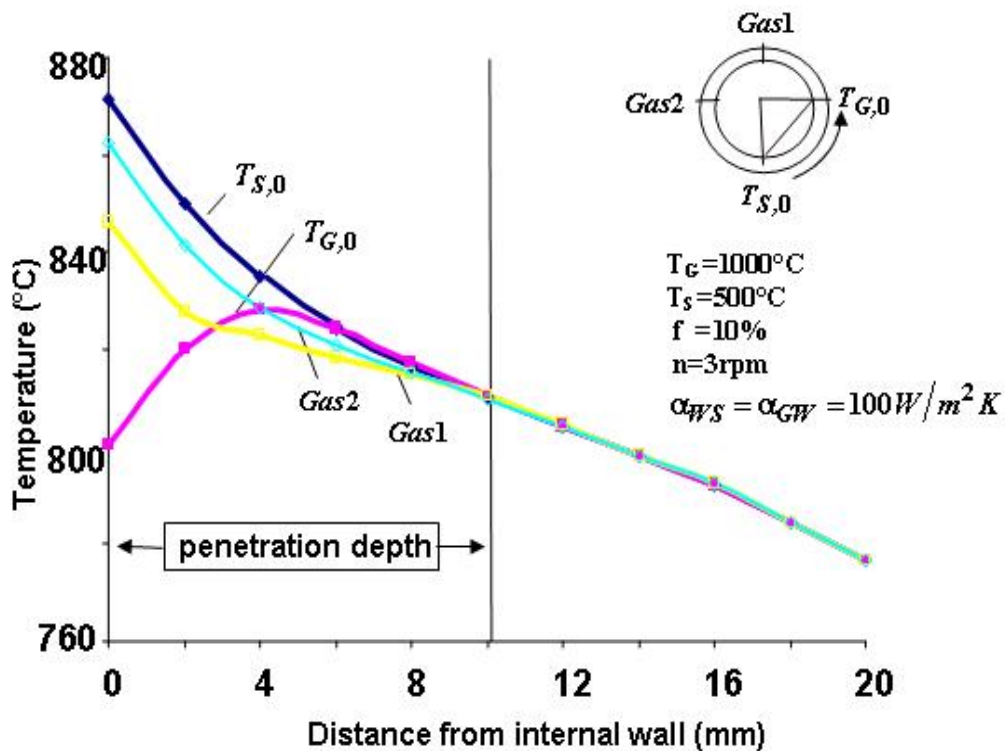


Figure 3-4. Temperature distribution on the kiln wall for a relatively short contact time and low filling degree

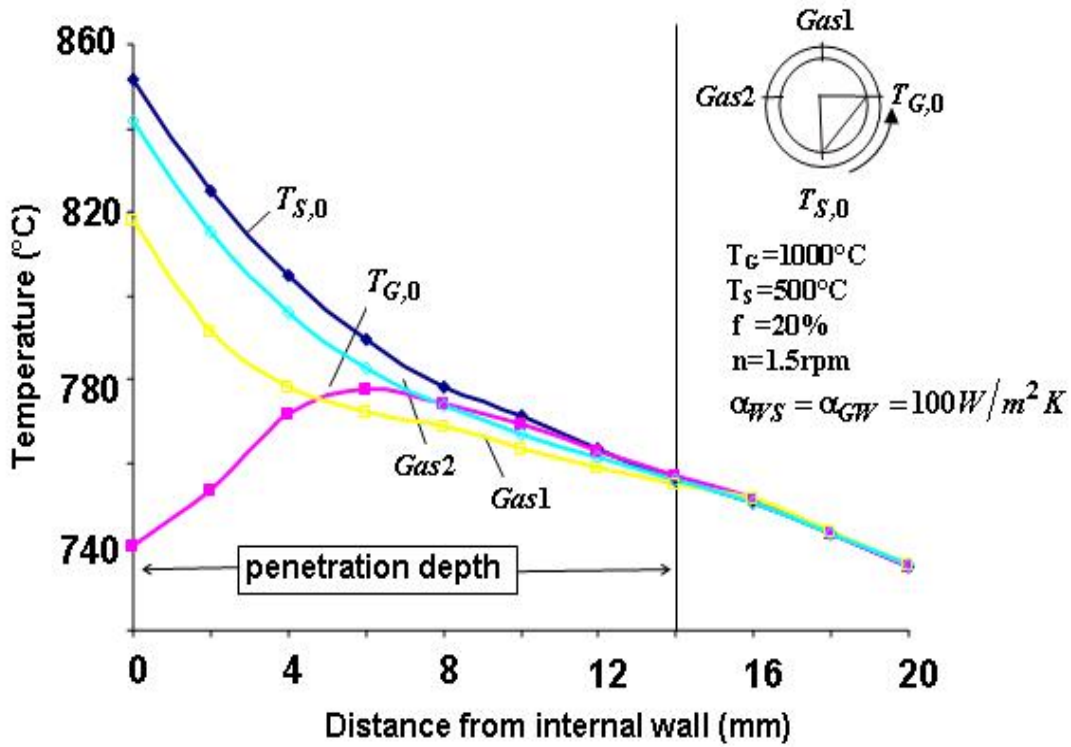


Figure 3-5. Temperature distribution on the kiln wall for a relatively short contact time and high filling degree

3.2.3 Heat flow

The heat flow from the wall to the solid is determined by the temperature gradients on the internal surface of the wall

$$\frac{\dot{Q}_{WS}}{L} = \int_{T_{S,0}}^{T_{G,0}} \lambda \frac{\partial T}{\partial r} \Big|_{r=R_i} R_i \cdot d\varphi \quad (3-11)$$

The amount of heat received by the wall from the gas

$$\frac{\dot{Q}_{GW}}{L} = \int_{T_{G,0}}^{T_{S,0}} \lambda \frac{\partial T}{\partial r} \Big|_{r=R_i} R_i \cdot d\varphi \quad (3-12)$$

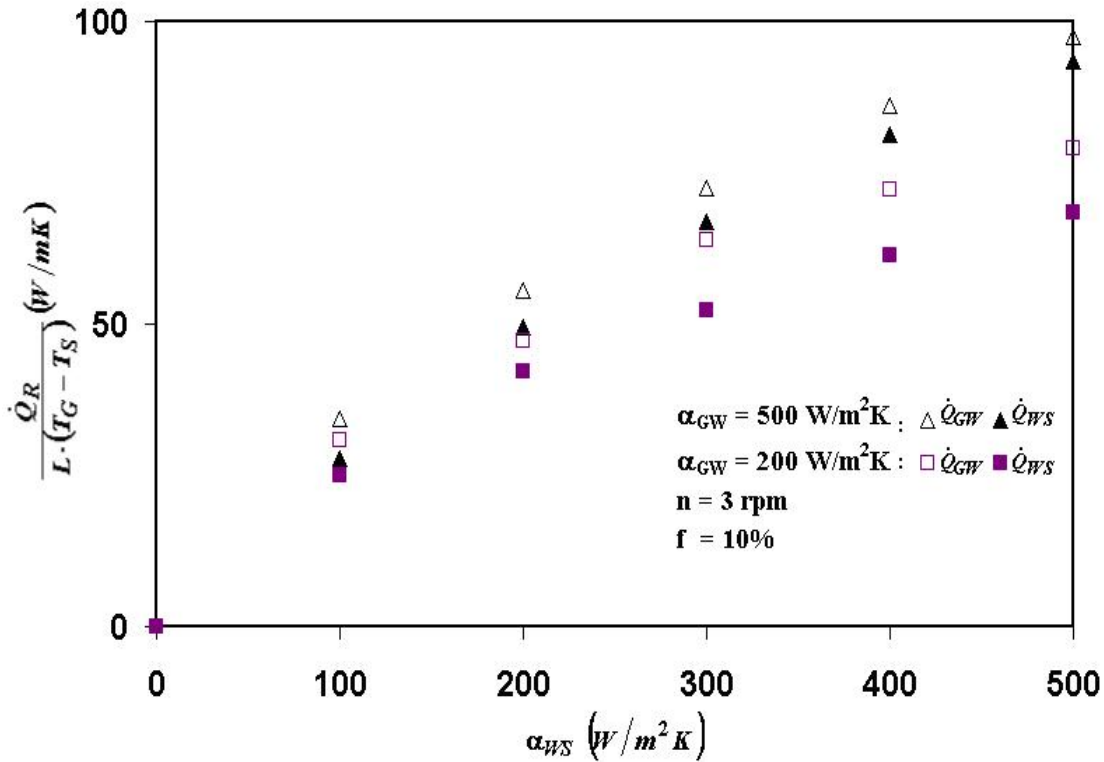


Figure 3-6. Comparison of numerical gas and solid regenerative heat flows

These two regenerative heat flows by the wall are shown in Figure 3-6 for some examples. It can be observed that the heat flows are more strongly influenced by the heat transfer coefficient wall-to-solid (α_{WS}) than the heat transfer coefficient gas-to-wall (α_{GW}).

The heat flow \dot{Q}_{GW} from the gas to the wall is higher than the heat flow \dot{Q}_{WS} from the wall to the solid. The difference is caused by the heat loss of the kiln to the environment, as described before with Eq. (3-8). The heat flows will be compared later with the analytically calculated heat flows which are explained in the following section.

3.3 Analytical solution

3.3.1 Temperature distribution

As shown previously with the numerical results, the penetration depth is much smaller than the thickness of the refractory wall. The wall thickness has no influence to the heat flow in the kiln. It is assumed that only a layer near to the surface of the kiln wall which is named as a thin lumped capacity layer (s) participates in the heat exchange. The thermal conductivity

of this layer is infinite in the radial direction and assumes to save the same amount of heat as the whole wall, as it is represented schematically in Figure 3-1. Thus, the temperature is constant in radial direction and depends only on the angular direction. Therefore, the model reduces to a 1-Dimensional problem. Since the thickness of this layer is very much smaller than the kiln diameter, its velocity (u) can be assumed to be constant and set equal to the surface velocity

$$u = 2 \cdot \pi \cdot R_i \cdot n \quad (3-13)$$

Remarkably, for the values of rotation speed greater than 0.3 rpm, the heat conduction in the angular direction can be neglected. With these simplifications, the temperature only depends on the circumference (one-dimensional).

For the further calculations, the coordinate x in circumferential direction is introduced according to Figure 3-1. Thus, the wall temperature in the solid region and in the gas region can be calculated using lumped capacity model

Solid region

$$\frac{T(x_S) - T_S}{T_{S,0} - T_S} = \exp\left(-\frac{\alpha_{WS} \cdot x_S}{\rho \cdot c \cdot u \cdot s}\right) \quad (3-14)$$

Gas region

$$\frac{T(x_G) - T_G}{T_{G,0} - T_G} = \exp\left(-\frac{\alpha_{GW} \cdot x_G}{\rho \cdot c \cdot u \cdot s}\right) \quad (3-15)$$

where x_S and x_G are the angular coordinates of solid and gas region, respectively; and s is still the unknown thickness of the lumped capacity layer. The initial temperatures $T_{G,0}$ and $T_{S,0}$ are obtained from the condition that the temperatures at the end of each region have to be equal to the inlet temperature of the other region

$$T_{G,0} = T(x_S = L_{WS}) \quad (3-16)$$

$$T_{S,0} = T(x_G = L_{GW}) \quad (3-17)$$

where L_{WS} and L_{GW} are the angular lengths of solid and gas region, respectively.

Finally, we get for the solid temperature distribution

$$\Theta_S = \frac{T(x_S) - T_S}{T_G - T_S} = \frac{e^{-St_G \cdot \varphi \cdot A} \cdot (e^{-St_G} - 1)}{e^{-St_G \cdot A} \cdot e^{-St_G} - 1} \quad (3-18)$$

and for the gas temperature distribution

$$\Theta_G = \frac{T(x_G) - T_S}{T_G - T_S} = \frac{e^{-St_G \cdot \varphi} \cdot (1 - e^{-St_G \cdot A})}{e^{-St_G \cdot A} \cdot e^{-St_G} - 1} + 1 \quad (3-19)$$

with the Stanton number

$$St_G = \frac{\alpha_{GW} \cdot L_{GW}}{\rho \cdot c \cdot u \cdot s} \quad (3-20)$$

and the heat resistance ratio

$$A = \frac{\alpha_{WS} \cdot L_{WS}}{\alpha_{GW} \cdot L_{GW}} \quad (3-21)$$

The lengths of the solid and the gas in contact with the rotating wall can be replaced by the internal kiln diameter and the filling degree

$$L_{WS} = \varepsilon \cdot D \quad (3-22)$$

$$L_{GW} = D \cdot (\pi - \varepsilon) \quad (3-23)$$

Inserting Eqs. (3-22) and (3-13) into Eq. (3-20), the Stanton number yields to

$$St_G = \frac{\alpha_{GW} \cdot (\pi - \varepsilon)}{\rho \cdot c \cdot \pi \cdot n \cdot s} \quad (3-24)$$

For infinite rotational speed ($St_G = 0$), both regions have the same value

$$\frac{T - T_S}{T_G - T_S} = \frac{1}{1 + \frac{\alpha_{WS} \cdot L_{WS}}{\alpha_{GW} \cdot L_{GW}}} \quad (3-25)$$

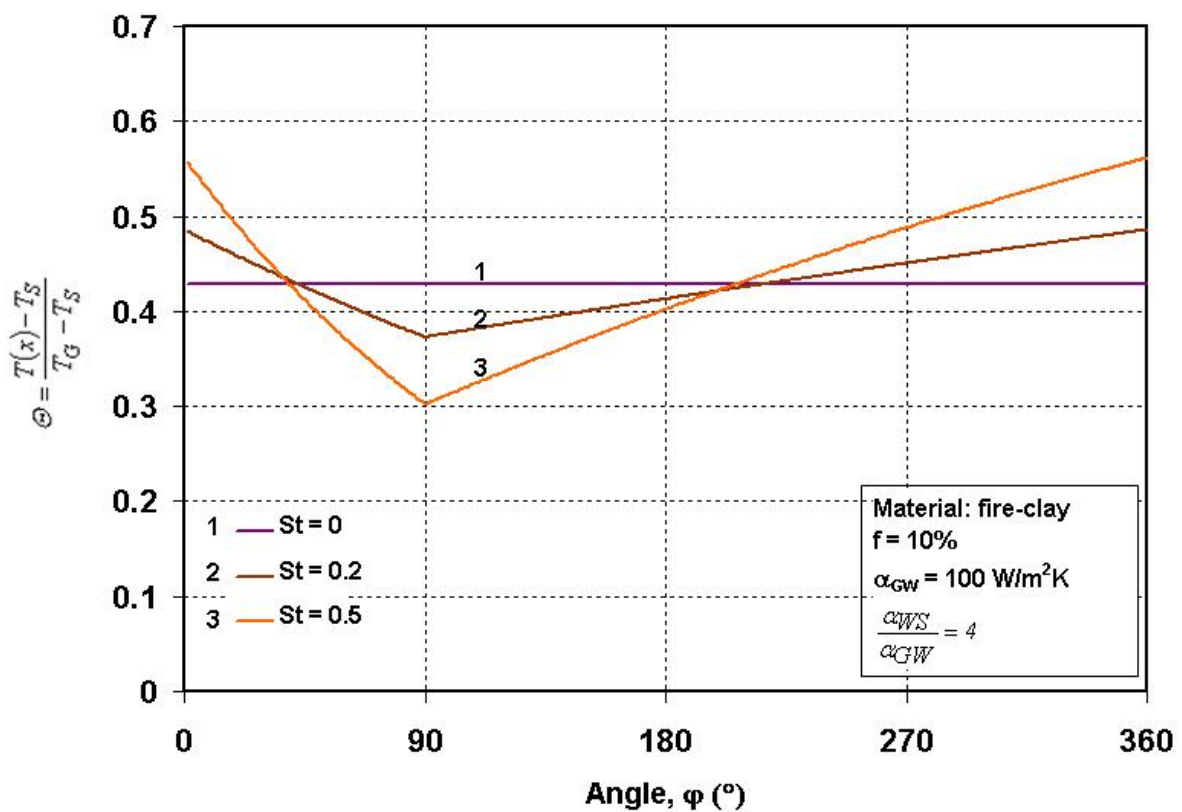


Figure 3-7. Dimensionless kiln wall temperature distribution for different Stanton number

Figure 3-7 shows the dimensionless temperature distribution for various Stanton number at heat transfer coefficient ratio = 4. As the Stanton number decreases, the inner wall temperature difference decreases. At a low rotational speed ($n = 0.5 \text{ rpm}$, $St = 0.5$) the fluctuation of the inner wall is high. However, at infinite rotational speed ($St = 0$) there are no more temperature difference of the inner wall according to Eq. 3-25. This fact indicates that the heat transportation coefficient which involved the rotational speed indeed influences the temperature fluctuation of the inner wall. The fluctuation of the inner wall influences the thermal stresses of the refractory wall. This result is important since the life time of the refractory wall depends on the change of temperatures.

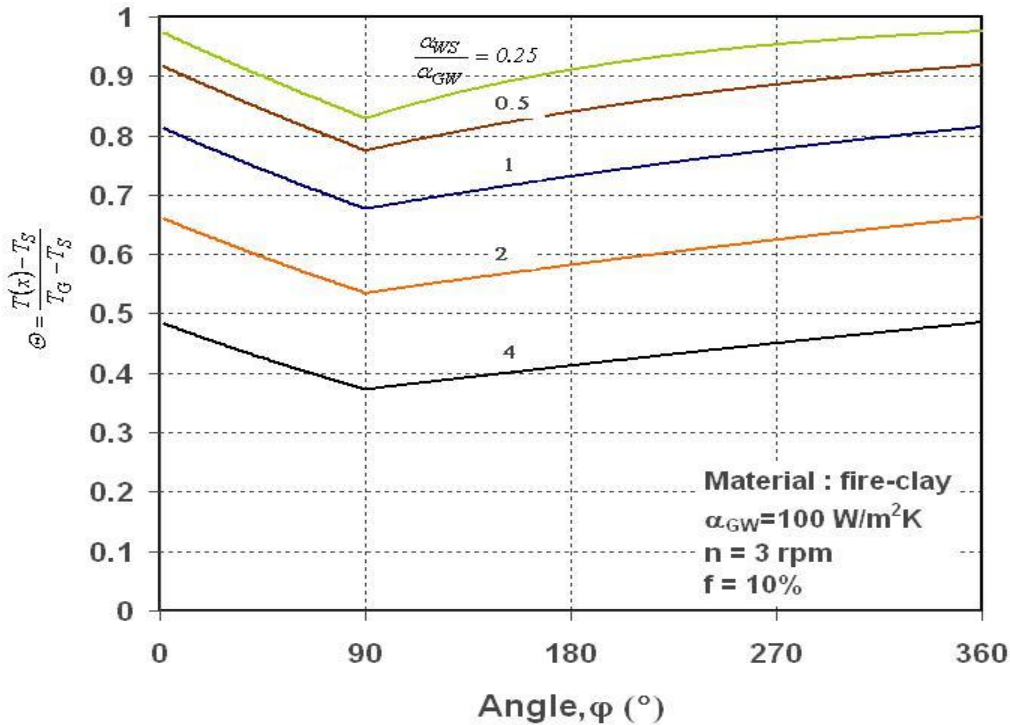


Figure 3-8. Influences of wall-solid heat transfer coefficient to the dimensionless temperature

Figure 3-8 illustrates the influence of wall-solid heat transfer coefficient to the dimensionless temperature distribution of the inner kiln wall at typical rotational speed ($n = 3 \text{ rpm}$). The level of the inner wall temperature increases towards the gas temperature at low wall-solid heat transfer coefficient and the level decreases towards the solid temperature at higher values of this coefficient. This fact is due to at high value of heat transfer coefficient wall-solid the heat is perfectly transferred from wall to solid. As a consequence, the temperature of the wall tends to decrease towards the solid bed temperature (T_S). In the case

of constant rotational speed, the fluctuation of the inner wall decreases at higher value of the wall-solid heat transfer coefficient which can be seen clearly in Figure 3-9 with the same parameters. At the same magnitude of both heat transfer coefficients, the fluctuation of the inner wall is around 15% at rotational speed 1 rpm. The temperature difference becomes smaller at higher rotational speed, and no more temperature difference at infinite rotational speed.

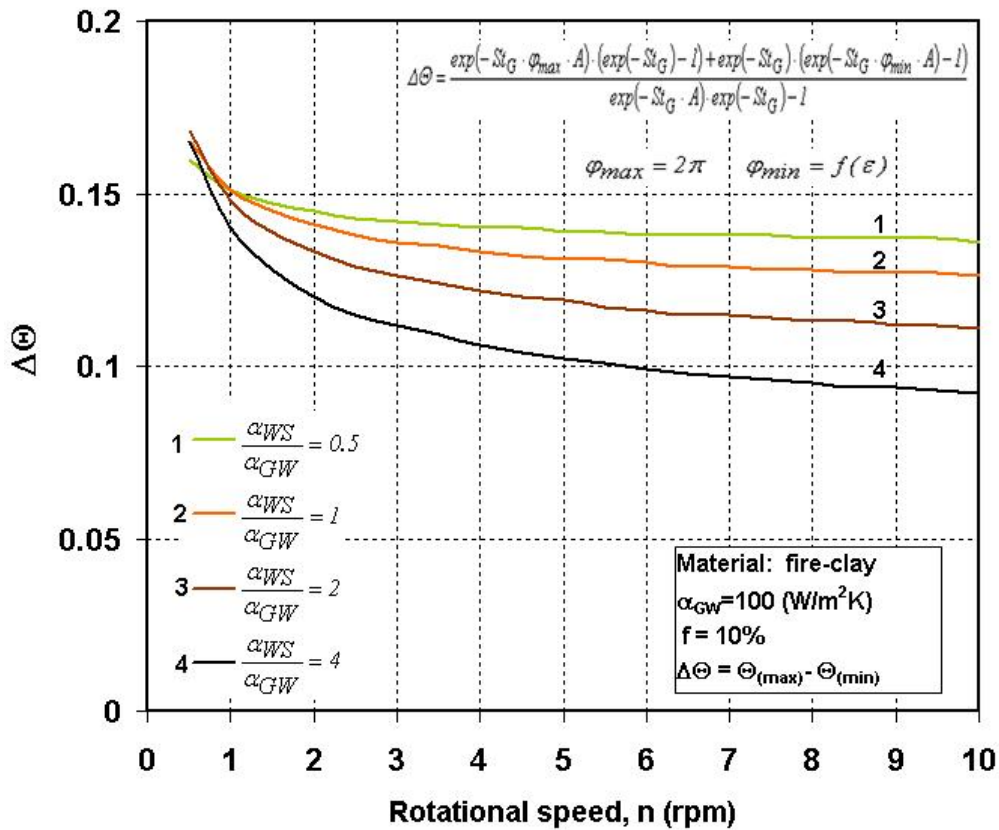


Figure 3-9. The maximum and minimum dimensionless inner wall temperature differences

3.3.2 Heat flow

The calculation of the regenerative heat flow is as follows

$$\dot{Q}_R = \int_0^{L_{GW}} \alpha_{GW} (T(x) - T_G) dx_G = \int_0^{L_{WS}} \alpha_{WS} (T(x) - T_S) dx_S \quad (3-26)$$

The amount of the heat which is transported from the freeboard gas to the wall is transferred again to the solid $\dot{Q}_{GW} = \dot{Q}_{WS}$. Thus, the heat loss is neglected in this model. After inserting Eq. (3-18) or (3-19) into Eq. (3-26), the regenerative heat flow related to the kiln length L is as follows

$$\dot{Q}_R = \alpha_{WS} \cdot L_{WS} \cdot (T_G - T_S) \cdot \frac{(e^{-St_G} - 1) \cdot (e^{-St_G \cdot A} - 1)}{A \cdot St_G \cdot (1 - e^{-St_G} \cdot e^{-St_G \cdot A})} \quad (3-27)$$

In the numerical model the radiation has to be linearized; therefore in order to verify the validation of the linearization, the heat flow using actual temperature from the numerical model and mean wall temperature from the analytical model is compared.

$$\dot{Q}_{T=R_i} = \varepsilon \cdot \sigma \cdot (T_G^4 - T_W^4) \quad (3-28)$$

For the analytical model, linearization of Eq. 3-6 is used

$$\dot{Q}_{T=T_{r=R_i}} = \alpha_{GW} \cdot (T_G - T_W) \quad (3-29)$$

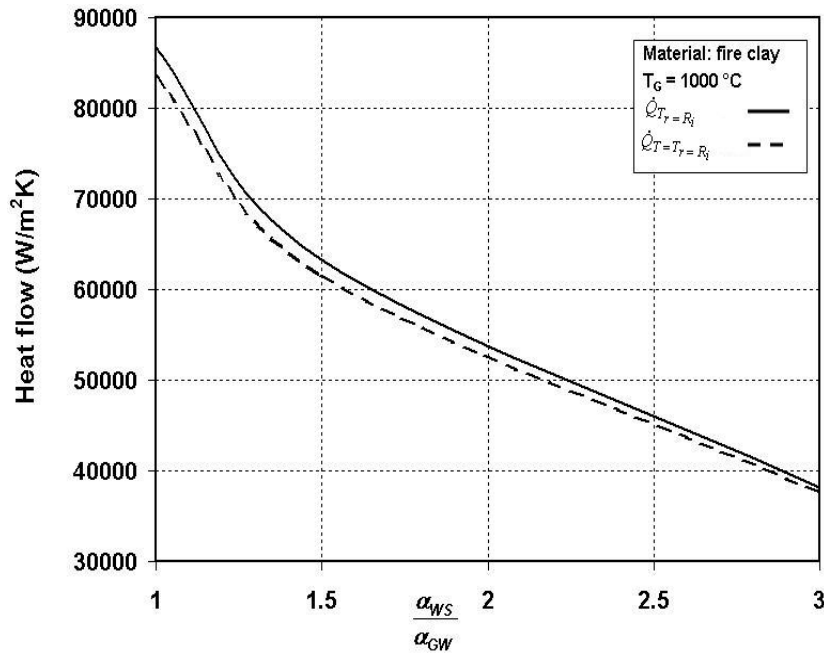


Figure 3-10. Comparison between heat flow with mean wall temperature and actual temperature

The error between the heat flow with mean temperature and linearization of radiation ($\dot{Q}_{T_r=R_i}$) and with the actual temperature $\dot{Q}_{T=T_r=R_i}$ is less than 2% (see Figure 3-10)

3.3.3 Thin lumped capacity layer

The calculation of the Stanton number requires the thickness s of the thin lumped capacity layer. The wall can be regarded as a semi-infinite body as could be seen in Figure 3-4 and Figure 3-5 for the numerical calculation. The distribution of the temperature in a semi-infinite body is given in Carslaw 1959. For the region of the contact solid-wall this equation can be written as

$$\frac{T(x) - T_S}{T_{S,0} - T_S} = \text{erf}(Z) + e^{Bi \cdot (2 \cdot Z + Bi)} \cdot [1 - \text{erf}(Z + Bi)] \quad (3-30)$$

with the dimensionless coordinate

$$Z = \frac{r}{2 \cdot \sqrt{a \cdot t_{WS}}} \quad (3-31)$$

and the Biot number

$$Bi = \frac{\alpha_{WS} \cdot \sqrt{t_{WS}}}{\sqrt{\lambda \cdot \rho \cdot c}} \quad (3-32)$$

where t_{WS} is the contact time between the rotating wall and the solid bed, and a is the thermal diffusivity of the wall. The symbols λ , ρ and c are the thermo-physical properties of the kiln wall. The contact time between the rotating wall and the solid depends on the rotation speed n and the filling angle ε along the solid bed

$$t_{WS} = \frac{l}{n} \cdot \frac{\varepsilon}{\pi} \quad (3-33)$$

The filling degree f is more commonly used than the filling angle ε . However, for the calculation, it is easier to use the filling angle. The relationship is as follows

$$f = \frac{A_{solid}}{A_{cycle}} = \frac{\frac{l}{2} \cdot R^2 \cdot (2 \cdot \varepsilon - \sin(2 \cdot \varepsilon))}{\pi \cdot R^2} \quad (3-34)$$

It can be written as follows

$$f = l/\pi \cdot (\varepsilon - \sin \varepsilon \cdot \cos \varepsilon) \quad (3-35)$$

The distribution of the temperature according to Eq. (3-30) is presented in Figure 3-11 for $Bi \rightarrow \infty$. The thickness of the lumped capacity layer Z_{lc} is assumed to store the same amount of heat as the total wall.

This results in

$$Z_{lc} = \int_0^{\infty} \left[1 - \frac{T(x) - T_S}{T_{S,0} - T_S}(Z) \right] dZ \quad (3-36)$$

It means that the above area of the temperature penetration in the wall is equal to the area of the lumped capacity layer with its constant temperature because of the infinite conductivity.

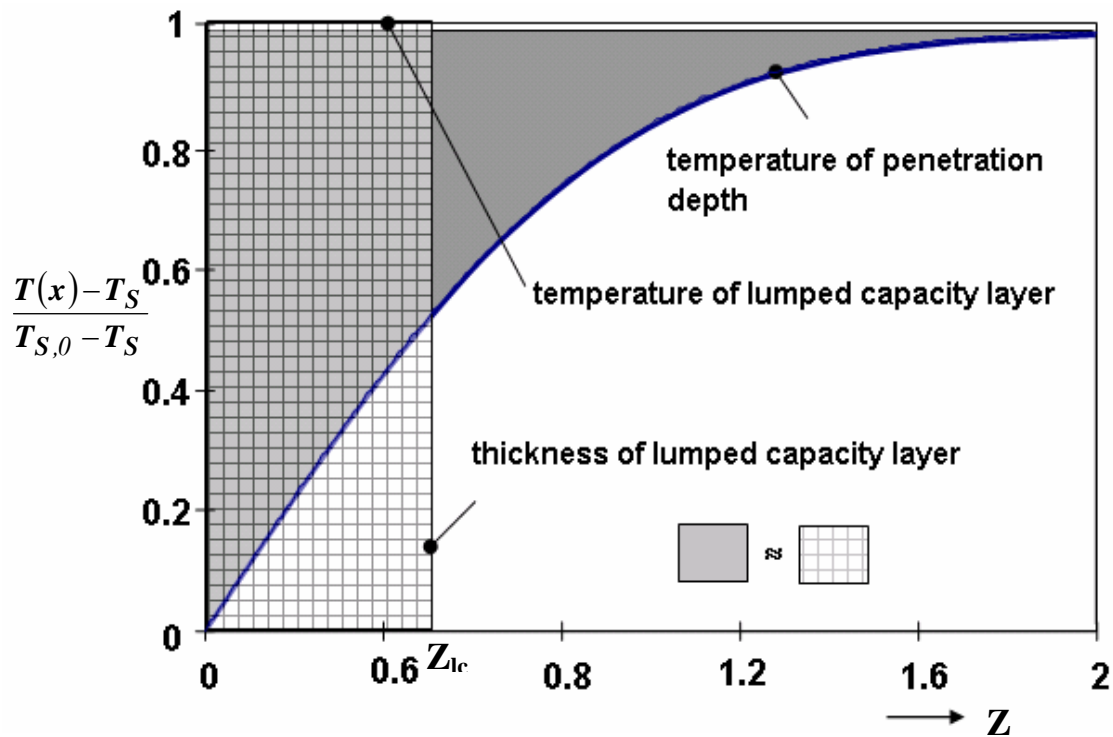


Figure 3-11. Definition of the lumped capacity layer

The integration depends only on the Biot number. A typical Biot number for rotary kilns is 1. Its value can be approximated by the correlation as shown in Figure 3-12.

$$Z_{lc} = 0.8l \cdot \ln(1 + 4 \cdot Bi) \quad (3-37)$$

for $Bi \leq 1$

Finally using Eqs. (3-31) and (3-33) the lumped capacity layer can be written as follows

$$s = Z_{lc} \cdot 2 \cdot \sqrt{a \cdot \frac{l}{n} \cdot \frac{\varepsilon}{\pi}} \quad (3-38)$$

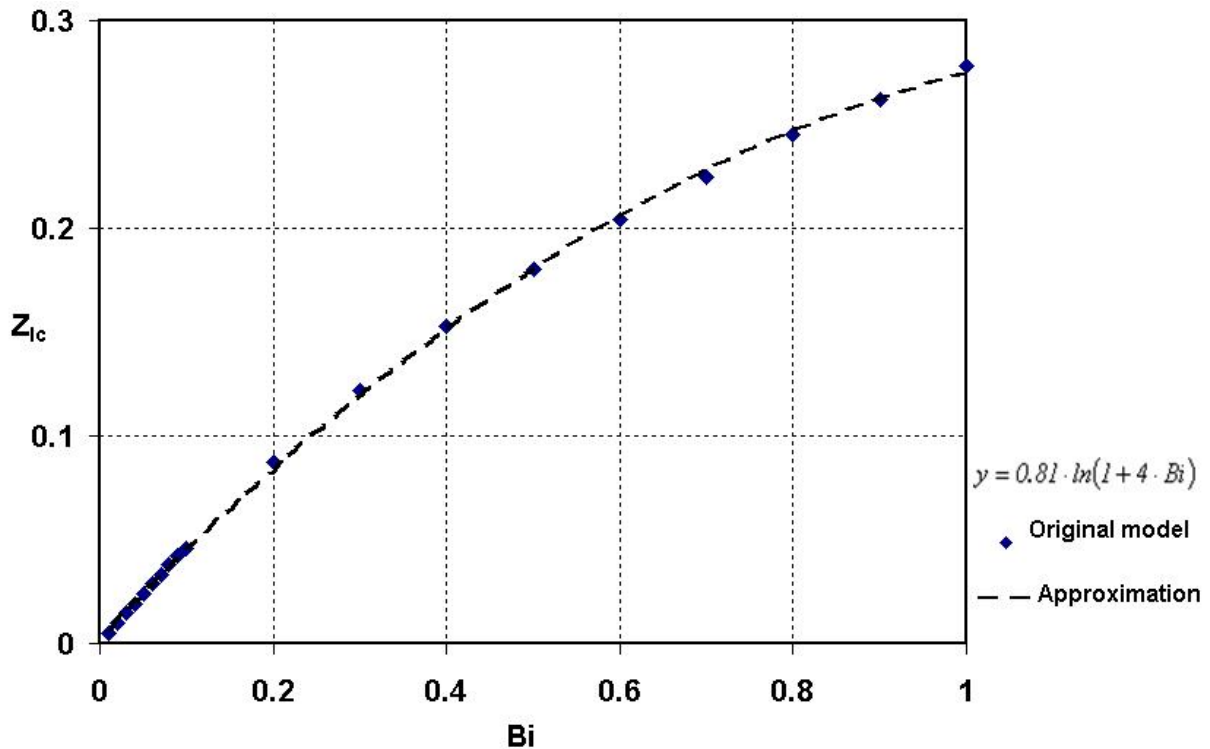


Figure 3-12. Determination of the lumped capacity layer

By replacing Z_{lc} with the Biot number according to Eq. (3-36) and the contact time by Eq. (3-33) we can see that this layer depends on the material properties of the kiln wall, the wall-to-solid heat transfer coefficient (α_{WS}), the rotation speed (n) and the filling angle (ε), and that it is independent of the kiln diameter.

Some examples for the thickness of this layer are shown in Figure 3-13. This thickness is much smaller than the penetration depth. A similar calculation is valid also for the lumped capacity layer in the contact region of gas-to-wall. This layer is a little bit larger than the wall-to-solid one because it also has to transport the heat loss. However, the wall-to-solid lumped capacity layer provides a better match to the numerical calculations.

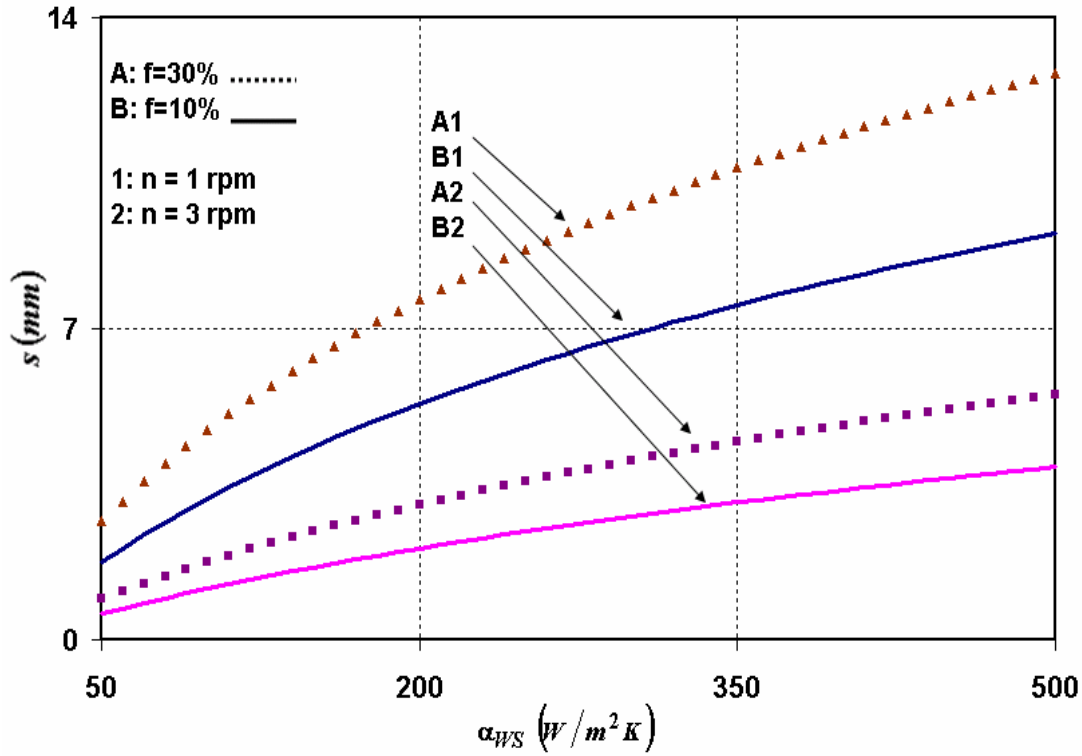


Figure 3-13. Thickness of the lumped capacity layer

3.3.4 Comparison of analytical and numerical results

In order to validate the assumptions that are made in the analytical model, we will compare this model with the numerical one. Therefore, the influencing parameters will be analyzed. It makes sense to introduce an overall regenerative heat transfer coefficient

$$\dot{Q}_R = \alpha_R \cdot L \cdot \varepsilon \cdot D \cdot (T_G - T_S) \quad (3-39)$$

The above equation, the regenerative heat flow is defined using the temperature difference between gas and solid and the area $L \cdot \varepsilon \cdot D$ of the contact solid-to-wall. From Eq. (3-27) we get for the overall heat transfer coefficient with respect to the heat transfer coefficient wall-to-solid

$$\frac{\alpha_R}{\alpha_{WS}} = \frac{(e^{-St_G} - 1) \cdot (e^{-St_G \cdot A} - 1)}{A \cdot St_G \cdot (1 - e^{-St_G} \cdot e^{-St_G \cdot A})} \quad (3-40)$$

This ratio depends only on two dimensionless parameters, Stanton number (St_G) and the heat resistance ratio (A). The effect of the influencing dimensional parameters can be shown as follows.

By replacing the two contact lengths according to Eqs. (3-26) and (3-26), the heat resistance ratio is replaced by

$$A = \frac{\alpha_{WS}}{\alpha_{GW}} \cdot \frac{\varepsilon}{\pi - \varepsilon} \quad (3-41)$$

According to Eqs. (3-20), (3-23), and (3-38), the Stanton number can be written as follows

$$St_G = \frac{\alpha_{GW}}{\pi \sqrt{\lambda \cdot \rho \cdot c \cdot n}} \cdot \sqrt{\frac{\pi}{\varepsilon}} \cdot \frac{l}{2} \cdot \frac{\pi - \varepsilon}{Z_{lc}(Bi)} \quad (3-42)$$

The wall-to-solid heat transfer coefficient is not included directly in the Stanton number, but it influences the lumped capacity layer (s) as it is utilized in Z_{lc} . From Eqs.(2-39) and (2-40) we get for the Biot number

$$Bi = \alpha_{WS} \frac{\sqrt{\varepsilon \cdot \pi}}{\pi \sqrt{\lambda \cdot \rho \cdot c \cdot n}} \quad (3-43)$$

These three dimensionless parameters show that the regenerative heat transfer is influenced by four dimensional parameters: the filling angle (ε), the heat transfer coefficient wall-to-solid (α_{WS}), the heat transfer coefficient gas-to-wall (α_{GW}), and the heat transfer coefficient

$$\alpha_T = \pi \cdot \sqrt{\lambda \cdot \rho \cdot c \cdot n} \quad (3-44)$$

This introduced new coefficient (unit of W/m^2K) is named here as the heat transportation coefficient. It should be emphasized here that the kiln diameter exerts no influence.

As a consequence, the overall heat transfer coefficient can be described as a series of three heat transfer resistances

$$\alpha_R \cdot L_{WS} \approx \frac{I}{\frac{I}{\alpha_{WS} \cdot L_{WS}} + \frac{I}{\alpha_{GW} \cdot L_{GW}} + \frac{I}{\alpha_T \cdot (L_{GW} + L_{WS})}} \quad (3-45)$$

By inserting Eqs. (3-22) and (3-23) into (3-45), we get for the overall heat transfer coefficient

$$\alpha_R \approx \frac{I}{\frac{I}{\alpha_{WS}} + \frac{I}{\alpha_{GW}} \cdot \frac{\varepsilon}{\pi - \varepsilon} + \frac{I}{\alpha_T} \cdot \frac{\varepsilon}{\pi}} \quad (3-46)$$

This simple correlation is important at an industrial level since the effort to solve the 2-dimensional problem can be omitted. The approximation matches with the analytical model with an error of only $\pm 1.7\%$ as shown in Figure 3-14 for two different gas-wall heat transfer coefficients.

The heat transportation coefficient (α_T) depends on the material properties of the wall. For typical refractory and rotational speeds around $n = 1 \sim 3rpm$, the heat transportation coefficient is in the range of $500 \sim 3000 W/m^2K$. as shown in Figure 3-15. These values are much higher than the other heat transfer coefficients. Thus, the overall heat transfer coefficient is mainly influence by α_{WS} and α_{GW} . On the basis of their numerical calculations, Gorog et al. 1982, reported that the operating parameters have only a slight influence on the regenerative heat transfer, which is in agreement with the analytical results.

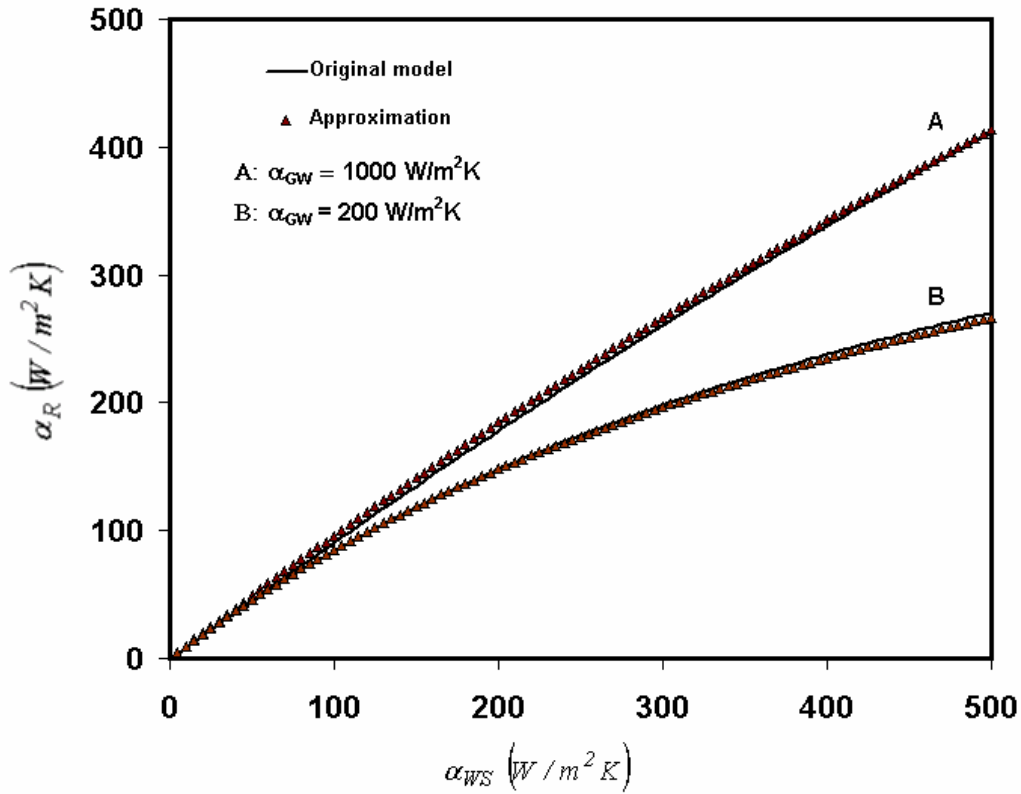


Figure 3-14. Approximation of the overall heat transfer coefficient

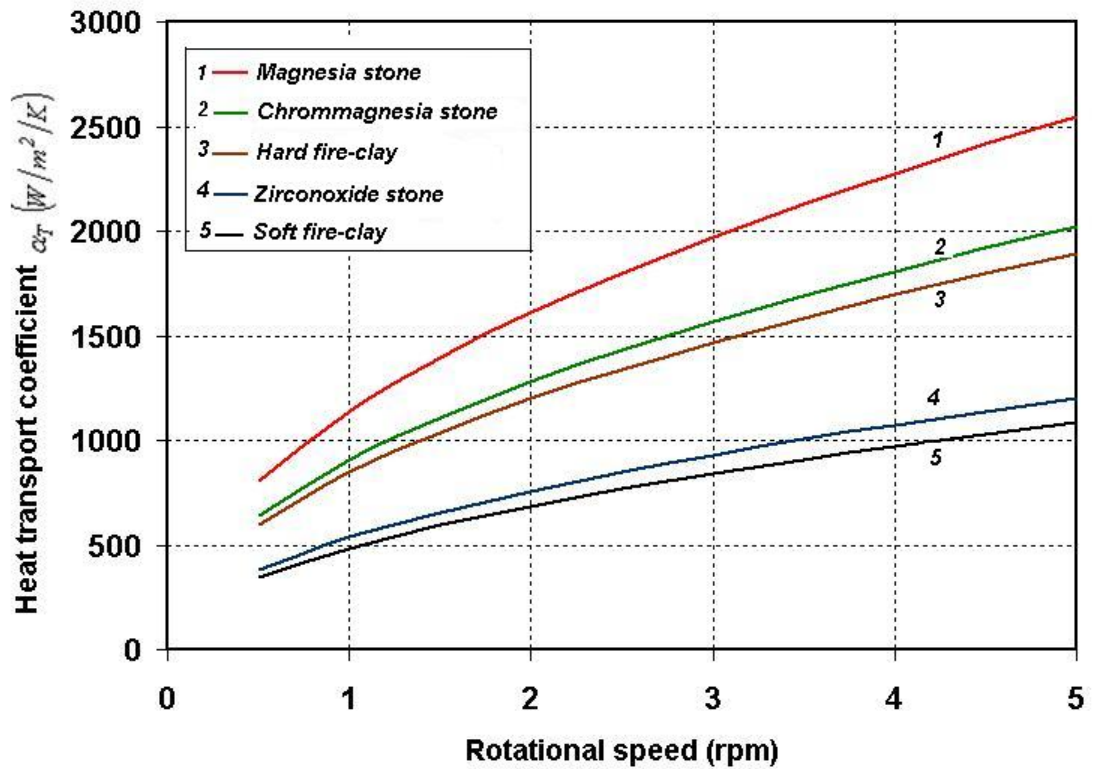


Figure 3-15. Heat transportation coefficient

Figure 3-16 shows the regenerative heat transfer coefficient as a function of the heat transfer coefficient wall-to-solid for four heat transfer coefficients gas-to-wall as parameters. The solid lines refer to the analytical calculations and the symbols represent numerically calculated values. These values are nearly the same for the lab-scale kiln 0.4 m ID and technical kiln 4 m ID. This confirms the results of the analytical model, namely that the diameter has no influence on the heat transfer. It can be observed that the deviations between numerically and analytically calculated heat transfer coefficients are less than 5%.

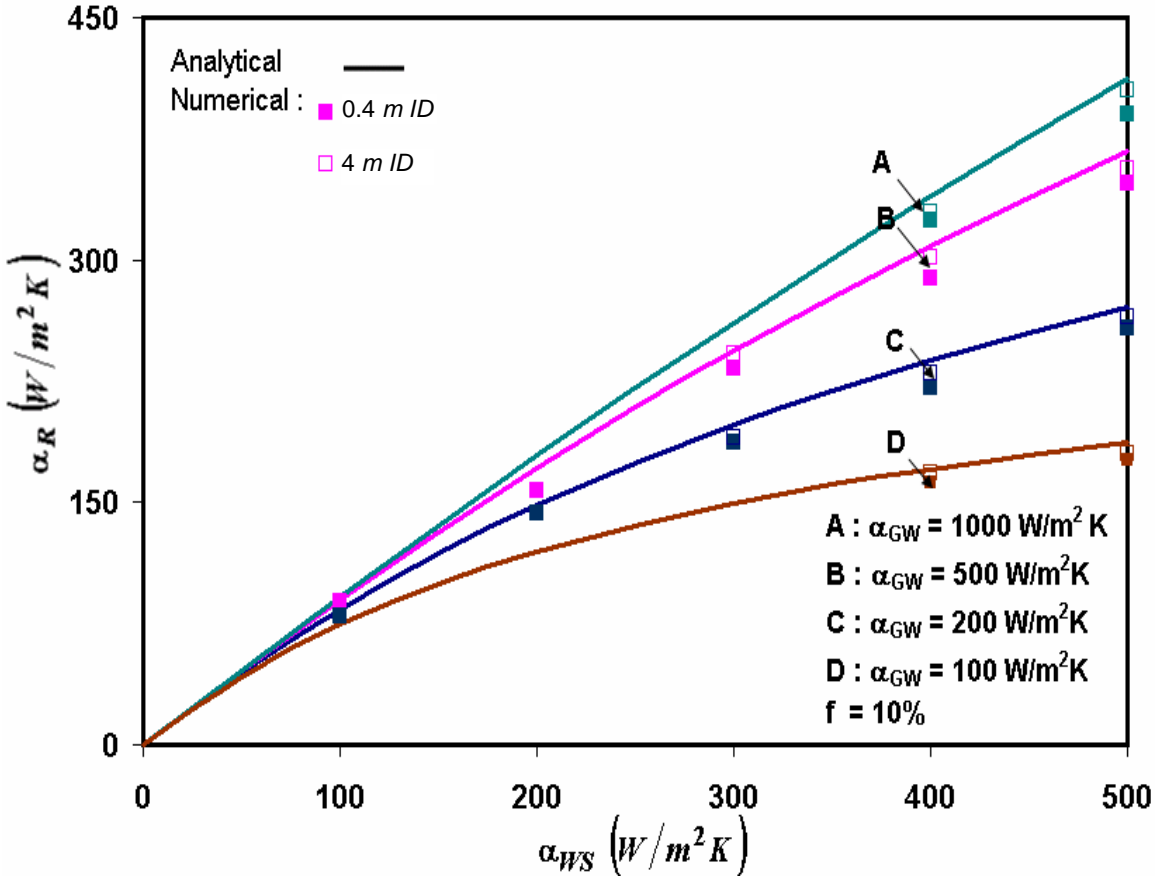


Figure 3-16. Comparison of numerical and analytical regenerative heat transfer coefficient

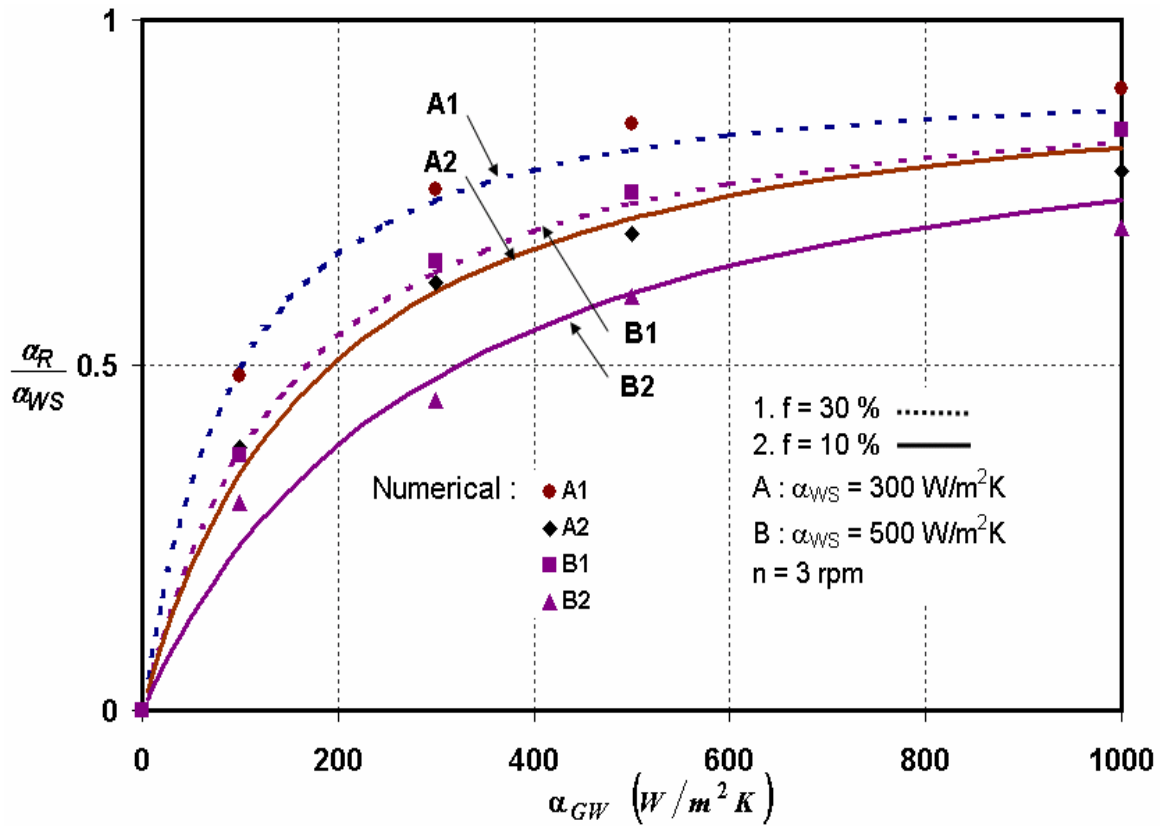


Figure 3-17. Influence of the gas-to-wall heat transfer coefficient on the regenerative heat transfer coefficient at various filling degrees

Numerically and analytically calculated values are also compared in Figure 3-17. Here the regenerative heat transfer coefficient is depicted as a function of the gas-to-wall heat transfer coefficient for two values of the wall-to-solid heat transfer coefficient and the filling degree. The deviations are again less than $\pm 5\%$. From the results obtained above we can conclude that the regenerative heat transfer model developed in this study is a proper approximation for the overall heat transfer by the wall.

This figure also shows that for higher values of the gas-to-wall heat transfer coefficient and the filling degree, α_R is about 80% of α_{WS} . In this case, the regenerative overall heat transfer is again mainly influenced by the wall-to-solid heat transfer. However, for low values of α_{GW} the coefficient α_R is much smaller than α_{WS} . In this case the overall heat transfer is mainly determined by the gas-to-wall heat transfer.

From the two figures above, the rate determining steps on the overall heat transfer can be discussed. The regenerative heat transfer coefficient is similar to the wall-to-solid heat transfer coefficient for low values of the wall-to-solid heat transfer coefficient (see Figure

3-16). This means that the wall-to-solid heat transfer is the rate determining step and the gas-to-wall heat transfer has a negligible influence.

3.3.5 Comparison of regenerative and direct heat flows

In order to consider the importance of the regenerative heat flow by the wall in a rotary kiln, the regenerative heat flow is compared with the direct heat flow from the gas to the solid. This heat is mainly transferred to the solid bed (\dot{Q}_{GS}) by radiation in industrial kilns. The heat flow depends on many parameters such as temperature and composition of the gas, etc. Thus, it is different for each kiln and process. Therefore, the heat flow is again linearized and approximated applying the law of convection as follows

$$\dot{Q}_D = \dot{Q}_{GS} = \alpha_{GS} \cdot L_{GS} \cdot (T_G - T_S) \quad (3-47)$$

where L_{GS} is the length of the bed surface

$$L_{GS} = D \cdot \sin \varepsilon \quad (3-48)$$

The heat transfer coefficient between gas and solid α_{GS} should be considered as a parameter as well as the other heat transfer coefficients. From Eqs. (3-27), (3-41), and (3-47), the ratio between the regenerative and the direct heat flow is as follows

$$\frac{\dot{Q}_R}{\dot{Q}_D} = \frac{\alpha_{GW}}{\alpha_{GS}} \cdot \frac{\pi - \varepsilon}{\sin \varepsilon} \cdot \frac{(e^{-St_G} - 1) \cdot (e^{-St_G \cdot A} - 1)}{St_G \cdot (1 - e^{-St_G} \cdot e^{-St_G \cdot A})} \quad (3-49)$$

From the above equations, we can see that the heat flow ratio is influenced only by two ratios of heat transfer coefficients and the filling angle

$$\frac{\dot{Q}_R}{\dot{Q}_D} = (\alpha_{WS}/\alpha_{GW}, \alpha_{GS}/\alpha_{GW}, \varepsilon) \quad (3-50)$$

The regenerative heat transportation coefficient (α_T) and the kiln diameter once again have no influence.

Figure 3-18 presents the ratio of the regenerative heat flow and the direct heat flow from the gas depending on the ratio of the heat transfer coefficients α_{WS}/α_{GW} with the ratio α_{GS}/α_{GW} as the parameter. The influence of \dot{Q}_R increases with α_{WS} and decreases with α_{GS} . The solid line refers to low filling degree and the dashed line refers to high filling degree. Increasing the filling degree from 0.01 to 0.03 increases the heat transfer contact area by a factor of 2 (see Figure 3-19).

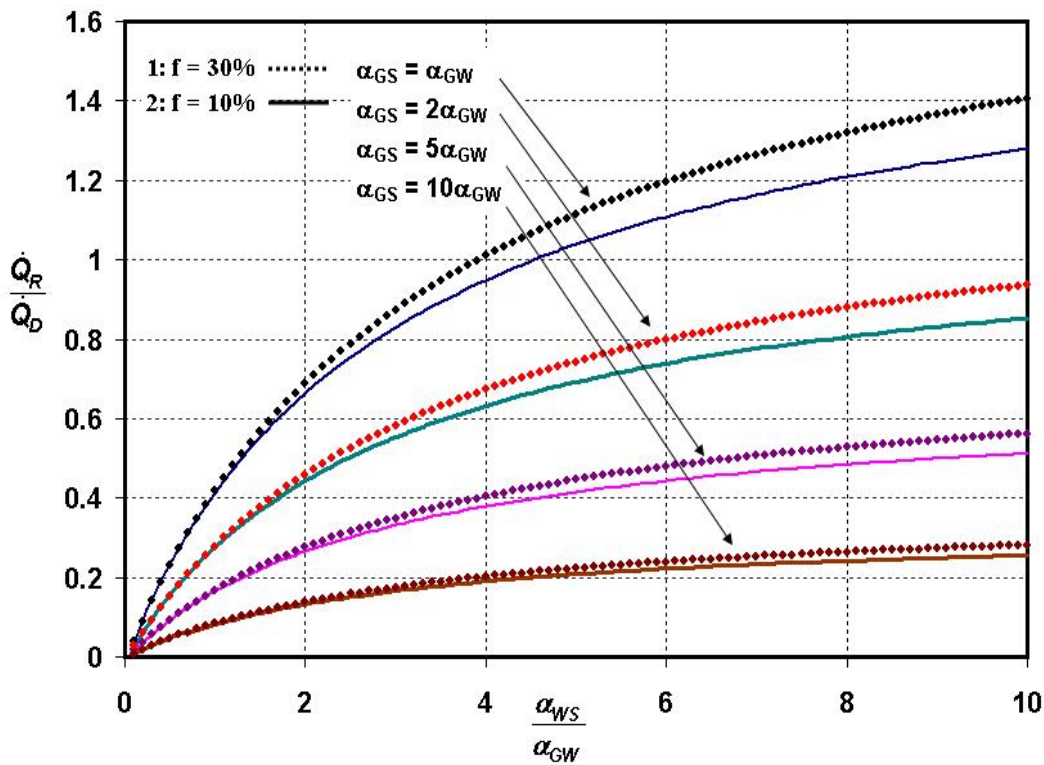


Figure 3-18. Comparison of regenerative heat transfer by the wall and direct heat transfer from the gas

Therefore, the heat transfers to the bed are higher at high filling degree. However, this effect is overcome with a high radiation effect at the freeboard gas. Thus, the filling angle ε has a relatively low influence at high radiative heat transfer coefficient. As the heat transfer coefficient from the gas-solid increases, the wall temperature decreases toward the solid

temperature. Thus, the regenerative heat flow decreases with radiative heat transfer coefficient. The exact values of the heat transfer coefficients are not very well known, as previously explained, and depend on a lot of operation and process parameters. Despite of this, we have attempted to give an application to the technical cases.

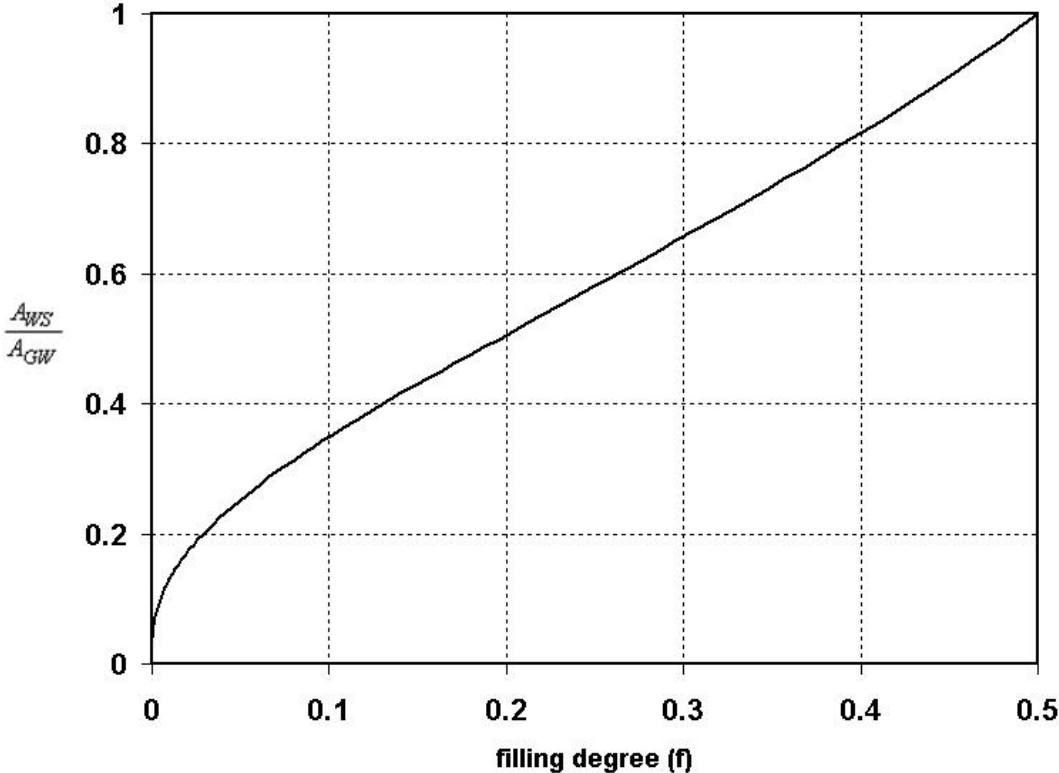


Figure 3-19. Area contact ratio versus filling degree in directly heated rotary kiln

Tscheng and Watkinson, 1979 and Barr et al., 1989 concluded from their experiments that the value of α_{GS} is 5 to 10 times higher than α_{GW} for the rolling motion. This type of motion is characterized by a high velocity and a high turbulence of the particle in the cascading layer. The heat transfer into the bed is mainly determined from this layer [Dhanjal, S.K., et al., 2004]. The heat transfer from the wall into the plug flow region has a relatively low influence because of the low conductivity of this region.

In industrial rotary kilns with large diameter, and thus high beam length and high gas temperature, the heat transfer coefficient gas-to-wall is higher than the heat transfer coefficient wall-to-solid or of the same magnitude $\alpha_{WS}/\alpha_{GW} < 1$. In this type of kiln, when the rolling motion occurs the ratio of the regenerative heat flow is only around 5-20%. Thus, the effect of the wall is relatively low with respect to the direct heat flow from the gas.

Moreover, in laboratory kilns with small kiln diameters and not such high temperatures, for example, the heat is mainly transferred by convection. The gas-to-wall heat transfer coefficient is much lower than the wall-to-solid heat transfer coefficient, therefore, the ratio of the heat transfer coefficients can be extended to 10 as reported by Tscheng and Watkinson, 1979. In this type of kiln with the rolling motion, the ratio of the regenerative heat flow can be in the range of 20-40%. In this case the effect of the wall cannot be neglected. In a slumping motion, the solid bed is continuously elevated and leveled off again and again by successive avalanches on the surface. Under this condition, the heat transfer to the bed surface is not so high and is expected to be in the range of 2 to 5 times higher than the heat transfer to the exposed wall. Under this type of motion, the influence of the wall is more dominant than in the rolling motion.

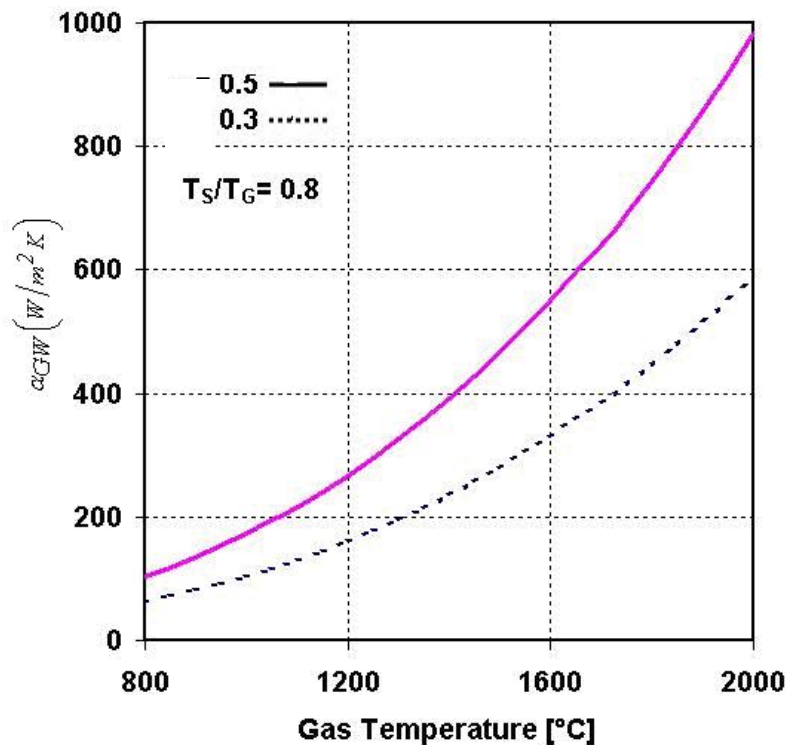


Figure 3-20. Influence of the gas temperature on the gas-to-wall heat transfer coefficients

The heat transfer from the gas to the wall is determined by radiation, therewith, depends strongly on the gas temperature as explained in Eq.(3-6). This profile is shown in Figure 3-20 for two gas emissivities. The dotted line refers to a low gas emissivity (clear kiln atmosphere) and the solid line presents a high gas emissivity (high concentration of dust, soot, ash, etc.). In the hot region of technical rotary kilns, the α_{GW} can reach the value of

$1000 \text{ W/m}^2\text{K}$ especially for higher gas emissivity. In the flue gas region of technical rotary kilns or in laboratory kilns with small kiln diameters the value of α_{GW} is around $50 \text{ W/m}^2\text{K}$.

In Figure 3-21 shows an example where the heat transfer ratio \dot{Q}_R/\dot{Q}_D is depicted as a function of the combustion gas temperature for $\alpha_{WS} = 100 \text{ W/m}^2\text{K}$. From the figure it is clear that the \dot{Q}_R decreases with an increase in the gas temperature. In the combustion region of technical rotary kilns, the temperature is estimated around $1500\text{-}2000^\circ\text{C}$. In this region, the ratio of regenerative heat flow is approximately less than 10%. The contribution of heat flow by the wall in this region is very small even in the slumping motion. In the flue gas region of technical rotary kilns or in laboratory kilns the maximum gas temperature is around 1000°C . Furthermore, by comparing the magnitudes of both the regenerative and direct heat transfer rates, the relative importance of regenerative heating may be established over a wide range of operating conditions.

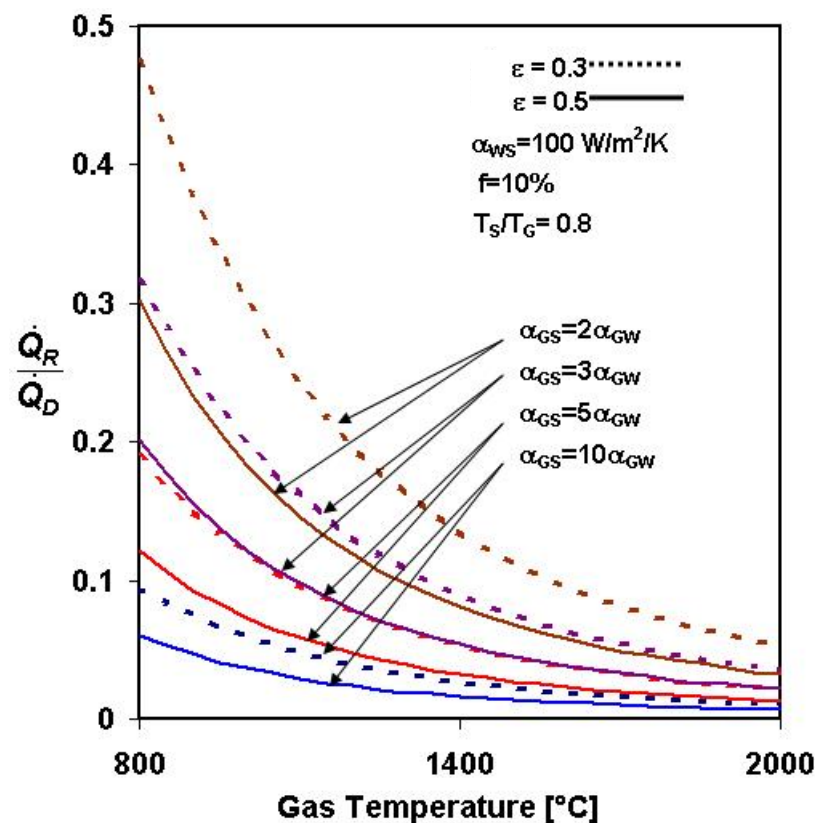


Figure 3-21. Influence of the gas temperature on the heat flow ratio

4 Regenerative action of the wall in an indirectly heated rotary kiln

4.1 Electrical heating

The studies to predict the heat transfer in the indirect rotary kiln with electrical heaters are relatively rare. Most of the previous studies are either focused on the experimental plants or to improve the final quality of the products. Marias et al., 2005 investigated a mathematical model for the pyrolysis of aluminium waste, but it has to be solved numerically with Matlab and Fluent. The goal of this study is to investigate a simplified analytical model with a simple kiln construction, therefore the impact of the parameters influencing the process are easy to understand. The previous model is extended to examine the relationship existing among the heat transfer processes at any kiln cross-section. The definition and approximate derivation of the thickness of a fictitious layer in the kiln wall is not necessary, the real wall thickness can be used instead.

4.1.1 Description of the model

The kiln wall plays a major role in the total amount of the heat transferred within the furnace. Indeed, it receives the thermal power released by the heating furnaces, stores the heat in the kiln wall and releases it towards the solid bed particles due to the rotation. The kiln is supposed to be a cylinder with inner diameter ID , of length L and of thickness s . There are 4 typical materials for the indirect heated kiln wall, the thermophysical properties are summarized in Table 4-1

Wall Material	λ (W/m^2K)	ρ (kg/m^3)	c (J/kgK)	Emissivity (ϵ)
Stainless Steel ($Fe-304$)	29	7530	640	0.2
SiC	40	2700	1650	0.8-0.9
Sapphire (Al_2O_3)	6	3600	1260	0.1
Graphite	20	1730	1920	0.7-0.85

Table 4-1. Thermophysical properties of indirectly heated rotary kiln wall at 1000°C (Mills, K.C, 2002, Touloukian et al. 1970)

As can be seen, the thermal conductivity of each material is low; therefore the wall temperature in any axial kiln position is essentially small. Thus, a cross-section model can be established over the length of the kiln as the basis for an overall heat transfer simulation.

The specific heat transfer paths occurring along the axial kiln and at a cross-section of a kiln are shown in Figure 4-1 and Figure 4.2, respectively; and described as follows:

- \dot{Q}_{el} the heat given from the heating furnace (electrical power dissipated into heat).
This value is assumed to be constant,
- \dot{Q}_{GS} the heat transfer between the kiln wall and the solid bed within the gas side,
- \dot{Q}_{WS} the heat transfer between the covered kiln wall and the solid bed.

The thermal conduction in the radial direction is assumed to be infinite; thus, the temperature in radial direction can be assumed to be constant (one dimensional problem). The gas in the rotary kiln is assumed to be inert; therefore, only heat transfer radiation considered is between uncovered kiln wall and solid bed (\dot{Q}_{GS}).

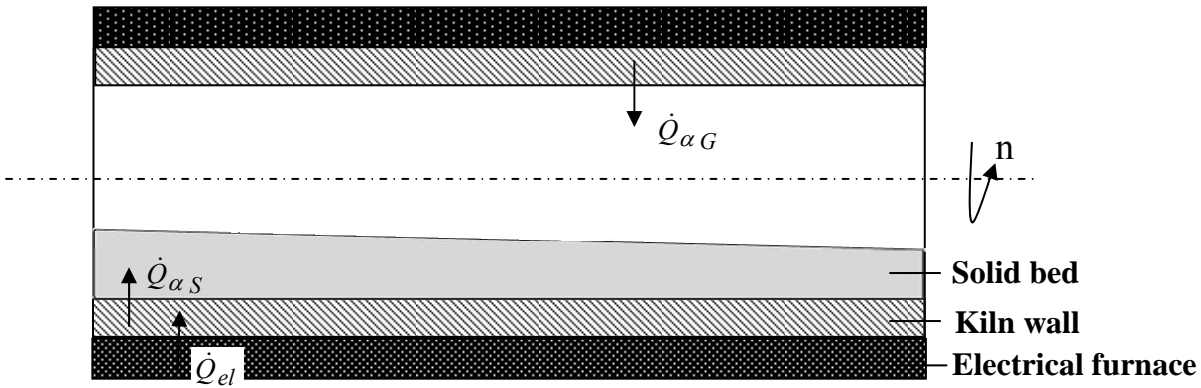


Figure 4-1. Schematic diagram of heat transfer path in an indirect rotary kiln

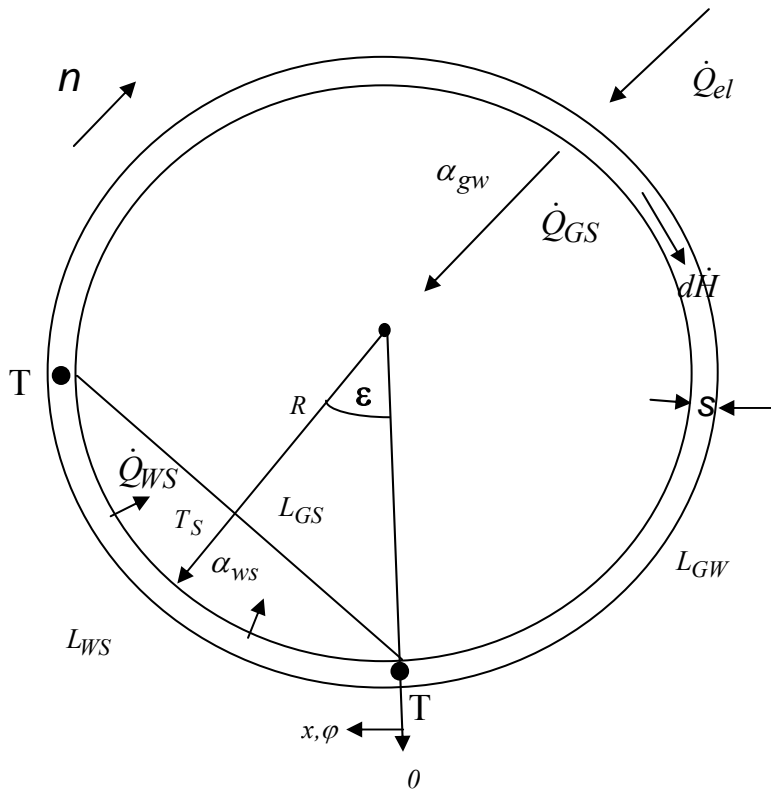


Figure 4-2. Cross sectional heat transfer of indirect rotary kiln

It is supposed that the total amount of electrical power received by the heaters is completely released as heat power and this heat is perfectly distributed over the circumference of the kiln.

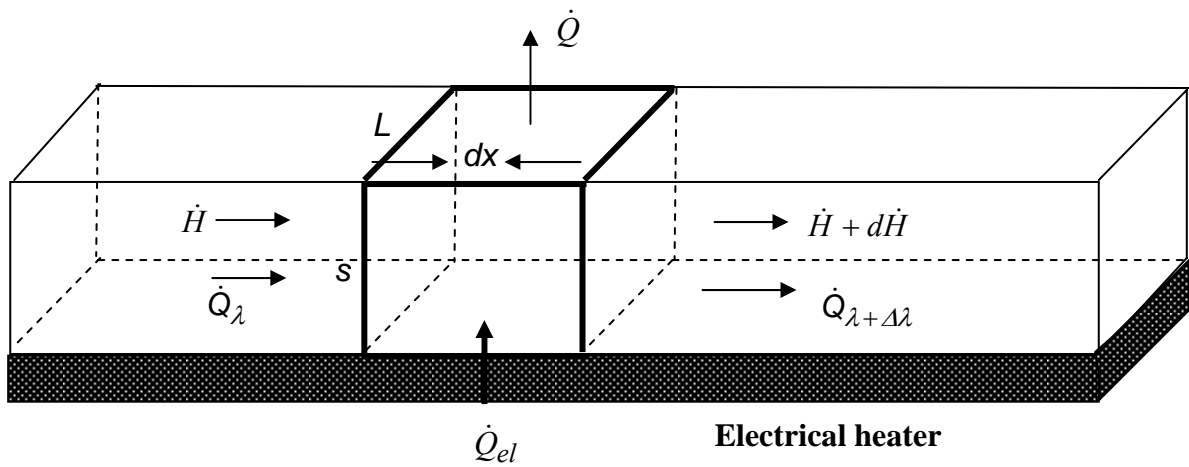


Figure 4-3. Heat flow through an extended kiln wall

The Fourier's law for an energy balance on an element thickness Δx of the kiln wall is described as follows (Figure 4-3)

$$\dot{Q}_\lambda + \dot{Q}_{el} + \dot{H} = \dot{Q}_{\lambda+\Delta\lambda} + (\dot{H} + d\dot{H}) + \dot{Q} \quad (4-1)$$

The rotational speed of a rotary kiln is high, the heat conduction is negligible.

$$\dot{H} + d\dot{H} = \dot{Q}_{el} - \dot{Q} \quad (4-2)$$

$$\dot{M} \cdot c \cdot dT = \dot{q}_{el} \cdot L \cdot R \cdot d\varphi - \alpha \cdot L \cdot R \cdot d\varphi \cdot (T - T_S) \quad (4-3)$$

Its velocity is assumed to be constant and can be set equal to the surface velocity

$$u = 2 \cdot \pi \cdot R \cdot n \quad (4-4)$$

Therefore the mass flow of the kiln wall because of the rotation is equal to

$$\dot{M} = u \cdot L \cdot s \cdot \rho \quad (4-5)$$

From Equations (4-3), (4-4) and (4-5) the heat balance is described as follows

$$\rho \cdot c \cdot u \cdot s \cdot dT = \dot{q}_{el} \cdot L \cdot R \cdot d\varphi - \alpha \cdot L \cdot R \cdot d\varphi \cdot (T - T_S) \quad (4-6)$$

For further calculation a circumferential coordinate is introduced

$$dx = R \cdot d\varphi \quad (4-7)$$

Therefore Equation (4-6) is reduced to

$$\rho \cdot c \cdot u \cdot s \cdot \frac{dT}{dx} = \dot{q}_{el} - \alpha \cdot (T - T_S) \quad (4-8)$$

The temperature distributions in the two regions are described with a lumped capacity model as follows:

wall-solid contact region

$$\rho \cdot c \cdot u \cdot s \cdot \frac{dT}{dx_S} = \dot{q}_{el} - \alpha_{WS} \cdot (T - T_S) \quad (4-9)$$

gas-wall contact region

$$\rho \cdot c \cdot u \cdot s \cdot \frac{dT}{dx_G} = \dot{q}_{el} - \alpha_{GS} \cdot (T - T_S) \quad (4-10)$$

where α_{WS} and α_{GS} are the heat transfer coefficients on the wall-solid and gas-solid regions, respectively. The heat from the wall to the solid bed is transferred mainly by radiation. However, as mentioned previously in Chapter 3 the radiation has to be linearized. As shown in Figure 3-9, the error because of the linearization is much smaller as the uncertainty of the heat transfer coefficient. The density and specific thermal capacity of the kiln wall are assumed to be constant because the temperature differences along the kiln wall are relatively small. This model is valid at any point along the kiln axis.

4.1.2 Temperature distribution

The kiln wall temperature can be calculated with lumped capacity model (integration of Equations (4-9) and (4-10))

$$T(x_S) - T_S = \frac{\dot{q}_{el}}{\alpha_{WS}} \left(1 - \exp\left(\frac{-\alpha_{WS}}{\rho \cdot c \cdot u \cdot s} \cdot x_S\right) \right) + (T_{S,0} - T_S) \cdot \exp\left(\frac{-\alpha_{WS}}{\rho \cdot c \cdot u \cdot s} \cdot x_S\right) \quad (4-11)$$

$$T(x_G) - T_S = \frac{\dot{q}_{el}}{\alpha_{GS}} \left(1 - \exp\left(\frac{-\alpha_{GS}}{\rho \cdot c \cdot u \cdot s} \cdot x_G\right) \right) + (T_{G,0} - T_S) \cdot \exp\left(\frac{-\alpha_{GS}}{\rho \cdot c \cdot u \cdot s} \cdot x_G\right) \quad (4-12)$$

The boundary condition for the initial temperatures $T_{S,0}$ and $T_{G,0}$ are obtained from the condition that the temperatures at the end of each region have to be equal to the inlet temperature of the other region

Solid region ($0 \leq x \leq L_{WS}$):

$$T_{S,0} = T1 \text{ and } T(x_G) = T2 \quad (4-13)$$

Gas side ($0 \leq x \leq L_{GW}$):

$$T_{G,0} = T2 \text{ and } T(x_G) = T1 \quad (4-14)$$

wall-solid contact region

$$T(x_S) = \frac{q_{el}}{\alpha_{WS}} \cdot \left[(1 - \exp(-St_S)) + \exp(-St_S) \cdot \left(\frac{\frac{\alpha_{WS}}{\alpha_{GS}} \cdot \left(\exp\left(-St_S \cdot \frac{l}{A}\right) - 1\right) + \exp\left(-St_S \cdot \frac{l}{A}\right) \cdot (\exp(-St_S) - 1)}{\exp\left(-St_S \cdot \frac{l}{A}\right) \cdot \exp(-St_S) - 1} \right) \right] + T_S \quad (4-15)$$

gas-wall contact region

$$T(x_G) = \frac{q_{el}}{\alpha_{GS}} \cdot \left[\left(1 - \exp\left(-St_S \cdot \frac{l}{A}\right) \right) + \exp\left(-St_S \cdot \frac{l}{A}\right) \cdot \left(\frac{\frac{\alpha_{WS}}{\alpha_{GS}} \cdot \exp(-St_S) \cdot \left(\exp\left(-St_S \cdot \frac{l}{A}\right) - 1\right) + (\exp(-St_S) - 1)}{\exp\left(-St_S \cdot \frac{l}{A}\right) \cdot \exp(-St_S) - 1} \right) \right] + T_S \quad (4-16)$$

where the Stanton number

$$St_S = \frac{\alpha_{WS}}{\rho \cdot c \cdot u} \cdot \frac{L_{WS}}{s} \quad (4-17)$$

and the heat resistance ratio

$$A = \frac{\alpha_{WS} \cdot L_{WS}}{\alpha_{GS} \cdot L_{GS}} \quad (4-18)$$

and

$$u = 2 \cdot \pi \cdot R \cdot n \quad (4-19)$$

The length can be replaced by the radius and the filling angle

$$L_{WS} = 2\varepsilon \cdot R \quad (4-20)$$

$$L_{GS} = 2 \cdot \sin(\varepsilon) \cdot R \quad (4-21)$$

The heat resistance ratio is reduce to

$$A = \frac{\alpha_{WS} \cdot \varepsilon}{\alpha_{GS} \cdot \sin(\varepsilon)} \quad (4-22)$$

A heat transportation coefficient is introduced here as

$$\alpha_n = \rho \cdot c \cdot n \cdot s \quad (4-23)$$

the Stanton number can be described by inserting Eqs. (4-23), and (4-20) into Eq.(4-17)

$$St_S = \frac{\alpha_{WS}}{\alpha_n} \cdot \frac{\varepsilon}{\pi} \quad (4-24)$$

Therefore the physical meaning of the Stanton number is the ratio of heat which is transferred from the wall to the heat which is transported by the wall.

If the heat transfer coefficients are the same ($\alpha_{WS} = \alpha_{GS}$), the kiln wall temperature has a constant value

$$T = \frac{\dot{q}_{el}}{\alpha_{WS}} + T_S \quad (4-25)$$

At low kiln wall temperature and low emissivity of kiln wall material (steel), the radiation heat transfer between wall and solid is relatively low. Sometimes there exists an opaque gas effect i.e. no radiation heat transfer. For the limiting case ($\alpha_{GS} = 0$) the long equations (4-15) and (4-16) are reduced to

$$T(x_S) = \frac{\dot{q}_{el}}{\alpha_{WS}} \cdot \left((1 - \exp(-St_S)) + \frac{\exp(-St_S) \cdot \left(-\frac{\alpha_{WS}}{\alpha_n} \cdot \frac{\sin(\varepsilon)}{\varepsilon} \cdot \frac{\varepsilon}{\pi} + \exp(-St_S) - 1 \right)}{\exp(-St_S) - 1} \right) + T_S \quad (4-26)$$

$$T(x_G) = \frac{\dot{q}_{el}}{\alpha_{WS}} \cdot \left(-\frac{\alpha_{WS}}{\alpha_n} \cdot \frac{\sin(\varepsilon)}{\varepsilon} \cdot \frac{\varepsilon}{\pi} + \frac{-\frac{\alpha_{WS}}{\alpha_n} \cdot \frac{\sin(\varepsilon)}{\varepsilon} \cdot \frac{\varepsilon}{\pi} \cdot \exp(-St_S) + \exp(-St_S) - 1}{\exp(-St_S) - 1} \right) + T_S \quad (4-27)$$

The dimensionless temperature is defined as the difference of kiln wall temperature to solid temperature related to the heat flux given and wall-solid heat transfer coefficient

$$\Theta = \frac{T - T_S}{\frac{\dot{q}_{el}}{\alpha_{WS}}} \quad (4-28)$$

The dimensionless temperature distribution at the solid region is defined by

$$\Theta_S = (1 - \exp(-St_S \cdot x_S)) + \exp(-St_S \cdot x_S) \cdot \left[\frac{\frac{\alpha_{WS}}{\alpha_{GS}} \left(\exp\left(-St_S \cdot \frac{1}{A}\right) - 1 \right) + \exp\left(-St_S \cdot \frac{1}{A}\right) \cdot (\exp(-St_S) - 1)}{\exp(-St_S) \cdot \exp\left(-St_S \cdot \frac{1}{A}\right) - 1} \right] \quad (4-29)$$

and at the gas region

$$\Theta_G = \frac{\alpha_{WS}}{\alpha_{GS}} \cdot \left(1 - \exp\left(-St_S \cdot \frac{I}{A} \cdot x_G\right) \right) + \exp\left(-St_S \cdot x_G \cdot \frac{I}{A}\right) \cdot \left[\frac{\frac{\alpha_{WS}}{\alpha_{GS}} \exp(-St_S) \left(\exp\left(-St_S \cdot \frac{I}{A}\right) - 1 \right) + (\exp(-St_S) - 1)}{\exp(-St_S) \cdot \exp\left(-St_S \cdot \frac{I}{A}\right) - 1} \right] \quad (4-30)$$

For a high rotational speed ($St_S = 0$), both regions have the same result

$$\Theta_S = \Theta_G = \Theta = \frac{1 + \frac{\varepsilon}{\sin(\varepsilon)}}{\frac{\alpha_{GS}}{\alpha_{WS}} + \frac{\varepsilon}{\sin(\varepsilon)}} \quad (4-31)$$

Figure 4-4 (a) shows that the difference of the kiln wall temperature to the solid bed temperature is compared for different heat transfer coefficients (kiln wall material is steel). The parameter estimation is for the same value of wall-solid and convective outer wall heat transfer coefficients. The level of the kiln inner wall temperature increases toward the outer wall temperature as the radiation heat transfer coefficient (α_{GS}) decreases.

The maximum inner wall temperature is reached when there is no radiation heat transfer from the wall ($\alpha_{WS}/\alpha_{GS} = \infty$), corresponding to Eqs. (4-26) and (4-27). In the circumferential direction, the wall temperature is cyclic due to the kiln rotation (see Figure 4-4 (b)). This figure is depicted at the ratio of heat transfer coefficient = 4 for various Stanton number. The kiln wall decreases as it immersed to the solid bed ($0^\circ \sim 90^\circ$) and increases again as it touches the gas region ($90^\circ \sim 360^\circ$). For a typical rotational speed $n = 1-3 \text{ rpm}$ i.e. Stanton number 0.03-0.01; the temperature differs only less than 1°K . At infinite rotational speed i.e. Stanton number is zero; the inner wall temperature is unchanged. Eqs. (4-18), (4-20), (4-24), and (4-30) show that the dimensionless kiln wall temperature distribution is influenced by the wall-to-solid heat transfer coefficient, gas-solid heat transfer coefficient, heat transportation coefficient, and filling angle. The kiln diameter has no influence to the temperature distribution.

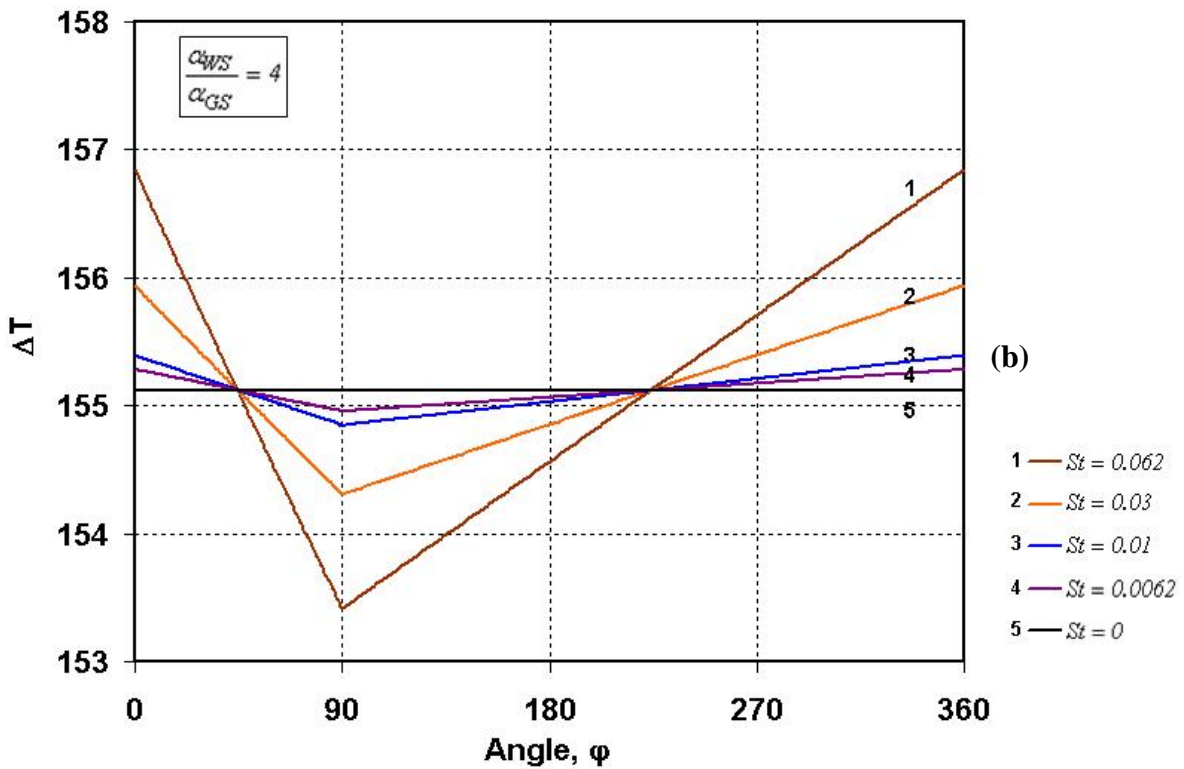
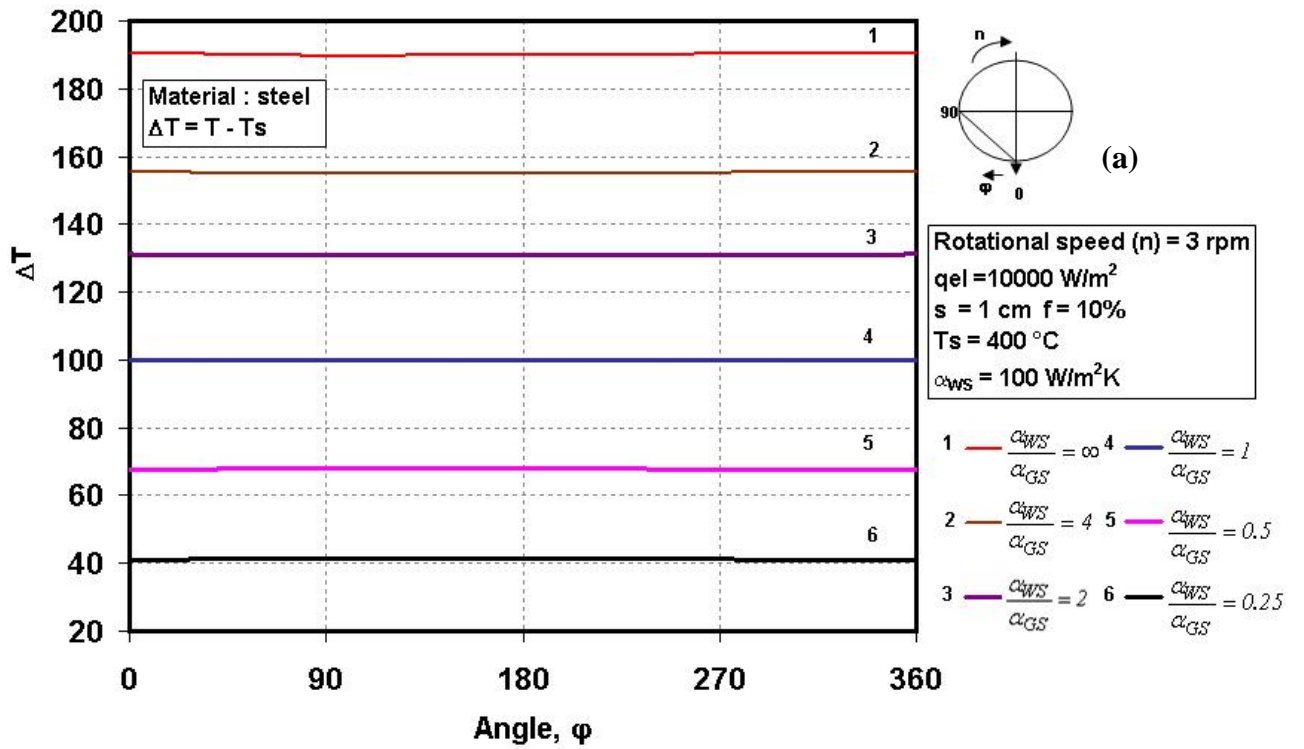


Figure 4-4. (a) Temperature distribution of kiln wall for different heat transfer coefficient
(b) Temperature distribution of kiln wall at ratio of heat transfer coefficient = 4

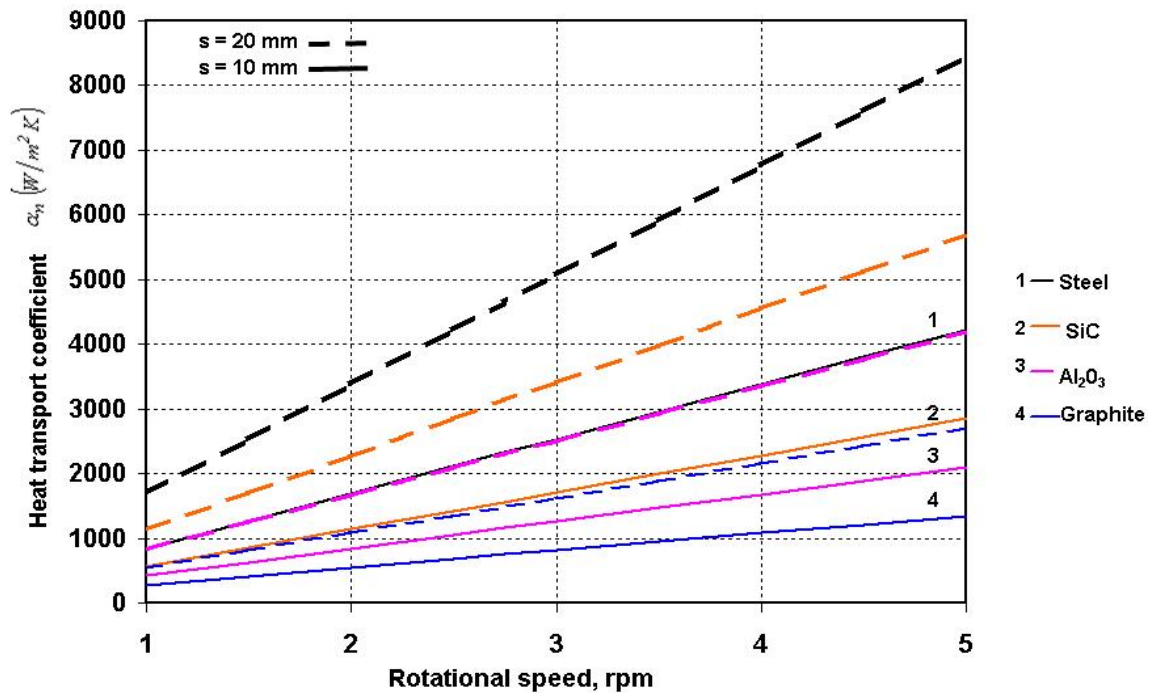


Figure 4-5. Heat transportation coefficient in indirectly heated rotary kiln with electrical heater

For the typical rotational speeds around $n = 1 \sim 3 \text{ rpm}$, the heat transportation coefficient is in the range of $300 \sim 5000 \text{ W/m}^2 \text{ K}$ (Figure 4-5). The solid line refers to the wall thickness of 1 cm and the spotted line refers to the wall thickness of 2 cm. The heat transportation coefficient increases with rotational speed and wall thickness. This value is mostly higher than the other heat transfer coefficient therefore the kiln speed has no significant influence to the kiln wall temperature distribution. The dimensionless temperature for various Stanton number are plotted in Figure 4-6 and Figure 4-7 under similar conditions as for the previous cases. These figures show that, for high wall-solid heat transfer coefficient in comparison with the radiation heat transfer coefficient the kiln wall decreases at the solid region and then increases at the gas region. Vice versa, the kiln wall temperature increases at the solid region and decreases at the gas region. For higher rotational speeds i.e. lower Stanton number, both the inner wall temperature and the difference between the maximum and minimum temperatures decreased.

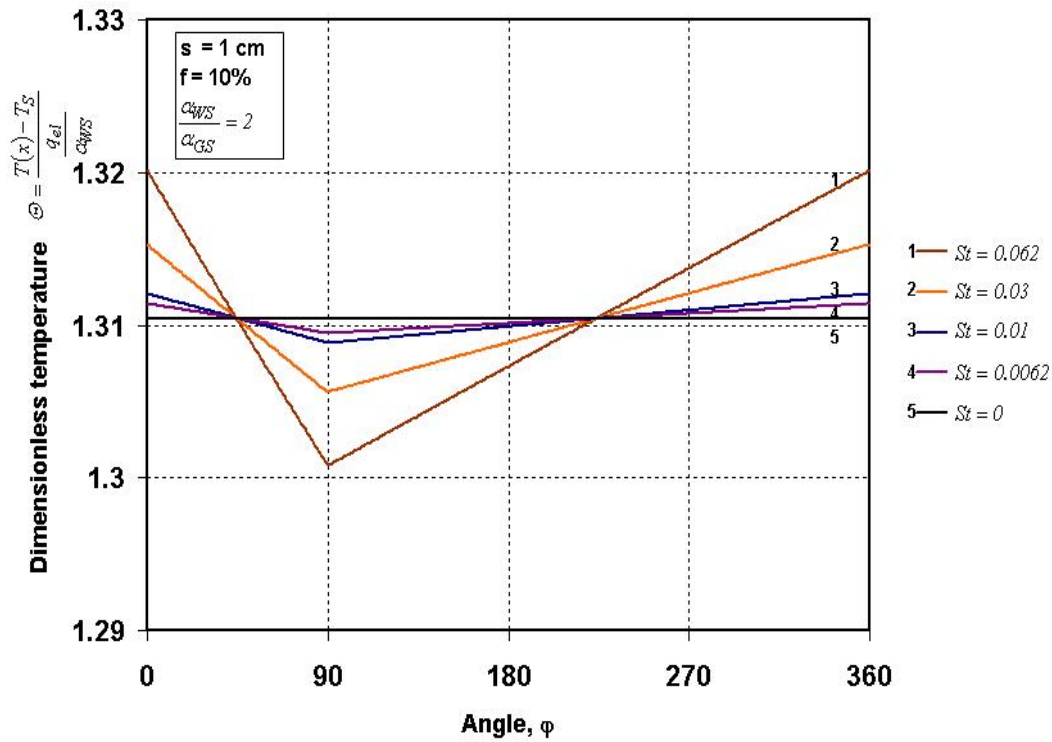


Figure 4-6. Temperature distribution of inner kiln wall at $\alpha_{WS}/\alpha_{GS} = 2$

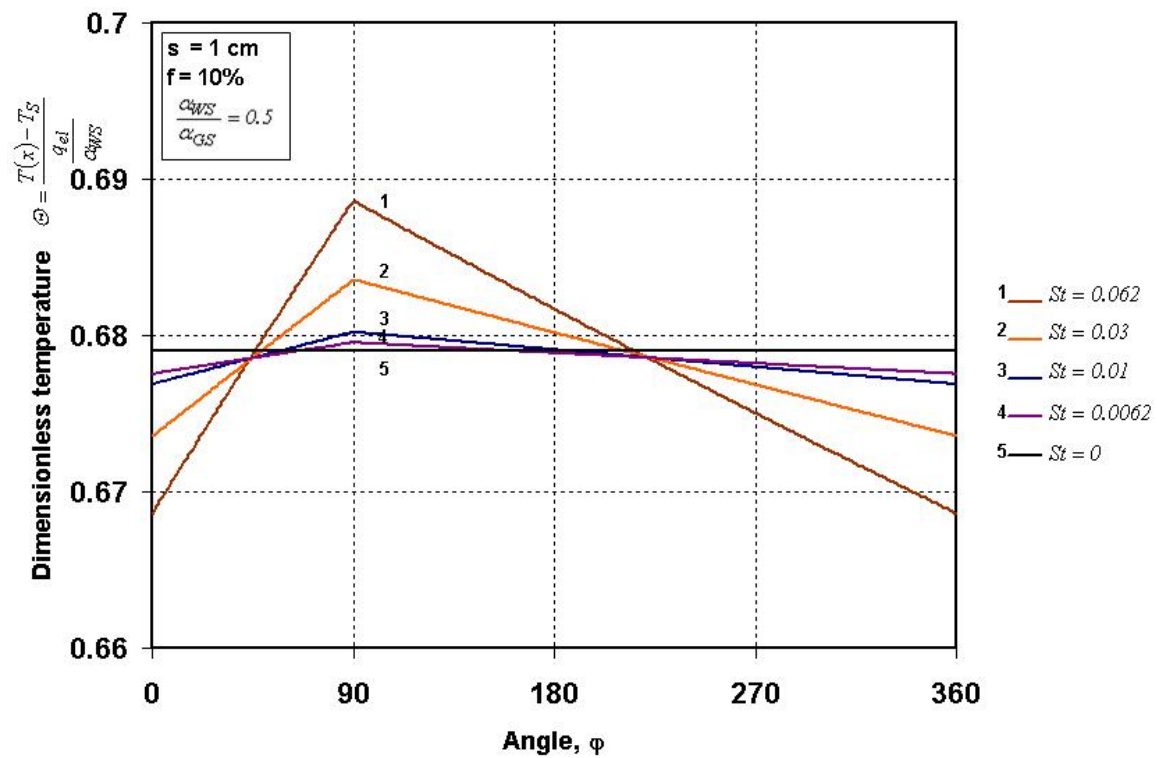
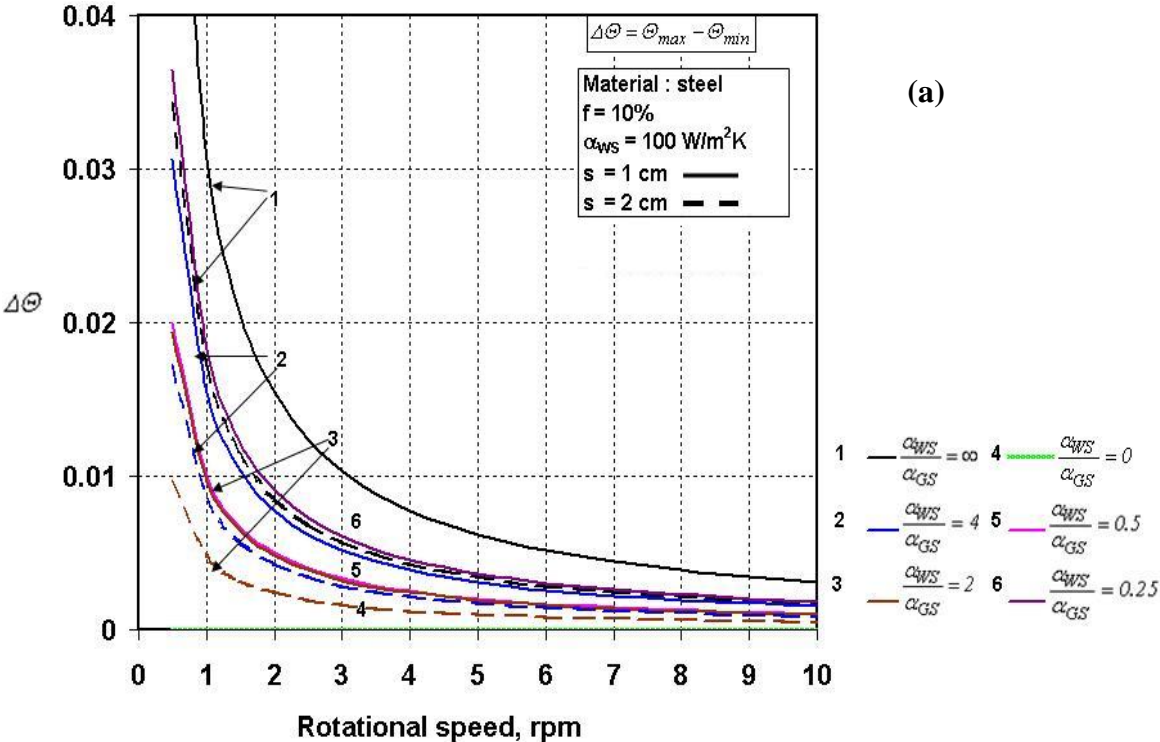


Figure 4-7. Temperature distribution of inner kiln wall at $\alpha_{WS}/\alpha_{GS} = 0.5$

Figure 4-8 (a-b) illustrates the dimensionless maximum temperature difference of the kiln wall temperatures for steel for two different filling degrees. The solid line represents the kiln wall thickness of 1 cm and the dotted line for 2 cm. The maximum and minimum inner wall temperature differences decrease with an increase of the wall thickness and the filling degree. At higher values of rotational speed, both the figures show that the temperature differences are low and can be neglected. At higher ratio of heat transfer coefficients (infinite) the temperature difference reaches to the higher value (no radiation heat transfer). However, as the radiation heat transfer coefficient increases both the inner wall temperature and its differences decrease. At the same magnitude of heat transfer coefficient the inner wall temperature remains constant according to Eq. (4-25). Furthermore, under some circumstances the radiative heat transfer coefficient can be higher than the wall-solid heat transfer coefficient. In this case, the temperature difference increases with the radiative coefficient in reverse direction.



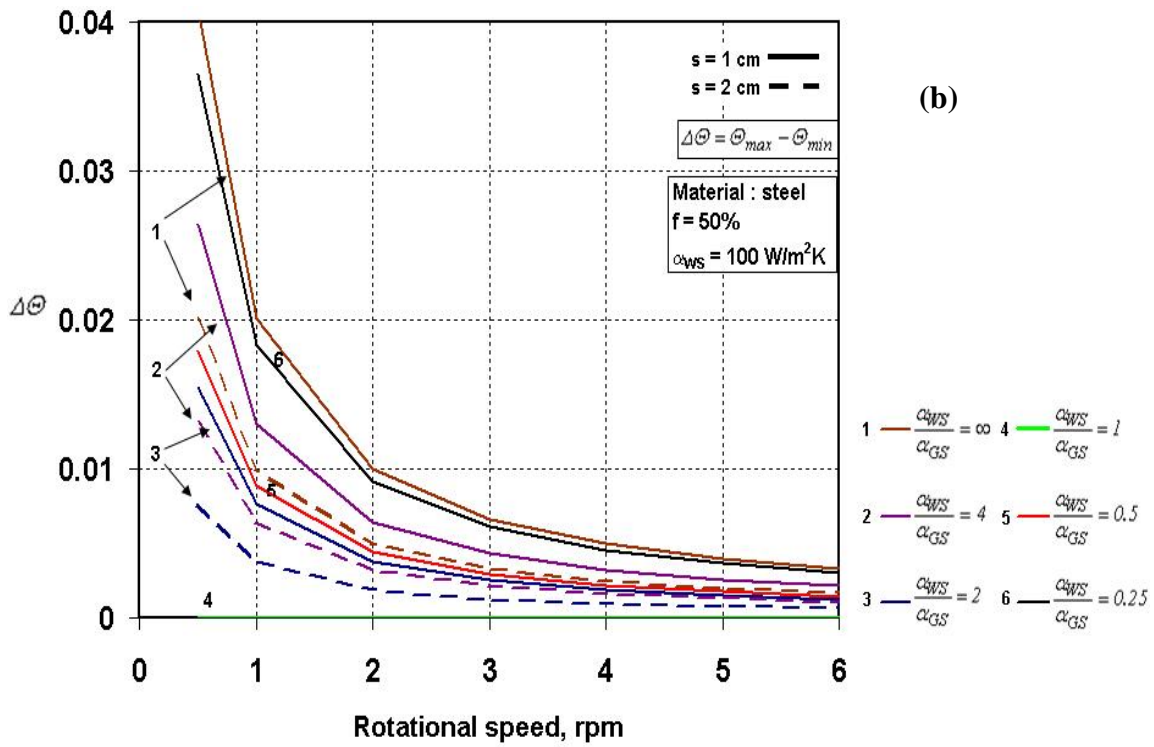
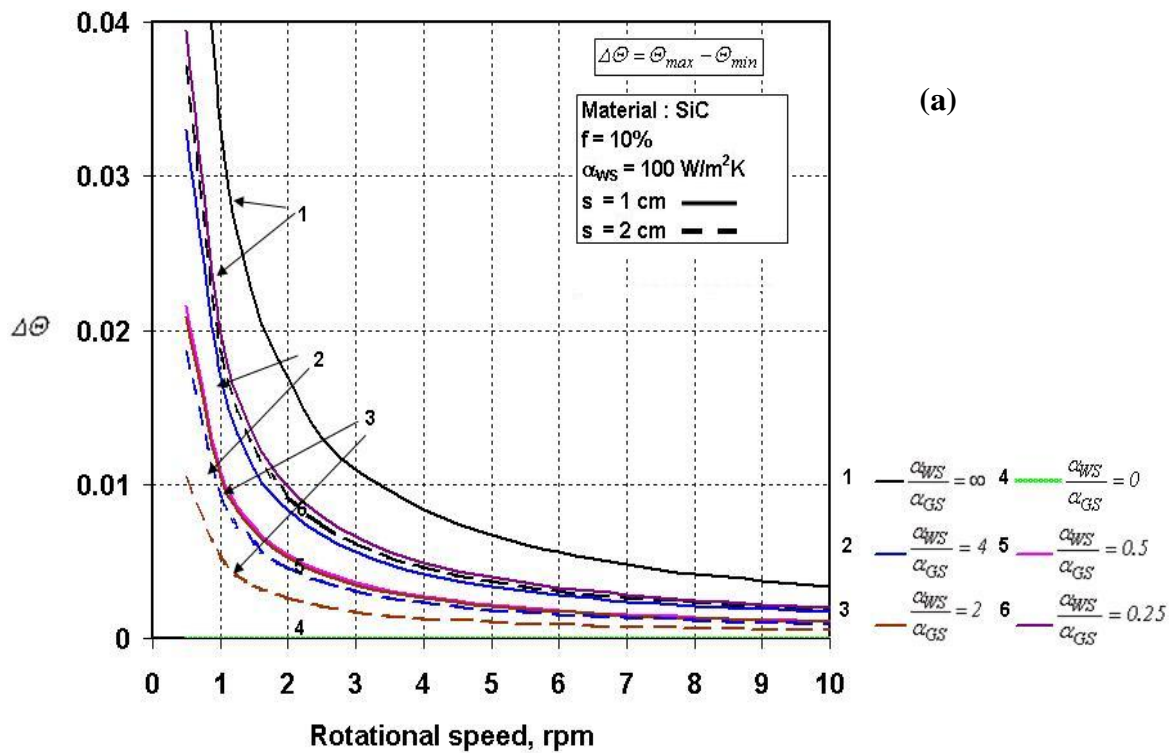


Figure 4-8. The maximum and minimum dimensionless temperature difference of the kiln wall for steel at various rotational speeds (a) filling degree 10% (b) filling degree 50%



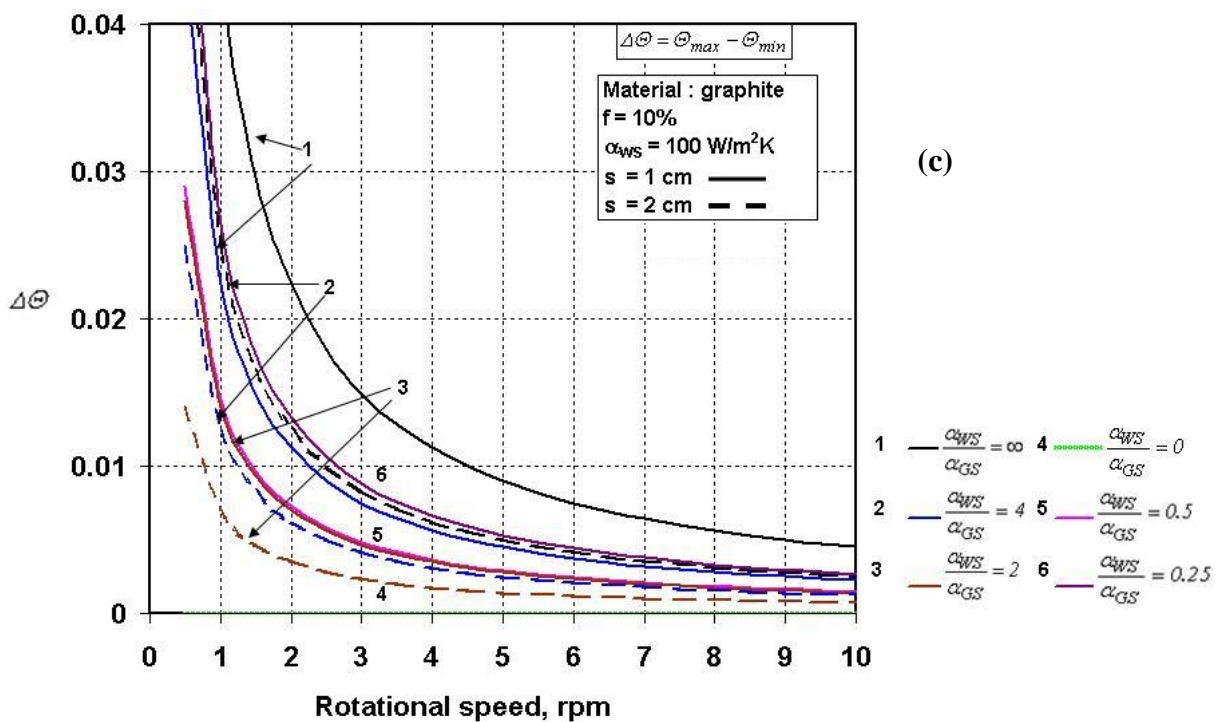
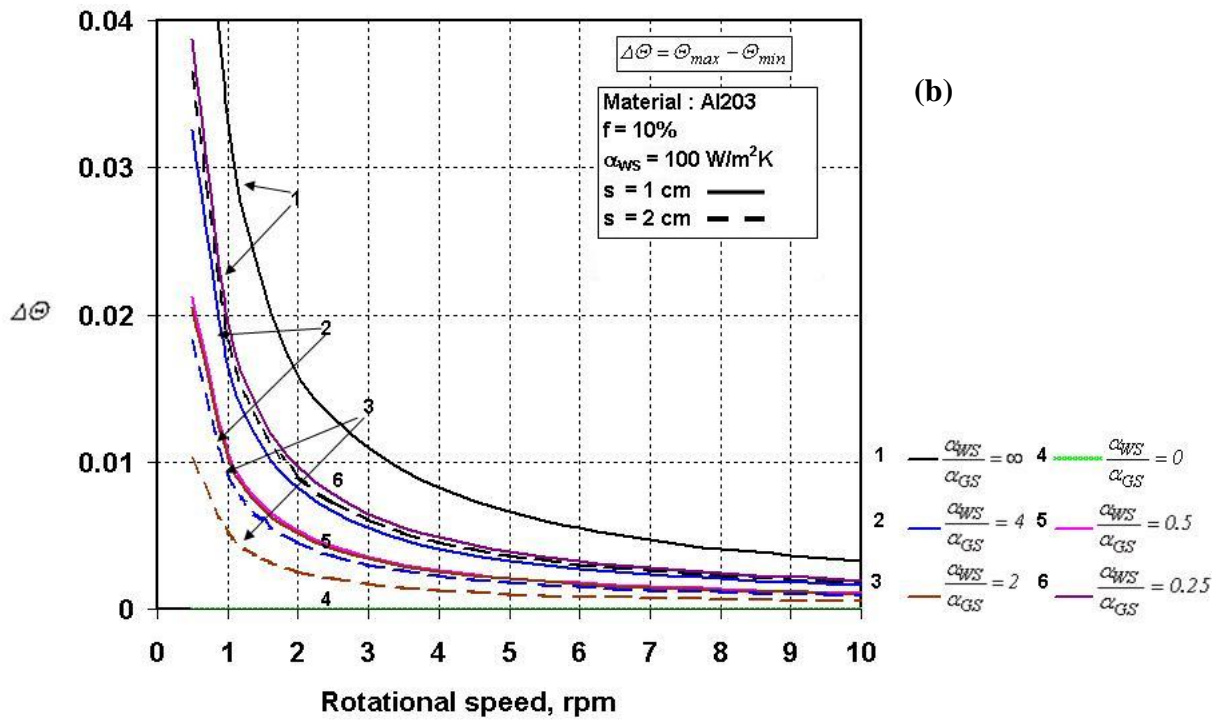


Figure 4-9. The maximum and minimum dimensionless temperature difference of the kiln wall some materials (a) SiC (b) Al₂O₃ (c) Graphite

Figure 4-9 (a-c) illustrates the dimensionless temperature difference of the inner wall other kiln wall materials at filling degree 10%. Increasing the kiln wall thickness from 1 to 2 *cm* decreases the wall temperature differences to 5%. At no radiation heat transfer coefficient, the inner wall temperature difference reaches to the larger value. The heat transfer coefficient ratios 2 and 0.5 have the same values but in reverse direction (according to Figure 4-6 and Figure 4-7). At typical rotational speed, Silicon Carbide (*SiC*) and Aluminium Oxide (*Al₂O₃*) have almost the same temperature profiles. However, graphite has the highest inner wall temperature difference in comparison to the other kiln wall materials. Nevertheless, at high rotational speeds all materials have the low temperature differences.

4.1.3 Heat flow

The amount of electrical power which is received from the heaters is released as heat power and distributed over the circumference of the kiln into two parts: covered wall-to-solid heat transfer (\dot{Q}_{WS}) and uncovered wall-to-solid heat flow (\dot{Q}_{GS}). A portion of this heat is lost to the surroundings. Therefore, it should be pointed out that the given electric heat flow (\dot{Q}_{el}) is the total electrical power supply received from the heaters minus the heat loss to the surroundings

$$\dot{Q}_{el} = \dot{Q}_{elT} - \dot{Q}_{elLOSS} \quad (4-32)$$

The heat flows per meter kiln length are obtained by

$$\frac{\dot{Q}_{WS}}{L} = \int_0^{L_{WS}} \alpha_{WS} \cdot (T(x_S) - T_S) \cdot dx_S \quad (4-33)$$

$$\frac{\dot{Q}_{GS}}{L} = \int_0^{L_{GS}} \alpha_{GS} \cdot (T(x_G) - T_S) \cdot dx_G \quad (4-34)$$

The integration from Eqs. (4-33) and (4-34)

$$\frac{\dot{Q}_{WS}}{L} = \frac{\dot{q}_{el}}{\alpha_{WS}} \left(L_{WS} \cdot \alpha_{WS} \cdot (\pi - \varepsilon) + \frac{L_{WS} \cdot \alpha_{WS}}{St_S} \cdot (1 - \exp(-St_S)) \cdot \left(\frac{(\alpha_{WS} - \alpha_{GS}) \cdot \left(\exp\left(-\frac{St_S}{A}\right) - 1\right)}{\alpha_{GS} \cdot \left(\exp(-St_S) \cdot \exp\left(-St_S \cdot \frac{1}{A}\right) - 1\right)} \right) \right) \right) \quad (4-35)$$

$$\frac{\dot{Q}_{GS}}{L} = \frac{\dot{q}_{el}}{\alpha_{WS}} \left(L_{GS} \cdot \alpha_{WS} \cdot (\pi - \varepsilon) + \frac{L_{WS} \cdot \alpha_{WS}}{St_S} \cdot \left(1 - \exp\left(-St_S \cdot \frac{1}{A}\right) \right) \cdot \left(\frac{(\alpha_{GS} - \alpha_{WS}) \cdot (\exp(-St_S) - 1)}{\alpha_{GS} \cdot \left(\exp(-St_S) \cdot \exp\left(-St_S \cdot \frac{1}{A}\right) - 1\right)} \right) \right) \right) \quad (4-36)$$

The total amount of heat flow to the solid is equal to the electric heat flow to the kiln

$$\frac{\dot{Q}_{el}}{L} = \frac{\dot{Q}_{WS}}{L} + \frac{\dot{Q}_{GS}}{L} \quad (4-37)$$

$$\frac{\dot{Q}_{el}}{L} = \dot{q}_{el} \cdot \pi \cdot D_i \quad (4-38)$$

At infinite rotational speed ($St_S = 0$), Eqs. (4-35) and (4-34) are reduced to

$$\frac{\dot{Q}_{WS}}{L} = \frac{\dot{q}_{el}}{\alpha_{WS}} \left(L_{WS} \cdot \alpha_{WS} \cdot (\pi - \varepsilon) + L_{WS} \cdot \alpha_{WS} \cdot \left(\frac{\alpha_{WS} - \alpha_{GS}}{\alpha_{GS} \cdot \left(1 + \frac{\alpha_{WS} \cdot \varepsilon}{\alpha_{GS} \cdot \sin(\varepsilon)} \right)} \right) \right) \right) \quad (4-39)$$

$$\frac{\dot{Q}_{GS}}{L} = \frac{\dot{q}_{el}}{\alpha_{WS}} \left(L_{GS} \cdot \alpha_{WS} \cdot (\pi - \varepsilon) + L_{WS} \cdot \alpha_{WS} \cdot \left(\frac{\alpha_{GS} - \alpha_{WS}}{\alpha_{GS} \cdot \left(1 + \frac{\alpha_{WS} \cdot \varepsilon}{\alpha_{GS} \cdot \sin(\varepsilon)} \right)} \right) \right) \right) \quad (4-40)$$

In Figure 4-10 the heat flow ratios are plotted against the heat transfer coefficient ratios. The figure shows that the infinite rotational speed ($St_S = 0$) has the same value as the other typical rotational speed ($n = 3 \text{ rpm}; St = 0.01$) and $n = 0.5 \text{ rpm}; St = 0.3$. Nevertheless, the value changes if the rotational speed is very low ($n = 0.05 \text{ rpm}; St = 2.9$) that never exists in any indirect rotary kiln. Therefore, the analytical solution for the heat flow to the solid bed can be further simplified with the equations of the infinite rotational speed Eqs. (4-39) and (4-40). Until this point it must be emphasized that changing the kiln speed does not alter the heat transfer conditions significantly, but it does strongly affect the residence time of the solids and hence overall kiln performance. This aspect of rotary kiln behaviour is beyond the scope of this work.

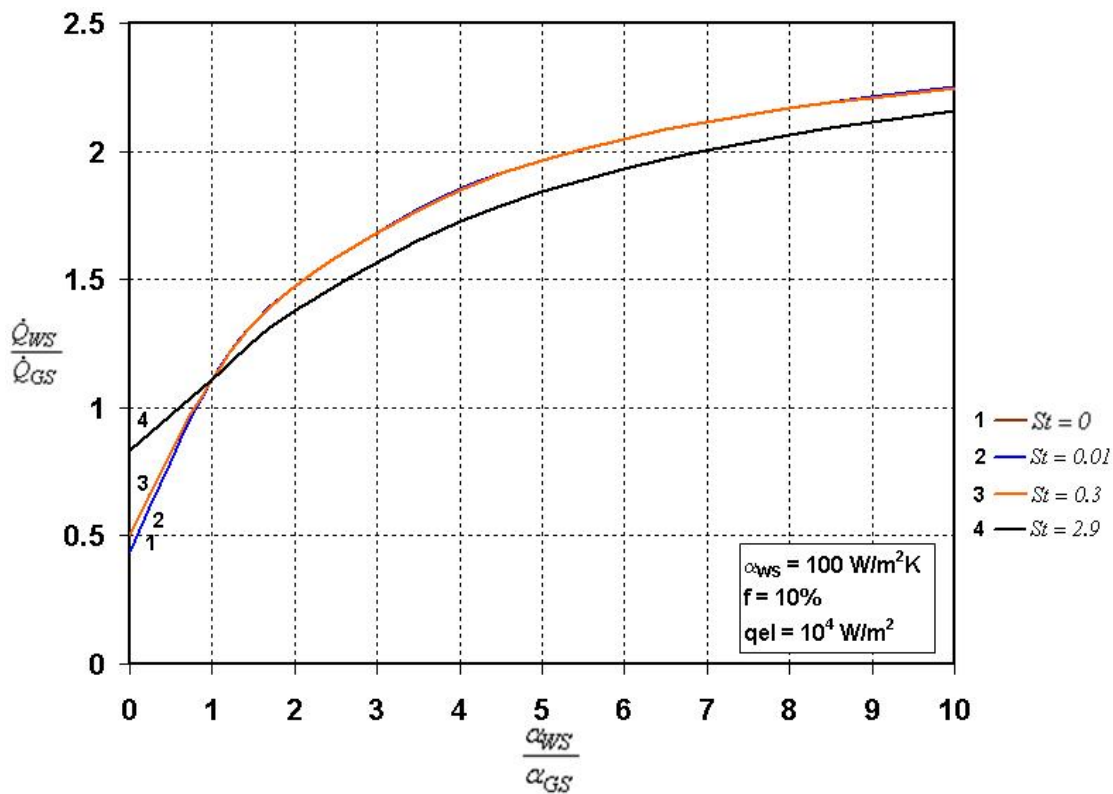


Figure 4-10. The ratio of heat flow in dependence to the ratio of heat transfer coefficient

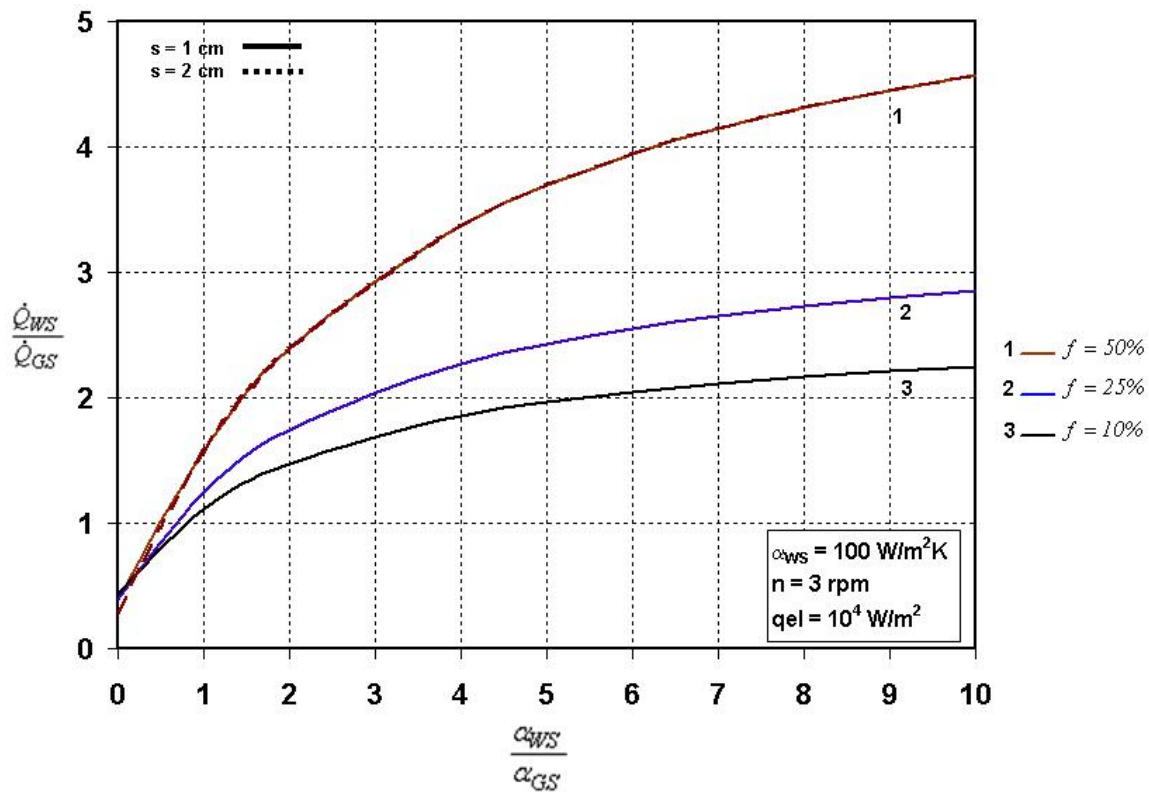


Figure 4-11. The ratio of heat flow for various filling degree

Figure 4-11 illustrates the heat flow ratios in dependence to the heat transfer coefficient ratios for different values of filling degree. The solid lines represent the thin wall and the dotted lines for thick wall, but the difference in this example is very low. The heat flow from wall to solid increases with α_{WS} and decreases with α_{GS} . At $\alpha_{WS}/\alpha_{GS} = 1$ and a lower value of filling degree, both types of the heat flow have almost the same value $\dot{Q}_{WS}/\dot{Q}_{GS} = 1.2$. This effect is caused by the fact that the inner wall temperature is constant and the area available for the heat transfer, at both the covered wall and exposed solid surface, is also the same (refer to Figure 4-12). Nevertheless, at the same magnitude of heat transfer coefficients the regenerative heat transfer (\dot{Q}_{WS}) is 50-60% in comparison to the overall heat transfer to the solid bed. At a value of α_{WS} is 10 times higher than α_{GS} at high filling degree, the heat flow from the wall to solid is almost 5 times higher than the direct heat flow from gas to solid.

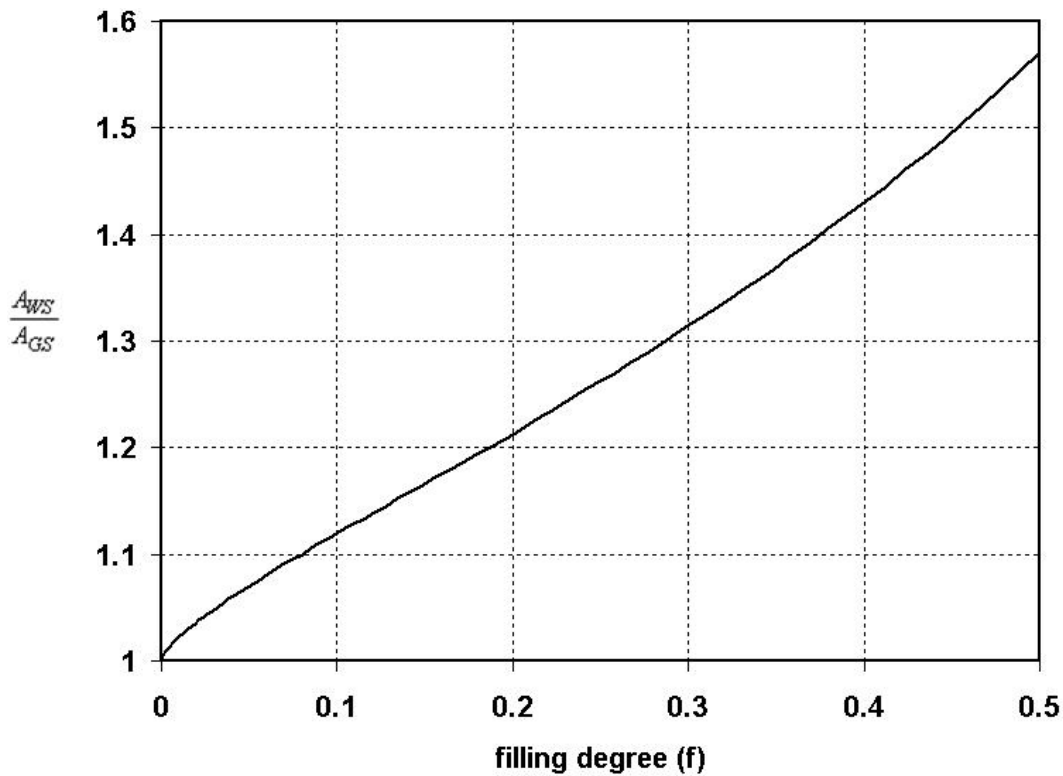


Figure 4-12. Area contact ratio versus filling degree in indirectly heated rotary kiln

4.2 Gas heating

In the manufacturing process of food and meals, the indirect rotary kilns with gas heating are widely used. The heating sources can be the combustion gas or steam jacket. However, the combustion gases usually exist at higher temperature (800°C), whereas the product induced a series of deterioration reactions that affects the final quality of the product. Thus, some countries are restricting the use of indirect heating with combustion gases for certain nutritional products (Wilkes et al., 1991). The advantage of this kiln is that it yields better product quality, reduces atmospheric contamination and decreases energy costs, by using water vapour from the drier itself as a steam source.

The objective of this work is to model the heat and energy balances for an indirect pilot plant rotary kiln with combustion gas or steam jacket, in order to obtain a simplified analytical model for the kiln.

4.2.1 Model Description

As mentioned previously in the chapter 4.1, the kiln wall has a significant influence on the heat transfer in the indirect heating rotary kiln. The typical materials for the kiln wall are already shown previously in Table 4.1 except graphite, since it is used only for the electrical furnaces. The steady state analytical model is based on the following assumptions: the thermal conduction in the radial direction is assumed to be infinite whereas at circumference is zero. Solid particles are of uniform size. There is no heat loss to the surroundings. There is only air present in the interior of the kiln (inert gas), thus there is no heat transfer from the gas to the kiln or to the solid bed. There is no evaporation of water from the solids. The heat transfer steps are shown previously in Figure 4-13.

In this system we use the same heat flow as in chapter 4.1, the difference is that the given heat flow comes from the hot combustion gas/steam jacket (\dot{Q}_0) instead of the electrical heaters (\dot{Q}_{el}). In order to simplify the modelling of the process, the heat transfer coefficients are divided into two parts: an effective conduction parameter and a single parameter.

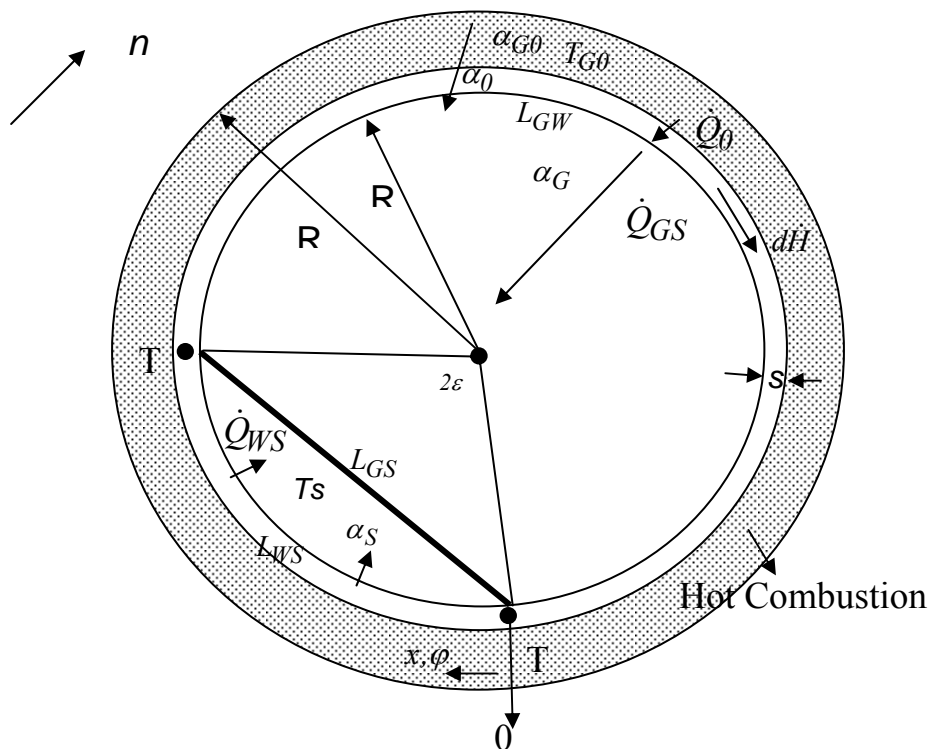


Figure 4-13. Indirectly heated rotary kiln with combustion gas or steam jacket

The effective parameters are described as follows:

- α_0 the heat transfer coefficient from the gas through the kiln wall

$$\frac{1}{\alpha_0} = \frac{1}{\alpha_{G0}} + \frac{s}{\lambda} \quad (4-41)$$

- α_G the heat transfer coefficient from the gas through the kiln wall to the solid bed surface

$$\frac{1}{\alpha_G} = \frac{1}{\alpha_{G0}} + \frac{s}{\lambda} + \frac{1}{\alpha_{GS}} \quad (4-42)$$

- α_S the heat transfer coefficient from the gas through the kiln wall to the covered solid bed

$$\frac{1}{\alpha_S} = \frac{1}{\alpha_{G0}} + \frac{s}{\lambda} + \frac{1}{\alpha_{WS}} \quad (4-43)$$

Because $\frac{s}{\lambda}$ is very low the temperature differences in radial direction can be neglected again.

The single parameters are :

- α_{G0} the convective heat transfer coefficient of the heating device. For the hot combustion gas system the range is $50 \leq \alpha_{G0} \leq 200 \text{ W/m}^2\text{K}$. For the steam jacket system the value is very higher and assumed to be infinite $\alpha_{G0} = \infty$.
- α_{GS} the radiative heat transfer coefficient between kiln wall and solid bed surface. It is supposed that the kiln wall has a lower value of the temperature, because of the properties of the wall. Thus, the value of this coefficient is considered low. The value can be zero if we have an opaque gas system (for low emissivities of the kiln wall material or very low kiln wall temperature)

- α_{WS} the conduction heat transfer coefficient between covered kiln wall and solid bed. This value depends on many parameters such as particles velocity, kiln diameter, etc., therefore this value will vary in the range $0 \leq \alpha_{WS} \leq 200 \text{ W/m}^2\text{K}$.

The energy balance, according to Fourier's law for the description of conduction on an element of thickness dx of the kiln wall, is described as follows Figure 4-14

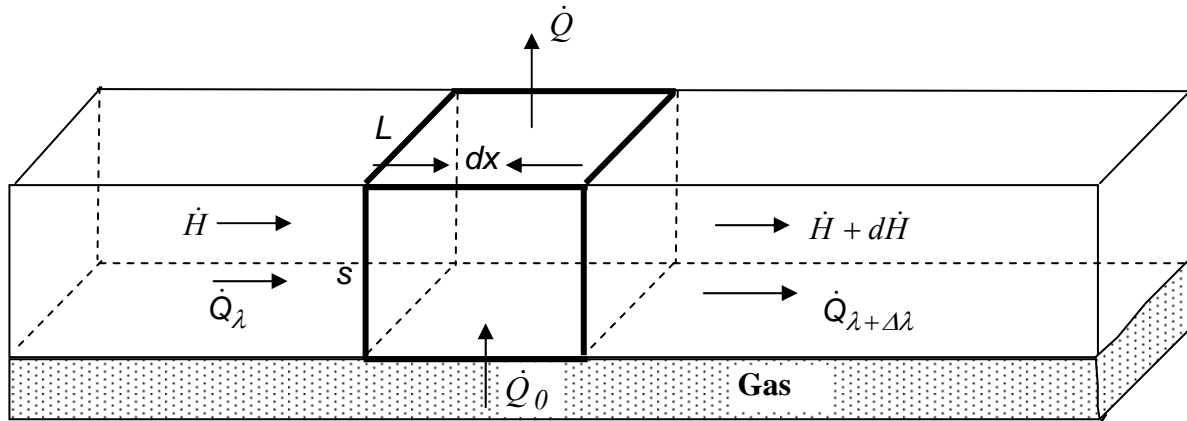


Figure 4-14. Heat flow through a kiln wall extended surface

The heat balance yields to

$$\dot{Q}_\lambda + \dot{Q}_0 + \dot{H} = \dot{Q}_{\lambda+\Delta\lambda} + (\dot{H} + d\dot{H}) + \dot{Q} \quad (4-44)$$

Since the rotational speed of the kiln is high, the heat conduction along the kiln length is negligible

$$d\dot{H} = \dot{Q}_0 - \dot{Q} \quad (4-45)$$

$$\dot{M} \cdot c \cdot dT = \alpha_0 \cdot L \cdot R \cdot d\varphi \cdot (T_{G0} - T) - \alpha \cdot L \cdot R \cdot d\varphi \cdot (T - T_S) \quad (4-46)$$

$$u = 2 \cdot \pi \cdot R \cdot n \quad (4-47)$$

$$\dot{M} = u \cdot L \cdot s \cdot \rho \quad (4-48)$$

By inserting the surface velocity and mass flow from previous Equations (4-4) and (4-5), respectively; into (4-46) the energy balance leads to

$$\rho \cdot c \cdot u \cdot s \cdot L \cdot dT = \alpha_0 \cdot L \cdot R \cdot d\phi \cdot (T_{G0} - T) - \alpha \cdot L \cdot R \cdot d\phi \cdot (T - T_S) \quad (4-49)$$

Finally, using the lumped capacity model the model is reduced to

$$\rho \cdot cp \cdot u \cdot s \cdot \frac{dT}{dx} = \alpha_0(T_{G0} - T) - \alpha(T - T_S). \quad (4-50)$$

The temperature distribution of the kiln wall in the solid and gas contact regions are described with a lumped capacity model

The solid region :

$$\rho \cdot cp \cdot u \cdot s \cdot \frac{dT}{dx_S} = \alpha_0(T_{G0} - T) - \alpha_S(T - T_S) \quad (4-51)$$

The gas region :

$$\rho \cdot cp \cdot u \cdot s \cdot \frac{dT}{dx_G} = \alpha_0(T_{G0} - T) - \alpha_G(T - T_S). \quad (4-52)$$

The density and specific thermal capacity of the kiln wall are assumed to be constant because the temperature differences along the kiln wall are relatively small.

4.2.2 Temperature distribution

The temperature distribution of the kiln wall for solid and gas contact regions lead to (Integration of Eqs. (4-51), (4-52))

$$T(x_S) - T_S = \frac{\left[\exp\left(\frac{-\alpha_0 - \alpha_S}{\rho \cdot c \cdot u \cdot s} x\right) \cdot (T_0 - T_S)(-\alpha_0 - \alpha_S) + \alpha_0(T_{G0} - T_S) \right] - \alpha_0(T_{G0} - T_S)}{-\alpha_0 - \alpha_S} \quad (4-53)$$

$$T(x_G) - T_S = \frac{\left[\exp\left(\frac{-\alpha_0 - \alpha_G}{\rho \cdot c \cdot u \cdot s} x\right) \cdot (T_0 - T_S)(-\alpha_0 - \alpha_G) + \alpha_0(T_{G0} - T_S) \right] - \alpha_0(T_{G0} - T_S)}{-\alpha_0 - \alpha_G} \quad (4-54)$$

The boundary conditions are

$$T_{S,0} = T1 \quad \text{and} \quad T(x_G) = T2 \quad (4-55)$$

$$T_{G,0} = T2 \quad \text{and} \quad T(x_G) = T1. \quad (4-56)$$

Finally the temperature distribution can be described as :

wall-solid contact region

$$T(x_S) = (T_{G0} - T_S) \cdot \left(\frac{\alpha_0}{\alpha_0 + \alpha_S} + \frac{\alpha_0 \cdot (\alpha_S - \alpha_G)}{(\alpha_0 + \alpha_S) \cdot (\alpha_0 + \alpha_G)} \cdot \frac{\exp\left(-St_S \cdot x_1 \cdot \left(1 + \frac{\alpha_0 \cdot \varepsilon}{\alpha_S \cdot \pi}\right)\right) \cdot \left(\exp\left(-St_S \cdot \left(\frac{l}{A} + \frac{\alpha_0 \cdot \varepsilon}{\alpha_S \cdot \pi}\right)\right) - 1\right)}{\exp\left(-St_S \cdot \left(1 + \frac{\alpha_0 \cdot \varepsilon}{\alpha_S \cdot \pi}\right)\right) \cdot \exp\left(-St_S \cdot \left(\frac{l}{A} + \frac{\alpha_0 \cdot \varepsilon}{\alpha_S \cdot \pi}\right)\right) - 1} \right) + T_S \quad (4-57)$$

gas-solid contact region

$$T(x_G) = (T_{G0} - T_S) \cdot \left(\frac{\alpha_0}{\alpha_0 + \alpha_G} + \frac{\alpha_0 \cdot (\alpha_S - \alpha_G)}{(\alpha_0 + \alpha_G) \cdot (\alpha_0 + \alpha_S)} \cdot \frac{\exp\left(-St_S \cdot x_2 \cdot \left(\frac{l}{A} + \frac{\alpha_0 \cdot \varepsilon}{\alpha_S \cdot \pi}\right)\right) \cdot \left(\exp\left(-St_S \cdot \left(1 + \frac{\alpha_0 \cdot \varepsilon}{\alpha_S \cdot \pi}\right)\right) - 1\right)}{\exp\left(-St_S \cdot \left(1 + \frac{\alpha_0 \cdot \varepsilon}{\alpha_S \cdot \pi}\right)\right) \cdot \exp\left(-St_S \cdot \left(\frac{l}{A} + \frac{\alpha_0 \cdot \varepsilon}{\alpha_S \cdot \pi}\right)\right) - 1} \right) + T_S \quad (4-58)$$

Dimensionless temperature distributions are introduced by normalization of the difference of wall temperature to solid temperature in relation to the maximum temperature difference of gas and solid

$$\theta_S = \frac{T(x_S) - T_S}{T_{G0} - T_S} = \frac{\alpha_0}{\alpha_0 + \alpha_S} + \frac{\alpha_0 \cdot (\alpha_S - \alpha_G)}{(\alpha_0 + \alpha_S) \cdot (\alpha_0 + \alpha_G)} \cdot \frac{\exp\left(-St_S \cdot x_1 \cdot \left(1 + \frac{\alpha_0 \cdot \varepsilon}{\alpha_S \cdot \pi}\right)\right) \cdot \left(\exp\left(-St_S \cdot \left(\frac{l}{A} + \frac{\alpha_0 \cdot \varepsilon}{\alpha_S \cdot \pi}\right)\right) - 1\right)}{\exp\left(-St_S \cdot \left(1 + \frac{\alpha_0 \cdot \varepsilon}{\alpha_S \cdot \pi}\right)\right) \cdot \exp\left(-St_S \cdot \left(\frac{l}{A} + \frac{\alpha_0 \cdot \varepsilon}{\alpha_S \cdot \pi}\right)\right) - 1} \quad (4-59)$$

$$\theta_G = \frac{T(x_G - T_S)}{T_{G0} - T_S} = \frac{\alpha_0}{\alpha_0 + \alpha_G} + \frac{\alpha_0 \cdot (\alpha_G - \alpha_S)}{(\alpha_0 + \alpha_G) \cdot (\alpha_0 + \alpha_S)} \cdot \frac{\exp\left(-St_S \cdot x_2 \cdot \left(\frac{l}{A} + \frac{\alpha_0 \cdot \varepsilon}{\alpha_S \cdot \pi}\right)\right) \cdot \left(\exp\left(-St_S \cdot \left(l + \frac{\alpha_0 \cdot \varepsilon}{\alpha_S \cdot \pi}\right)\right) - 1\right)}{\exp\left(-St_S \cdot \left(l + \frac{\alpha_0 \cdot \varepsilon}{\alpha_S \cdot \pi}\right)\right) \cdot \exp\left(-St_S \cdot \left(\frac{l}{A} + \frac{\alpha_0 \cdot \varepsilon}{\alpha_S \cdot \pi}\right)\right) - 1} \quad (4-60)$$

where the Stanton number is defined as

$$St_S = \frac{\alpha_S}{\alpha_n} \cdot \frac{\varepsilon}{\pi} \quad (4-61)$$

For a high rotational speed ($St_S = 0$), both contact regions have the same temperature

$$\theta = \theta_S = \theta_G = \frac{\alpha_0}{(\alpha_0 + \alpha_S) \cdot (\alpha_0 + \alpha_G)} \cdot \frac{\left(\left(l + \frac{\alpha_0 \cdot \varepsilon}{\alpha_S \cdot \pi}\right) \cdot (\alpha_0 + \alpha_G) + \left(\frac{\alpha_G \cdot \sin(\varepsilon)}{\varepsilon} + \frac{\alpha_0 \cdot \varepsilon}{\alpha_S \cdot \pi}\right) \cdot (\alpha_0 + \alpha_S)\right)}{1 + 2 \cdot \frac{\alpha_0 \cdot \varepsilon}{\alpha_S \cdot \pi} + \frac{\alpha_G \cdot \sin(\varepsilon)}{\alpha_S \cdot \varepsilon}} \quad (4-62)$$

From Eqs. (4-59), (4-60), and (4-62) one can see that the temperature distribution of the kiln wall is influenced by two dimensionless parameters (St_S, A), the effective heat transfer coefficients ($\alpha_0, \alpha_G, \alpha_S$), and the filling angle (ε). It should be emphasized here that the diameter once again has no influence on the temperature distribution and the rotational speed appears only in the heat transportation coefficient (Eq. (4-23)).

If the heat transfer coefficients are in the same magnitude ($\alpha_S = \alpha_G$), the kiln wall temperature is constant for any given kiln speed

$$\theta_S = \theta_G = \frac{\alpha_0}{\alpha_0 + \alpha_S} \quad (4-63)$$

For no radiation heat transfer ($\alpha_{GS} = 0$), Eqs. (4-15) and (4-16) are reduced to

$$\theta_S = \frac{\alpha_0}{\alpha_0 + \alpha_S} + \frac{\alpha_S}{(\alpha_0 + \alpha_S)} \cdot \frac{\exp\left(-St_S \cdot x_1 \cdot \left(1 + \frac{\alpha_0 \cdot \pi}{\alpha_S \cdot \varepsilon}\right)\right) \cdot \left(\exp\left(-St_S \cdot \left(\frac{\alpha_0 \cdot \pi}{\alpha_S \cdot \varepsilon}\right)\right) - 1\right)}{\exp\left(-St_S \cdot \left(1 + \frac{\alpha_0 \cdot \pi}{\alpha_S \cdot \varepsilon}\right)\right) \cdot \exp\left(-St_S \cdot \left(\frac{\alpha_0 \cdot \pi}{\alpha_S \cdot \varepsilon}\right)\right) - 1} \quad (4-64)$$

$$\theta_G = 1 - \frac{\alpha_S}{(\alpha_0 + \alpha_S)} \cdot \frac{\exp\left(-St_S \cdot x_2 \cdot \left(\frac{\alpha_0 \cdot \pi}{\alpha_S \cdot \varepsilon}\right)\right) \cdot \left(\exp\left(-St_S \cdot \left(1 + \frac{\alpha_0 \cdot \pi}{\alpha_S \cdot \varepsilon}\right)\right) - 1\right)}{\exp\left(-St_S \cdot \left(1 + \frac{\alpha_0 \cdot \pi}{\alpha_S \cdot \varepsilon}\right)\right) \cdot \exp\left(-St_S \cdot \left(\frac{\alpha_0 \cdot \pi}{\alpha_S \cdot \varepsilon}\right)\right) - 1} \quad (4-65)$$

Now the case is assumed that the wall temperature corresponds to the saturation temperature of the heating surface. Thus, if the heating surface is the condensing steam the heat transfer coefficient is very high/infinite typical values are 3000-10.000 W/m^2K ($\alpha_0 = \infty$) [Canales et al. 2001]. For this case, the inner wall temperature has the same value as the temperature of the steam

$$\theta_S = \theta_G = 1 \quad (4-66)$$

A typical circumferential dimensionless temperature distribution is presented in Figure 4-15 for the same value of wall-solid and convective outer wall heat transfer coefficients. The material of the wall is steel with high density and low heat capacity. The figure reveals that at a low radiation heat transfer the inner wall temperature rises towards the outer wall temperature (T_G). As the radiation heat transfer coefficient increases the inner wall temperature decreases towards the solid bed temperature. For the same heat transfer ratio, the inner wall temperature remains constant according to Eq. (4-63). Furthermore, if the heat transfer wall-solid is higher than the radiation of the wall, the inner wall temperature is decreasing at the solid side and increasing at the gas side. Vice versa, when the heat transfer wall-solid is lower the inner wall temperature increases at the solid side. This phenomenon is

clearly illustrated for different Stanton number in Figure 4-16 (a) and (b) for the higher and lower ratios, respectively. Typical rotational speed is $n = 1-3 \text{ rpm}$ with Stanton number $0.03 - 0.01$. Therefore, it reveals that the circumferential temperature variations for typical kiln speeds are less than 3 K , thus the inner wall temperature is expected to be constant. Furthermore, the temperature cycling in the wall is expected to be the greatest at a high radiation between wall-solid or in areas where there exists a large difference between outer wall hot combustion gas temperature (T_{G0}) and solid temperature (T_S).

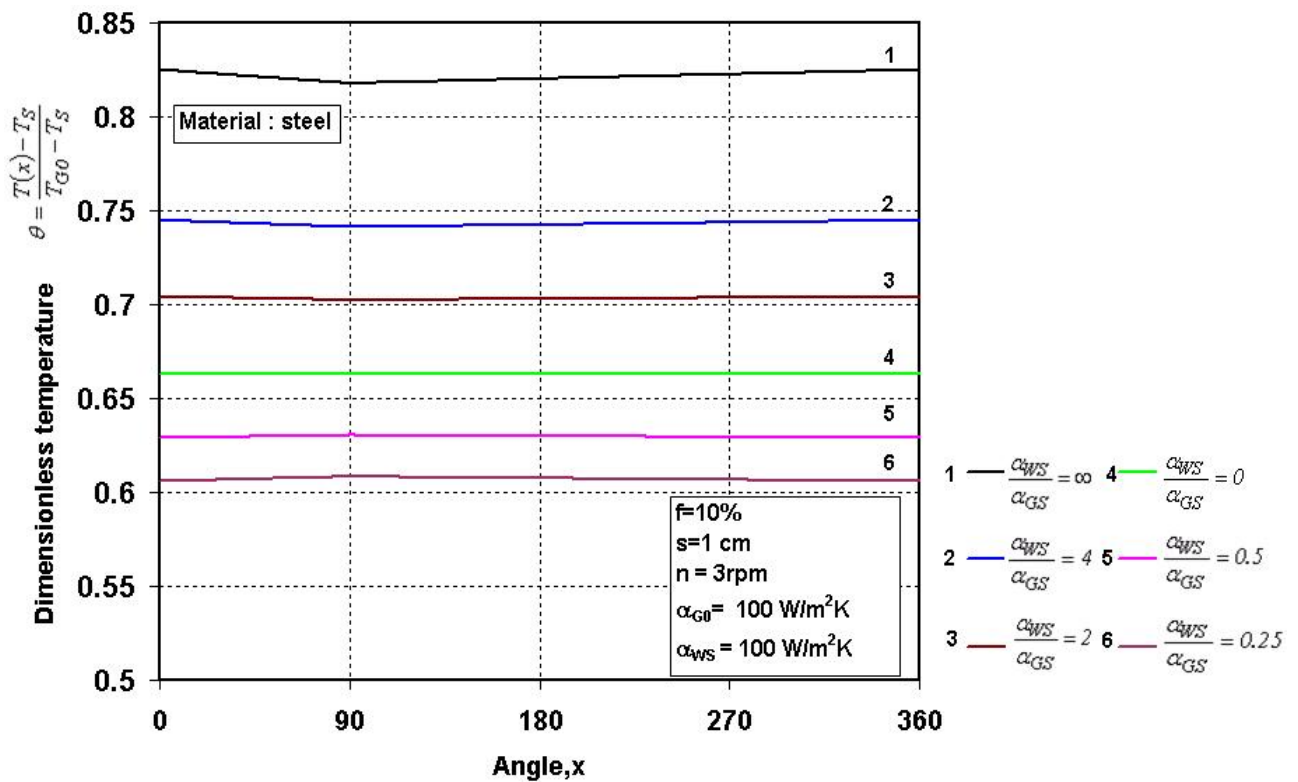


Figure 4-15. Inner wall temperature distribution along the circumference for steel

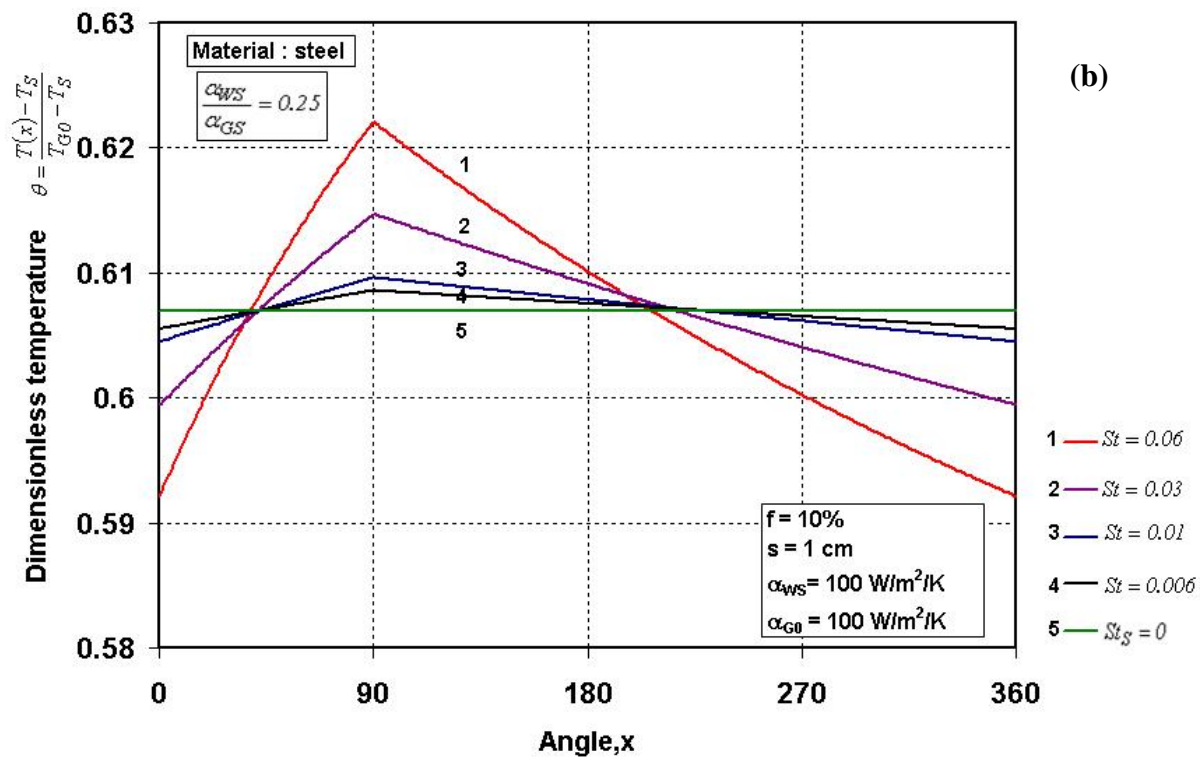
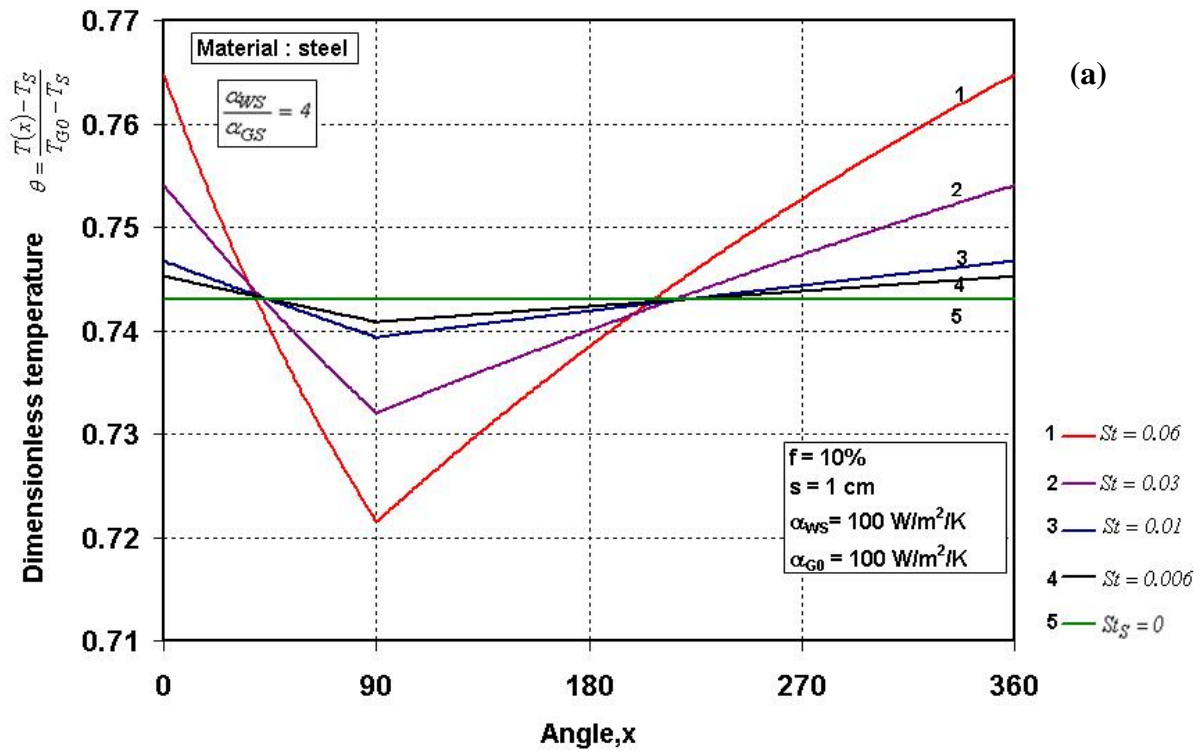


Figure 4-16. (a) Heat transfer coefficient ratios =4 (b) Heat transfer coefficient ratios = 0.25

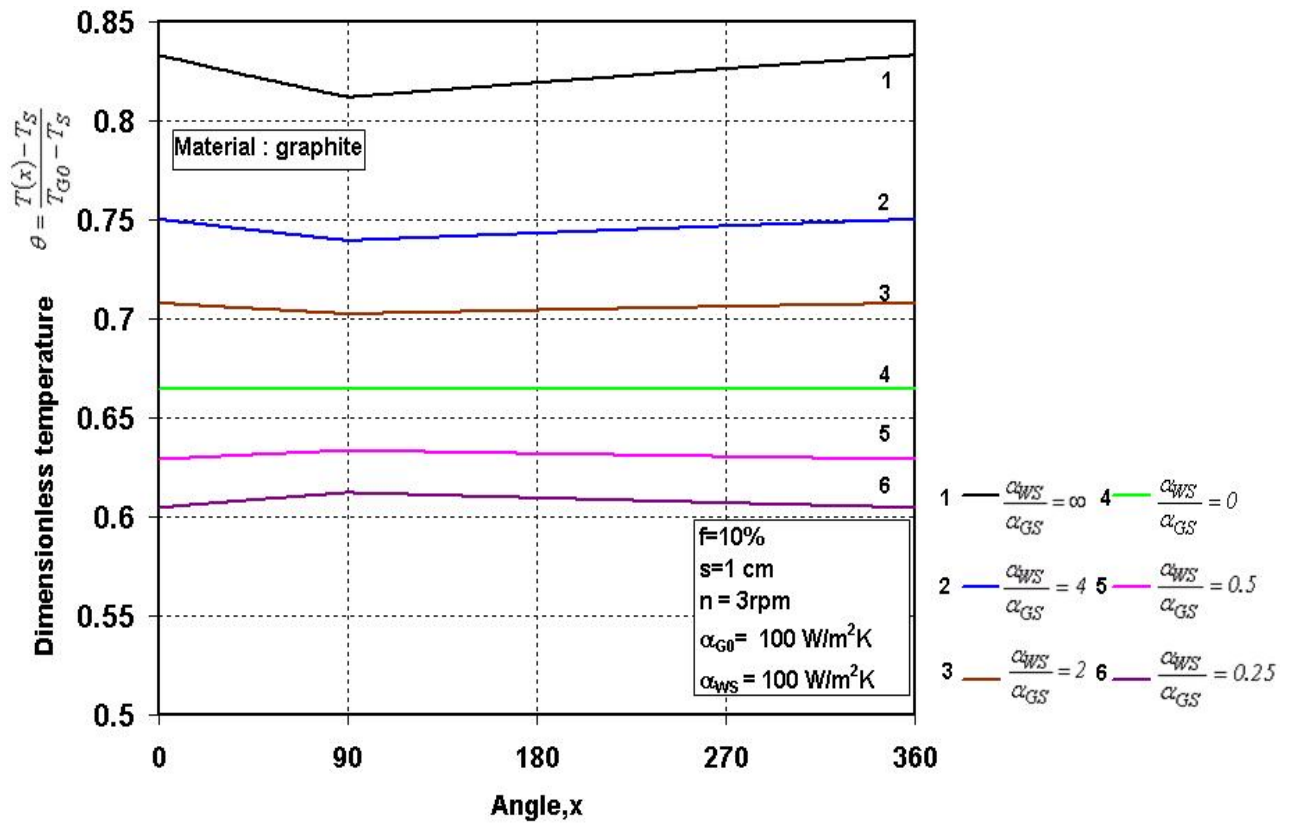


Figure 4-17. Inner wall temperature distribution along the circumference for graphite

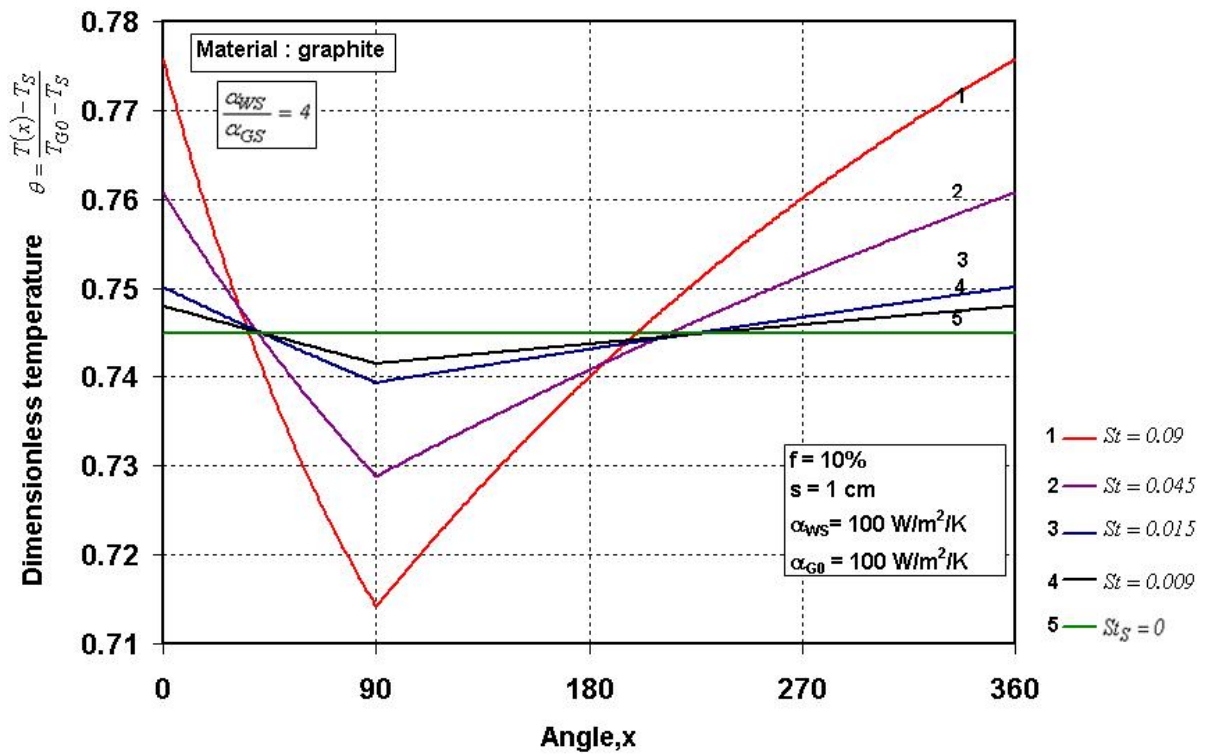


Figure 4-18. Inner wall temperature distribution for different Stanton number at heat transfer coefficient ratios =4

The dimensionless inner wall temperature distribution along the circumference is plotted again in Figure 4-17 for Graphite. This figure indicates that both the temperature level and the temperature cyclic on the inner wall are slightly higher than that of steel. A decrease in the heat transfer ratios by 50% reduces the inner wall by 3 to 5% towards the solid bed temperature. Graphite has a higher value of emissivity therefore the radiation heat transfer is high. In this example it is necessary to show all possibilities cases. Nevertheless, the temperature difference between the gas and solid side is less than 5 K for typical rotational speed with Stanton number 0.045 – 0.009 (see Figure 4-18). For lower kiln speed $n = 0.5 \text{ rpm}$ (Stanton number = 0.09), the gas and solid inner wall temperature increases by 10%. Thus, the inner wall temperature is expected to be constant for typical kiln speed.

Figure 4-19 shows a high filling degree for typical kiln wall material (steel). By increasing the filling degree, the gas region becomes smaller and the region occupied by the solid is larger; thus, the time that the wall spends beneath the solid increases and the time in contact with the gas decreases; and therefore both the inner wall temperature and the difference between the maximum and minimum temperature are reduced.

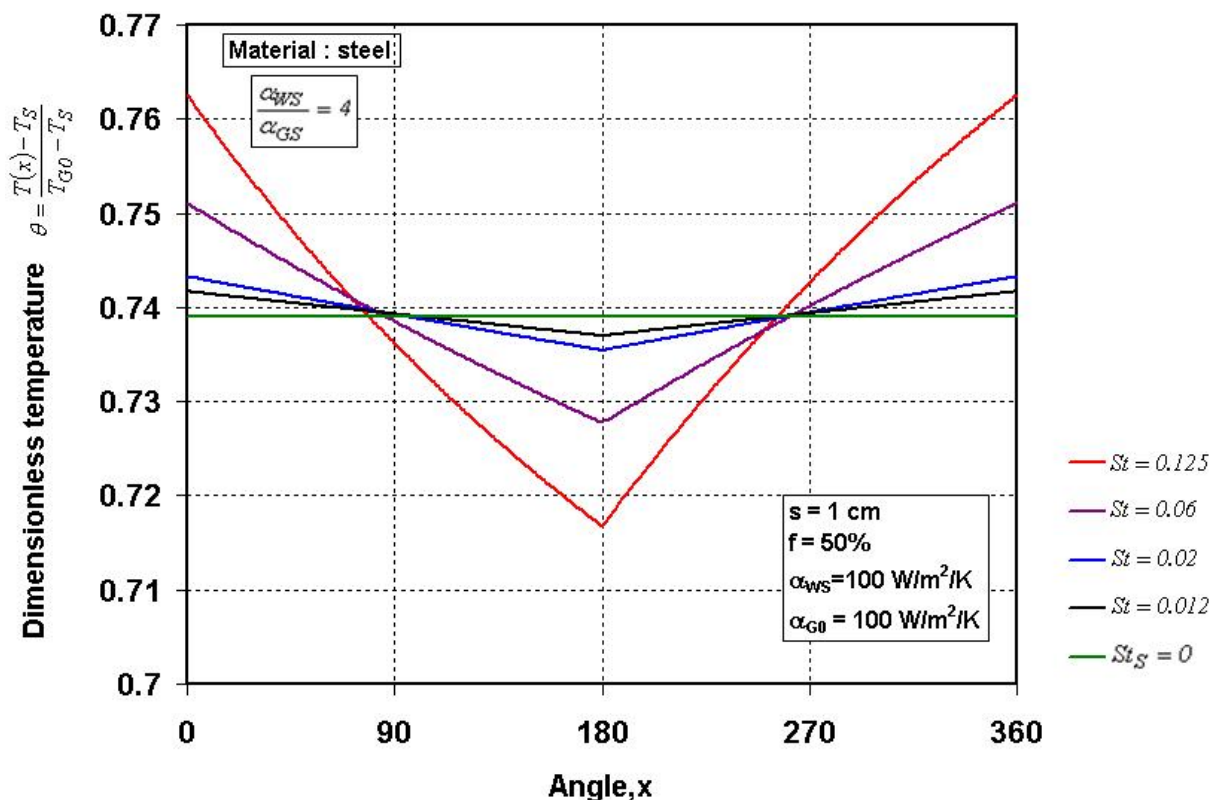


Figure 4-19. Inner wall temperature distribution for different Stanton number at filling degree 50%

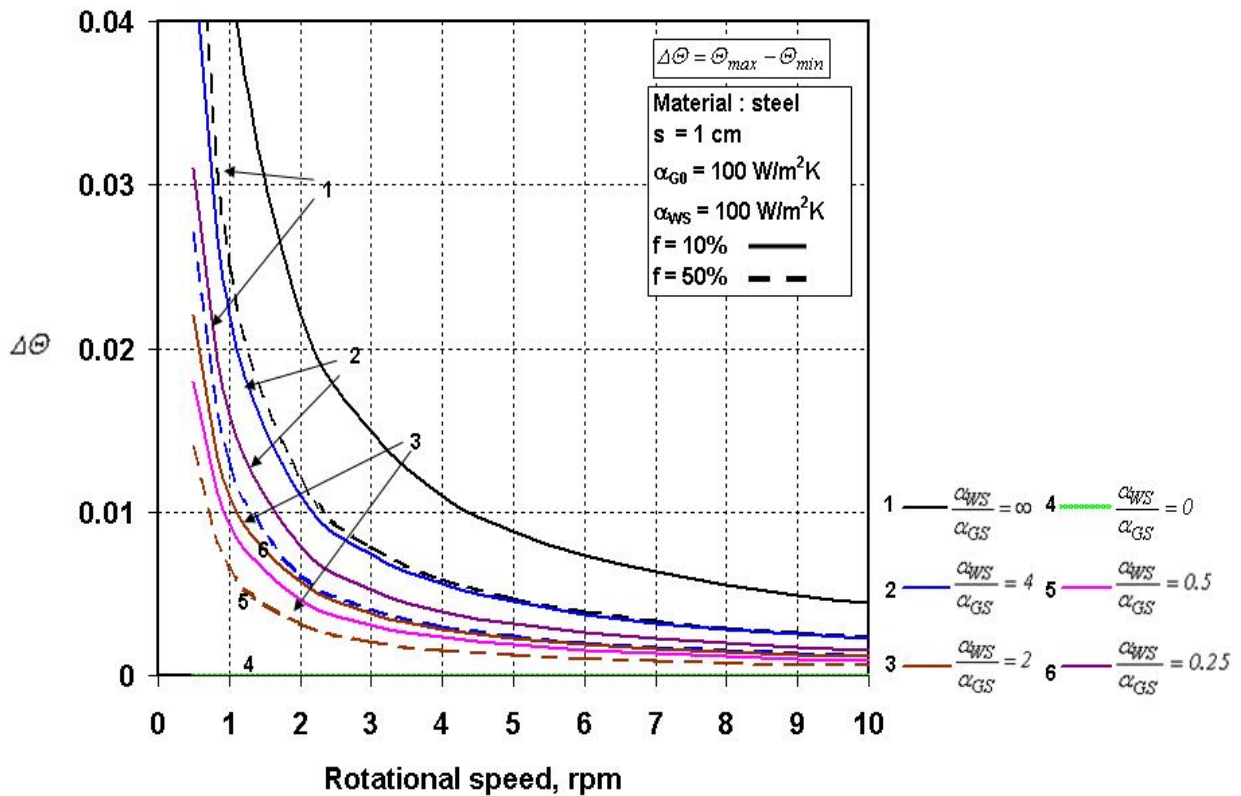


Figure 4-20. Maximum and minimum dimensionless temperature difference for two different filling degree

Nevertheless, an increase in the filling degree to 50% decreases the level of the inner wall temperature less than 2% which is not significant. This phenomenon is valid for all kiln wall material. Moreover, the circumferential wall temperature varies less than 3% for typical rotational speed with Stanton number 0.06-0.012. Therefore, the temperature cycling of the inner wall at typical rotational speed is independent of the filling degree and thermophysical material properties.

The influence of the rotational speed on the difference between the integrated exposed and covered inner wall temperature is shown in Figure 4-20. It is evident that, for the higher rotational speeds, the temperature difference decreases. Moreover, an increase in the filling degree by 50% decreases the temperature difference by 3%. A higher temperature difference is expected at infinite heat transfer coefficient ratios i.e. no radiative heat transfer. The difference decreases as the radiative heat transfer coefficient increases (inner wall temperature decrease at the solid side and increase at the gas side). On the other hand, when the radiative heat transfer is higher than the wall-solid heat transfer coefficient the temperature difference increases again but in a vice versa direction (inner wall temperature increase at the solid side and decrease at the gas side). A similar operating condition as the previous case is used in

Figure 4-21 to calculate the inner wall temperature for two filling degrees. The solid line refers to filling degree 10% and the dotted line to filling degree 50%. An increase in filling degree by 50% decreases the temperature difference by only 1%. Therefore, the solids fill ratio has no significant influence to the temperature difference. Furthermore, for low radiation heat transfer coefficients the difference between the dimensionless maximum and minimum inner wall temperature is higher. Increasing the radiation heat transfer coefficient by a factor of 2 decreases the inner wall temperature and the temperature differences. The temperature difference increases with the convective outer wall heat transfer coefficient, but in some stages the temperature difference reduced. There is no temperature difference on the inner wall temperature at infinite α_0 i.e. $\Delta\Theta = 0$.

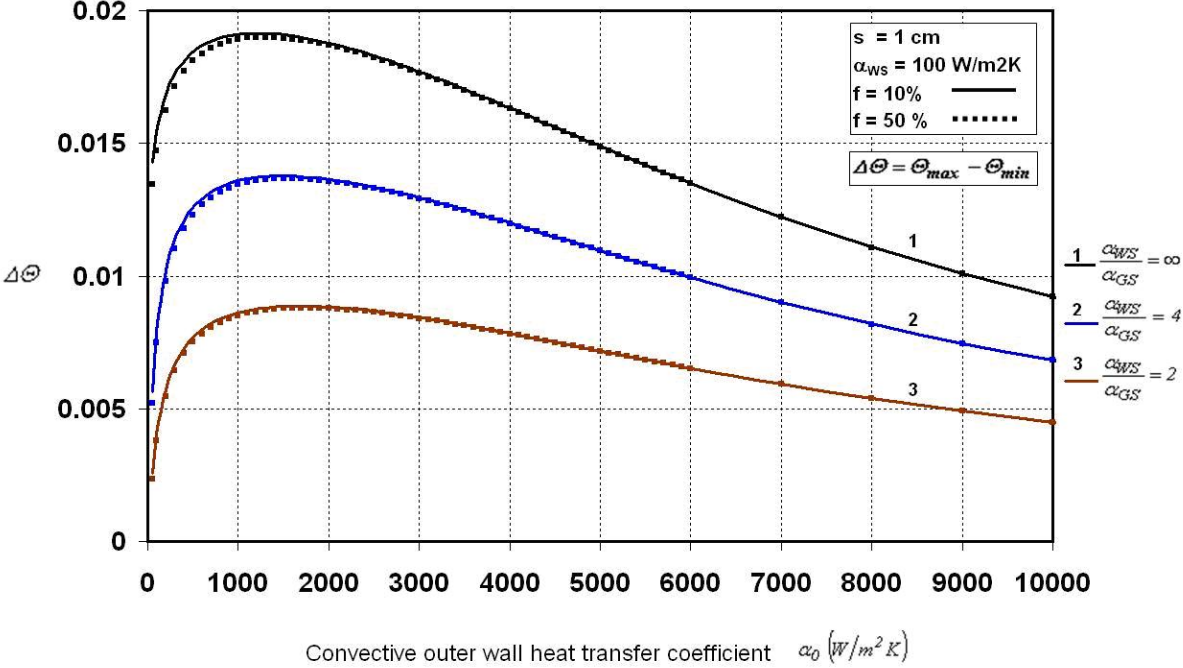


Figure 4-21. The influence of convective outer wall heat transfer coefficient to inner wall temperature difference

4.2.3 Heat flow

The heat flow to the solid bed is divided into two parts: covered wall-to-solid heat transfer (\dot{Q}_{WS}) and uncovered wall-to-solid heat flow (\dot{Q}_{GS}). The total heat flow is the sum of both

$$\dot{Q}_T = \dot{Q}_{WS} + \dot{Q}_{GS} \quad (4-67)$$

According to Eqs. (4-33) and (4-34), the heat flow along the kiln length is defined as

$$\dot{Q}_{WS}/L = (T_{G0} - T_S) \cdot \left[\frac{\alpha_S \cdot \alpha_0}{\alpha_0 + \alpha_S} \cdot L_{WS} + \frac{\frac{L_{WS} \cdot \alpha_S}{St_S} \cdot \alpha_S \cdot \alpha_0 \cdot (\alpha_S - \alpha_G)}{(\alpha_0 + \alpha_S)^2 \cdot (\alpha_0 + \alpha_S)} \cdot \frac{\left(1 - \exp\left(-St_S \left(l + \frac{\alpha_0}{\alpha_S} \cdot \frac{\varepsilon}{\pi}\right)\right)\right) \cdot \left(\exp\left(-St_S \left(\frac{l}{A} + \frac{\alpha_0}{\alpha_S} \cdot \frac{\varepsilon}{\pi}\right)\right) - 1\right)}{\exp\left(-St_S \cdot \left(\frac{l}{A} + \frac{\alpha_0}{\alpha_S} \cdot \frac{\varepsilon}{\pi}\right)\right) \cdot \exp\left(-St_S \left(l + \frac{\alpha_0}{\alpha_S} \cdot \frac{\varepsilon}{\pi}\right)\right) - 1} \right] \quad (4-68)$$

$$\dot{Q}_{GS}/L = (T_{G0} - T_S) \cdot \left[\frac{\alpha_G \cdot \alpha_0}{\alpha_0 + \alpha_G} \cdot L_{GS} + \frac{\frac{L_{GS} \cdot \alpha_S}{St_S} \cdot \alpha_G \cdot \alpha_0 \cdot (\alpha_S - \alpha_G)}{(\alpha_0 + \alpha_G)^2 \cdot (\alpha_0 + \alpha_S)} \cdot \frac{\left(1 - \exp\left(-St_S \left(l + \frac{\alpha_0}{\alpha_S} \cdot \frac{\varepsilon}{\pi}\right)\right)\right) \cdot \left(\exp\left(-St_S \left(\frac{l}{A} + \frac{\alpha_0}{\alpha_S} \cdot \frac{\varepsilon}{\pi}\right)\right) - 1\right)}{\exp\left(-St_S \cdot \left(\frac{l}{A} + \frac{\alpha_0}{\alpha_S} \cdot \frac{\varepsilon}{\pi}\right)\right) \cdot \exp\left(-St_S \left(l + \frac{\alpha_0}{\alpha_S} \cdot \frac{\varepsilon}{\pi}\right)\right) - 1} \right] \quad (4-69)$$

Later on it is easier to define the heat flow related to the kiln length and the maximum temperature differences

$$\dot{Q}_S^* = \frac{\dot{Q}_{WS}}{L \cdot (T_{G0} - T_S)} \quad (4-70)$$

$$\dot{Q}_G^* = \frac{\dot{Q}_{GS}}{L \cdot (T_{G0} - T_S)} \quad (4-71)$$

$$\dot{Q}_T^* = \dot{Q}_S^* + \dot{Q}_G^* \quad (4-72)$$

At infinite rotational speed ($St_S = 0$), the equations are simplified as

$$\frac{\dot{Q}_{WS}}{L} = (T_{G0} - T_S) \cdot \frac{\alpha_S \cdot \alpha_0}{\alpha_0 + \alpha_S} \left[L_{WS} + L_{WS} \cdot \frac{\alpha_S - \alpha_G}{(\alpha_0 + \alpha_S)} \cdot \frac{\left(\alpha_G \cdot \frac{\sin(\varepsilon)}{\varepsilon} + \alpha_0 \cdot \frac{\varepsilon}{\pi} \right) + \frac{1}{\alpha_S} \left(\alpha_0 \cdot \alpha_G \cdot \frac{\sin(\varepsilon)}{\varepsilon} \cdot \frac{\varepsilon}{\pi} + \alpha_0^2 \cdot \frac{\varepsilon^2}{\pi^2} \right)}{(\alpha_0 + \alpha_G) \cdot \left(1 + 2 \cdot \frac{\alpha_0}{\alpha_S} \cdot \frac{\varepsilon}{\pi} + \frac{\alpha_G}{\alpha_S} \cdot \frac{\sin(\varepsilon)}{\varepsilon} \right)} \right] \quad (4-73)$$

$$\frac{\dot{Q}_{GS}}{L} = (T_{G0} - T_S) \cdot \frac{\alpha_G \cdot \alpha_0}{\alpha_0 + \alpha_G} \left[L_{GS} + L_{WS} \cdot \frac{\alpha_S - \alpha_G}{(\alpha_0 + \alpha_S)} \cdot \frac{\left(\alpha_G \cdot \frac{\sin(\varepsilon)}{\varepsilon} + \alpha_0 \cdot \frac{\varepsilon}{\pi} \right) + \frac{1}{\alpha_S} \left(\alpha_0 \cdot \alpha_G \cdot \frac{\sin(\varepsilon)}{\varepsilon} \cdot \frac{\varepsilon}{\pi} + \alpha_0^2 \cdot \frac{\varepsilon^2}{\pi^2} \right)}{(\alpha_0 + \alpha_G) \cdot \left(1 + 2 \cdot \frac{\alpha_0}{\alpha_S} \cdot \frac{\varepsilon}{\pi} + \frac{\alpha_G}{\alpha_S} \cdot \frac{\sin(\varepsilon)}{\varepsilon} \right)} \right] \quad (4-74)$$

For a steam heating system ($\alpha_{G0} = \infty$) the model is simplified as

$$\dot{Q}_T = \alpha_S \cdot L_{WS} + \alpha_G \cdot L_{GS} \quad (4-75)$$

where

$$L_{WS} = 2\varepsilon \cdot R$$

$$L_{GS} = 2 \cdot \sin(\varepsilon) \cdot R \quad (4-76)$$

Figure 4-22 shows the influence of the filling degree on the heat flow to the solid bed. The heat flows are defined in comparison to the kiln length and maximum difference between temperature of the hot combustion gas and the temperature of solid bed. The heat transfer coefficient of the hot combustion gas and wall-solid are in the same magnitudes. The heat flow increases with the filling degree and decreases with the exposed wall-solid heat transfer coefficient. Increasing fill ratio by a factor of 2 increases the heat flow ratios less than 5%; which is a relatively low effect. On this basis, changes in fill ratios are not expected to strongly influence heat transfer within the kiln. At the same magnitude of the heat transfer coefficients ratio, the regenerative heat flow from the covered wall-solid bed is 50%-60% to the total heat flow received by the solid. At the condition that the covered wall-solid heat

transfer coefficient is 10 times higher than the exposed wall-solid heat transfer coefficient, the regenerative heat flow is 90% of the total heat flow. This fact explains that in externally heated rotary kilns the regenerative heat flow has a significant influence to the process.

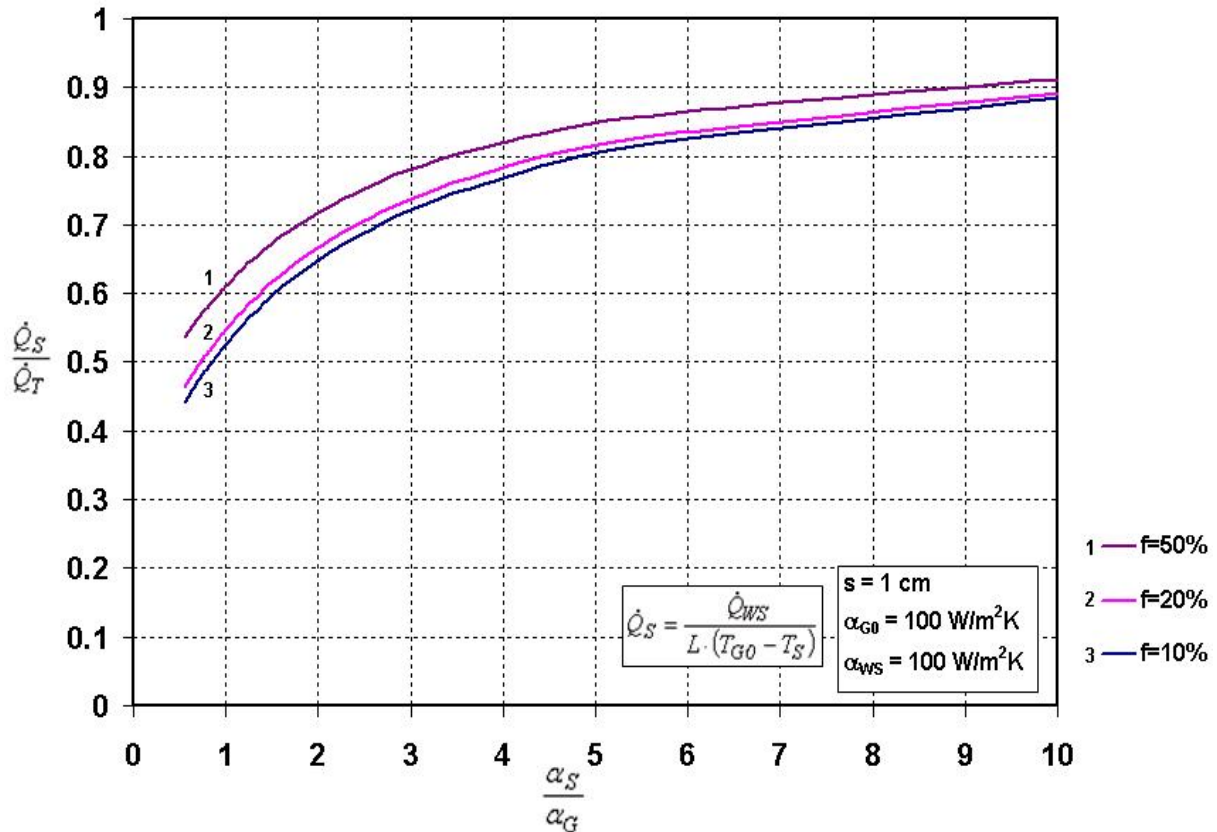


Figure 4-22. Influence of the heat transfer coefficient on the heat flow

4.2.4 Overall heat transfer coefficient

An overall heat transfer coefficient (α_{ov}) is introduced as the total heat flow received by the solid related to the kiln length, the covered wall length and the maximum temperature difference between hot combustion gas and solid bed

$$\frac{\dot{Q}_T}{L \cdot L_{WS} \cdot (T_{G0} - T_S)} = \alpha_{ov} \quad (4-77)$$

In order to determine the role of regenerative heating in the overall heat flow to the solids, dimensionless quantities on the overall heat transferred to the solid related to the heat transferred from the hot gas are used to calculate the total heat transferred to the solids.

$$\begin{aligned} \frac{\alpha_{ov}}{\alpha_0} = & \frac{1}{\frac{\alpha_0}{\alpha_S} + 1} + \frac{1}{\frac{\alpha_0}{\alpha_G} + 1} \cdot \frac{\sin(\varepsilon)}{\varepsilon} + \frac{1}{St_S} \cdot \frac{\left(\frac{\alpha_S}{\alpha_0} \cdot \frac{\alpha_0}{\alpha_G} - 1\right)}{\left(\frac{\alpha_0}{\alpha_S} + 1\right)^2 \left(\frac{\alpha_0}{\alpha_G} + 1\right)} \cdot \frac{(1 - \exp(-St_S \cdot X)) \cdot (\exp(-St_S \cdot Y) - 1)}{\exp(-St_S \cdot X) \cdot \exp(-St_S \cdot Y) - 1} \dots \\ & \dots + \frac{1}{St_S} \cdot \frac{\left(\frac{\alpha_S}{\alpha_0} \cdot \frac{\alpha_0}{\alpha_G} - 1\right)}{\left(\frac{\alpha_0}{\alpha_G} + 1\right)^2 \left(\frac{\alpha_0}{\alpha_S} + 1\right)} \cdot \frac{(1 - \exp(-St_S \cdot Y)) \cdot (\exp(-St_S \cdot X) - 1)}{\exp(-St_S \cdot X) \cdot \exp(-St_S \cdot Y) - 1} \end{aligned} \quad (4-78)$$

where

$$X = 1 + \frac{\alpha_0}{\alpha_S} \cdot \frac{\varepsilon}{\pi} \quad (4-79)$$

$$Y = \frac{\alpha_G}{\alpha_S} \cdot \frac{\sin(\varepsilon)}{\varepsilon} + \frac{\alpha_0}{\alpha_S} \cdot \frac{\varepsilon}{\pi} \quad (4-80)$$

At infinite rotational speed, the model is reduced to

$$\frac{\alpha_{ovWS}}{\alpha_0} = \frac{1}{\frac{\alpha_0}{\alpha_S} + 1} \cdot \left[1 + \frac{\alpha_S - \alpha_G}{(\alpha_0 + \alpha_S)} \cdot \frac{\left(\alpha_G \cdot \frac{\sin(\varepsilon)}{\varepsilon} + \alpha_0 \cdot \frac{\varepsilon}{\pi} \right) + \frac{1}{\alpha_S} \left(\alpha_0 \cdot \alpha_G \cdot \frac{\sin(\varepsilon)}{\varepsilon} \cdot \frac{\varepsilon}{\pi} + \alpha_0^2 \cdot \left(\frac{\varepsilon}{\pi} \right)^2 \right)}{(\alpha_0 + \alpha_G) \cdot \left(1 + 2 \cdot \frac{\alpha_0}{\alpha_S} \cdot \frac{\varepsilon}{\pi} + \frac{\alpha_G}{\alpha_S} \cdot \frac{\sin(\varepsilon)}{\varepsilon} \right)} \right] \quad (4-81)$$

$$\frac{\alpha_{ovGS}}{\alpha_0} = \frac{1}{\frac{\alpha_0}{\alpha_S} \cdot \frac{\alpha_S}{\alpha_G} + 1} \left[\frac{\sin(\varepsilon)}{\varepsilon} + \frac{\alpha_S - \alpha_G}{(\alpha_0 + \alpha_S)} \cdot \frac{\left(\alpha_G \cdot \frac{\sin(\varepsilon)}{\varepsilon} + \alpha_0 \cdot \frac{\varepsilon}{\pi} \right) + \frac{1}{\alpha_S} \left(\alpha_0 \cdot \alpha_G \cdot \frac{\sin(\varepsilon)}{\varepsilon} \cdot \frac{\varepsilon}{\pi} + \alpha_0^2 \cdot \left(\frac{\varepsilon}{\pi} \right)^2 \right)}{(\alpha_0 + \alpha_G) \cdot \left(1 + 2 \cdot \frac{\alpha_0}{\alpha_S} \cdot \frac{\varepsilon}{\pi} + \frac{\alpha_G}{\alpha_S} \cdot \frac{\sin(\varepsilon)}{\varepsilon} \right)} \right] \quad (4-82)$$

where

$$\alpha_{ov} = \alpha_{ovWS} + \alpha_{ovGS} \quad (4-83)$$

For no radiation between wall-solid, the overall heat transfer is reduced to

$$\frac{\alpha_{ov}}{\alpha_0} = \frac{1}{\frac{\alpha_0}{\alpha_S} + 1} \left[1 + \frac{\alpha_S}{\alpha_0 + \alpha_S} \cdot \frac{\alpha_S + \alpha_0 \cdot \frac{\varepsilon}{\pi}}{\alpha_S \cdot \frac{\pi}{\varepsilon} + 2 \cdot \alpha_0} \right] \quad (4-84)$$

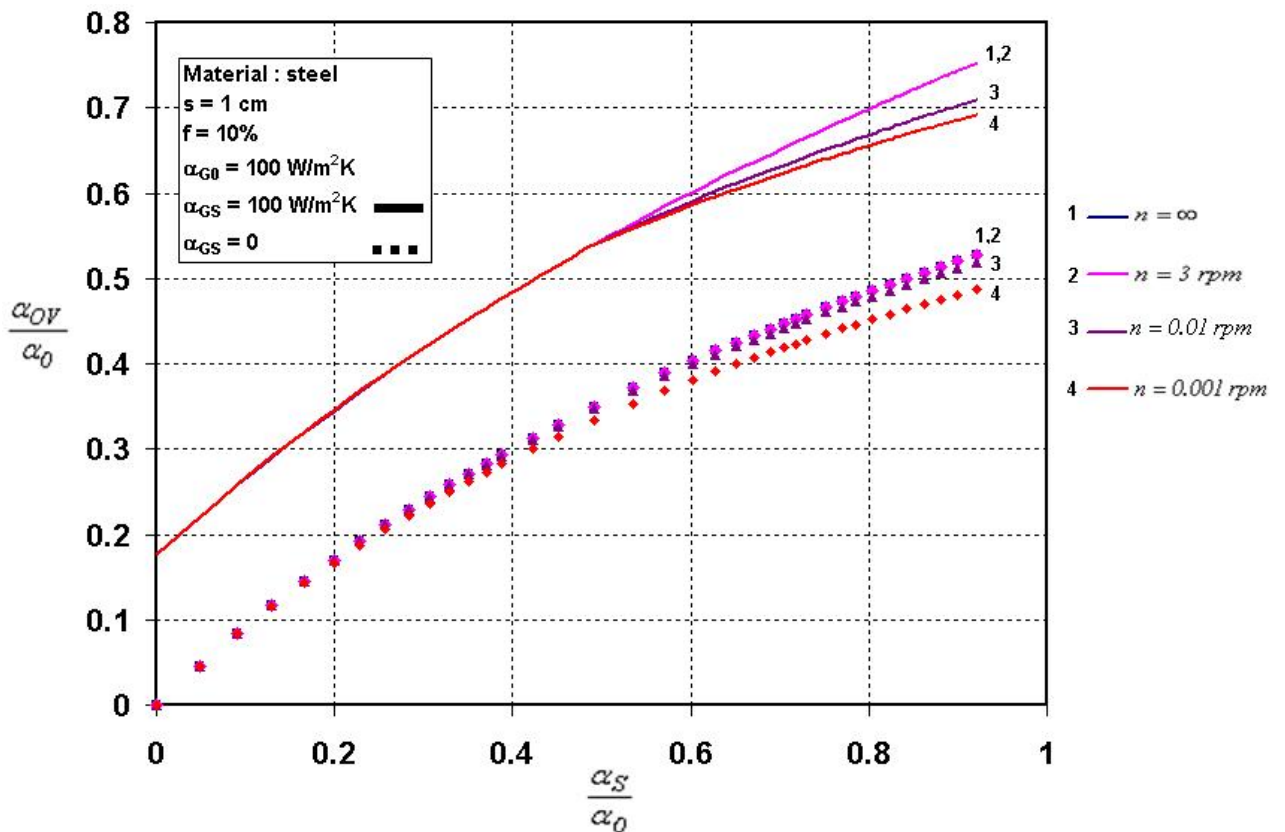


Figure 4-23. Dimensionless overall heat transfer coefficient at various rotational speed

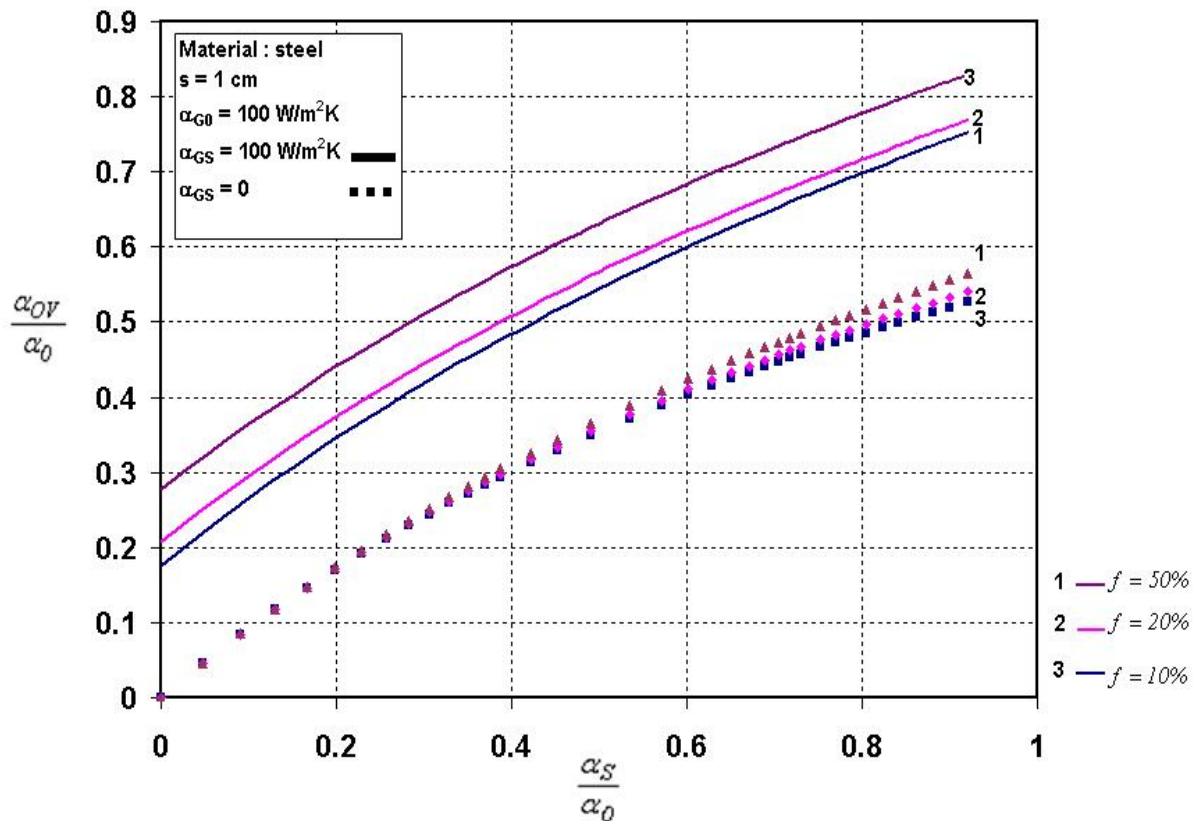


Figure 4-24. Influence of the effective heat transfer coefficient ratios on the dimensionless overall heat transfer coefficient to the solid

The influence of rotational speed on the dimensionless overall heat transfer coefficient is shown in Figure 4-23. The solid line refers to a high radiative heat transfer between the wall and solid, the dotted line refers to a low radiation. The outer wall convective heat transfer coefficient is constant at 100 W/mK . With an increase in the kiln speed from 3 to infinite rpm, the overall heat transfer remains unchanged. It is evident that, for typical rotational speeds, the infinite rotational speed is an appropriate assumption to calculate the total heat flow received by the solid. The heat flows remain constant with the kiln speed, the value changes for a very low rotational speed ($n < 0.01 \text{ rpm}$). Therefore, to evaluate the overall heat transferred to solid, instead of using a long equation according to (4-80), one can use a simplified model according to Eqs. (4-81) and (4-82). It must be noted although the kiln speed does not strongly influence the total heat flow received by the solids; it significantly alter the thermal load and residence time of the solids. For these reasons, kiln speed has an effect on kiln operation; however, it is beyond the scope of this work.

Figure 4-24 illustrates the influence of the effective heat transfer coefficient ratios on the dimensionless overall heat transfer coefficient to the solid bed under the similar conditions. An increase in the effective heat transfer coefficient ratios from 0 to 0.2, improves

the overall heat transfer coefficient to the solid bed to the outer wall heat transfer coefficient by 20% for no radiation heat transfer and 35% for high radiation heat transfer. For high contact between wall-solid and no radiation heat transfer, α_{ov} is about 60% of α_0 . Thus, the overall heat transfer to the solid bed is mainly influenced by the wall-solid heat transfer coefficient. However, if the radiative heat transfer is high the overall heat transfer coefficient is higher at low filling degree. This fact is due to the condition that the α_{ov} is related to the contact area of the covered wall, in which at a high filling degree the area of the covered wall is higher than the area of the exposed bed surface (see Figure 4-12). However this effect is overcome by the fact that the heat flow increases with the filling degree (see Figure 4-20). In the case of no radiation heat transfer, increasing the filling degree by a factor of 2 increases the overall heat transfer by only 1%. At this point on it is emphasized that the overall heat transfer coefficient is influenced by three heat transfer coefficient ($\alpha_{WS}, \alpha_{GS}, \alpha_{G0}$) and the filling angle ε has a relatively low influence.

4.2.5 Simplified resistance network

As shown previously in the previous chapter, the model to predict the overall heat transfer coefficient received by the solid is complex. It is necessary to develop a simple model to investigate the impact of the parameters easily. While pursuing this goal, the network in Figure 4-25 is formulated by the extension of the standard electricity resistance analogue including both the rotational kiln wall and the convective heat flow from the outer wall. This method is used to estimate a simplified exposed inner wall heat transfer coefficient and the covered inner wall heat transfer coefficient. The results of these calculations are presented in Figure 4-30 and Figure 4-31 and compared with the model formulated earlier in this chapter.

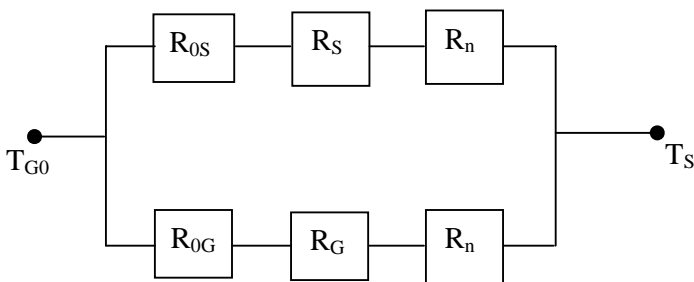


Figure 4-25. Resistance network

In order to approximate the overall heat transfer coefficient, the following steps are introduced.

To predict the resistance of the solid bed the following steps are used:

1. For no radiation heat transfer between the exposed wall and solid $\alpha_{GS} = 0$, the effective heat transfer coefficient in this region is also zero $\alpha_G = 0$ (according to Eq. 4-42). The previous model gives the overall heat transfer coefficient according to Eq. 4-81.

$$\alpha_{ov} = \frac{\alpha_0 \cdot \alpha_S}{\alpha_0 + \alpha_S} \cdot \left[1 + \frac{\alpha_S}{\alpha_0 + \alpha_S} \cdot \frac{\alpha_S + \alpha_0 \cdot \frac{\varepsilon}{\pi}}{\alpha_S \cdot \frac{\pi}{\varepsilon} + 2 \cdot \alpha_0} \right] \quad (4-85)$$

- 1.1. For infinite contact heat transfer between covered wall and solid $\alpha_{WS} = \infty$, and according to Eq. 4-43 the effective heat transfer coefficient in this region is equal to the convective gas heat transfer coefficient $\alpha_S = \alpha_0$. This is the resistance of the wall at the solid side coupled with the convective heat flow from outer wall at the solid region R_{0S} .

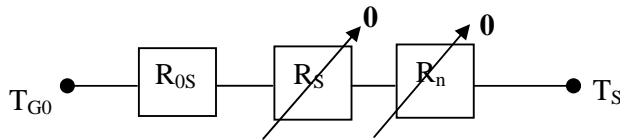


Figure 4-26. Resistance network at no radiation heat flow and infinite wall-solid heat flow

$$R_{0S} = \alpha_0 \cdot \left[\frac{1}{2} + \frac{1}{4} \cdot \frac{1 + \frac{\varepsilon}{\pi}}{2 + \frac{\pi}{\varepsilon}} \right] \quad (4-86)$$

1.2. For steam as heat source $\alpha_0 = \infty$, the effective heat transfer coefficient is equal to the wall-solid heat transfer coefficient $\alpha_S = \alpha_{WS}$. The result leads to the resistance of the covered wall-solid R_S .

$$R_S = \alpha_{WS} \quad (4-87)$$

These approximations give the heat flow and the overall heat transfer coefficient according to Figure 4-27 as follows

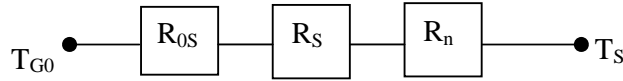


Figure 4-27. Resistance network for no radiation heat transfer

$$(R_{0S} + R_S) \cdot \frac{\dot{Q}_{ov}}{L} = (T_{G0} - T_S) \quad (4-88)$$

$$\frac{\dot{Q}}{L \cdot (T_{G0} - T_S)} = \frac{1}{\frac{1}{\alpha_0 \cdot \varepsilon \cdot D \cdot \left(\frac{1}{2} + \frac{1}{4} \cdot \frac{1 + \frac{\varepsilon}{\pi}}{\varepsilon \cdot \left(2 + \frac{\varepsilon}{\pi} \right)} \right)} + \frac{1}{\alpha_{WS} \cdot L_{WS}}} \quad (4-89)$$

$$\alpha_{ov} = \frac{1}{\frac{1}{\alpha_0 \cdot \left(\frac{1}{2} + \frac{1}{4} \cdot \frac{1 + \frac{\varepsilon}{\pi}}{\left(2 + \frac{\varepsilon}{\pi} \right)} \right)} + \frac{1}{\alpha_{WS}}} \quad (4-90)$$

The second step is to predict the resistance of the exposed wall-solid region without influence of the regenerative heat flow from the wall:

2. For no conduction heat transfer between covered wall and solid $\alpha_{WS} = 0$, the effective heat transfer coefficient in this region is also zero $\alpha_S = 0$ (according to Eq. 4-43). With this boundary condition the previous model gives the overall heat transfer coefficient according to Eq. 4-82.

$$\alpha_{ov} = \frac{\alpha_G \cdot \alpha_0}{\alpha_0 + \alpha_G} \left[\frac{\sin(\varepsilon)}{\varepsilon} - \frac{\alpha_G}{(\alpha_0 + \alpha_G)} \cdot \frac{\left(\alpha_G \cdot \frac{\sin(\varepsilon)}{\varepsilon} + \alpha_0 \cdot \frac{\varepsilon}{\pi} \right)}{\left(2 \cdot \alpha_0 + \alpha_G \cdot \frac{\sin(\varepsilon)}{\varepsilon} \cdot \frac{\pi}{\varepsilon} \right)} \right] \quad (4-91)$$

- 2.1. For infinite heat transfer coefficient between exposed wall and solid surface $\alpha_{GS} = \infty$, thus the effective heat transfer coefficient in this region is equal to the convective gas heat transfer coefficient $\alpha_G = \alpha_0$ (according to Eq. 4-42). This is the resistance of the exposed wall surface which is coupled with the convective heat flow from outer wall at the solid region R_{0G} .

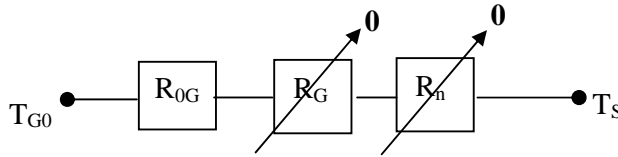


Figure 4-28. Resistance network for no conduction heat transfer and infinite radiation heat transfer

$$R_{0G} = \alpha_0 \left(\frac{1}{2} \cdot \frac{\sin(\varepsilon)}{\varepsilon} - \frac{1}{4} \cdot \frac{\frac{\sin(\varepsilon)}{\varepsilon} + \frac{\varepsilon}{\pi}}{2 + \frac{\sin(\varepsilon)}{\varepsilon} \cdot \frac{\pi}{\varepsilon}} \right) \quad (4-92)$$

- 2.2. For steam as a heat source $\alpha_0 = \infty$, the effective heat transfer coefficient is equal to the exposed wall-solid surface heat transfer coefficient $\alpha_G = \alpha_{GS}$ (according to Eq. 4-40). The result leads to the resistance of the exposed wall R_G

$$R_G = \alpha_{GS} \cdot \frac{\sin(\varepsilon)}{\varepsilon} \quad (4-93)$$

The results of these approximations give the heat flow and the overall heat transfer coefficient according to Figure 4-29 as follows

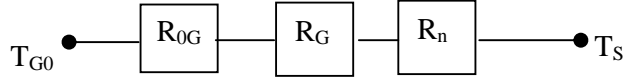


Figure 4-29. Resistance network for no conduction heat transfer

$$(R_{0G} + R_G) \cdot \frac{\dot{Q}_{ov}}{L} = (T_{G0} - T_S) \quad (4-94)$$

$$\frac{\dot{Q}_{ov}}{L \cdot (T_{G0} - T_S)} = \frac{l}{\alpha_0 \cdot \varepsilon \cdot D \cdot \left(\frac{l}{2} \cdot \frac{\sin(\varepsilon)}{\varepsilon} - \frac{l}{4} \cdot \frac{\frac{\sin(\varepsilon)}{\varepsilon} + \frac{\varepsilon}{\pi}}{2 + \frac{\sin(\varepsilon)}{\varepsilon} \cdot \frac{\pi}{\varepsilon}} \right)} + \frac{l}{\alpha_{GS} \cdot L_{GS}} \quad (4-95)$$

$$\alpha_{ov} = \frac{l}{\alpha_0 \cdot \left(\frac{l}{2} \cdot \frac{\sin(\varepsilon)}{\varepsilon} - \frac{l}{4} \cdot \frac{\frac{\sin(\varepsilon)}{\varepsilon} + \frac{\varepsilon}{\pi}}{2 + \frac{\sin(\varepsilon)}{\varepsilon} \cdot \frac{\pi}{\varepsilon}} \right)} + \frac{l}{\alpha_{GS} \cdot \frac{\sin(\varepsilon)}{\varepsilon}} \quad (4-96)$$

In Figure 4-30 the original model of the overall heat transfer coefficient according to Eq. (4-84) is plotted against the result of approximation model according to Eq. (4-89). It can be seen that for each value of covered wall-solid heat transfer coefficient the modified analogue of Figure 4-27 accurately predicts the overall heat transfer coefficient of the covered wall-solid.

In Figure 4-31 the original model according to Eq.(4-90) is plotted against the approximation model according to Eq. (4-95). In this case, it can be seen again that the

simplified resistance network of Figure 4-29 accurately predicts the overall heat transfer coefficient of the exposed wall-solid. For any of the cases in this investigation the error introduced by the use of this approximation is less than 1%. Therefore, the modified resistance network of Figure 4-25 may be used to predict accurately the overall heat flows and the overall heat transfer coefficients to the solid at any point along the kiln axis.

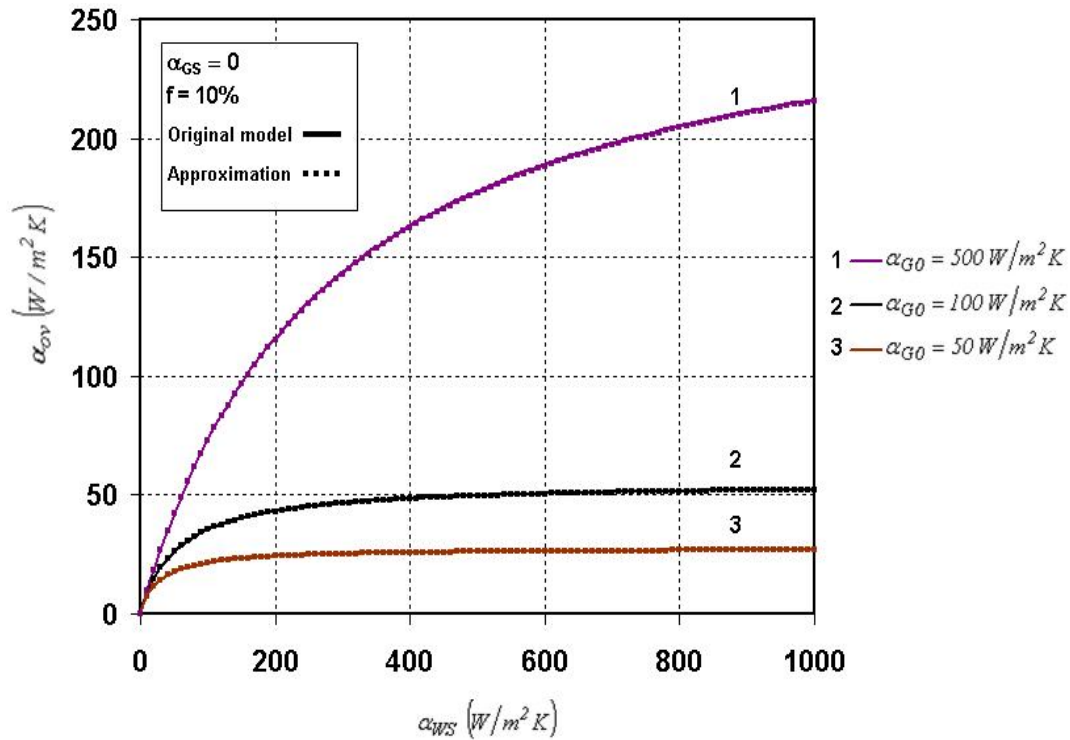


Figure 4-30. Approximation model predicted by resistance network versus the original model at $\alpha_{GS} = 0$

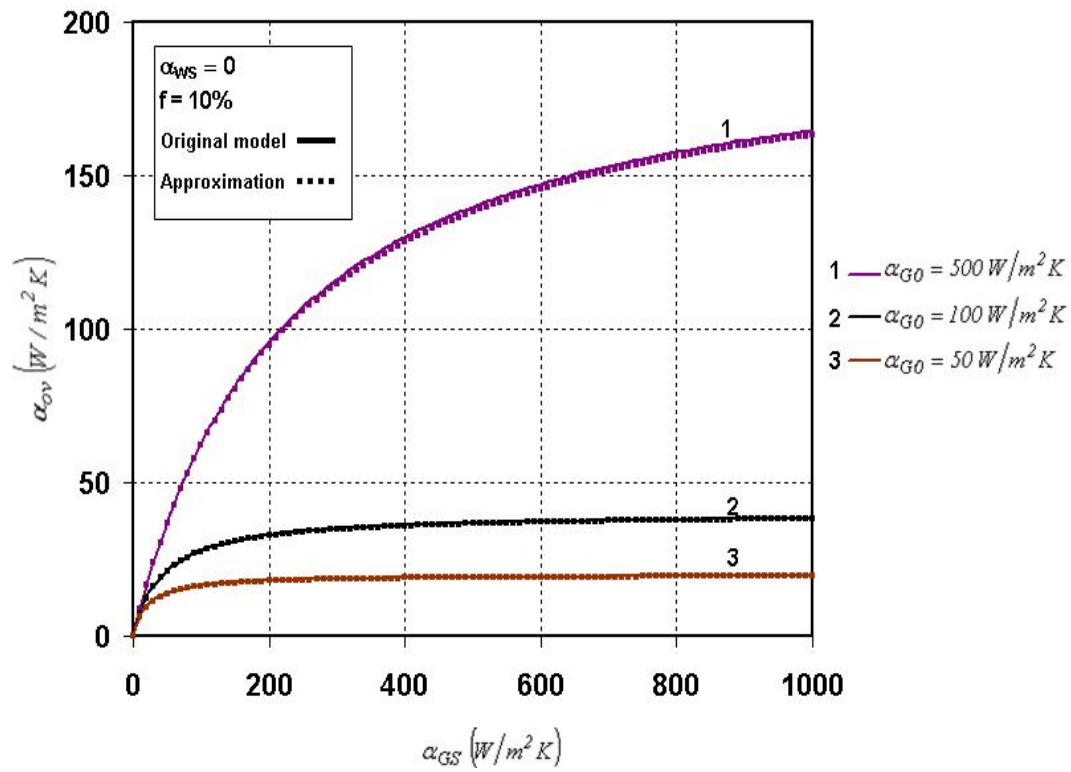


Figure 4-31. Approximation model predicted by resistance network versus the original model at $\alpha_{WS} = 0$

5 Experimental investigation of the temperature distribution in the kiln

5.1 Experimental apparatus and measuring technique

A series of two heat transfer trials were performed in the pilot kiln with the run conditions summarized in Table 5.1. The experimental facility employed for the flow measurements comprised a rotary kiln of 400 mm O.D. (250 mm I.D.) and 6.735 m long which was designed specifically to study the flow behaviour of granular material and the kiln wall in the kiln cross section. It was operated with a fixed rotational speed of 3.25 rpm, and was divided into 12 sections but only four sections were used for the experiment (Figure 5-1). At each section, five thermocouples were inserted through the wall into the bed and the gas to measure the temperature (Figure 5-2). The fuel used was natural gas (appendix) using a burner with a maximal capacity of 70 kW. This was premixed with excess number of 2.16, prior to the ignition for combustion. The material was dry quartz sand with specification being summarized in Table 5-1. The filling degree of the bed was 27 % and the fill angle of 69°.

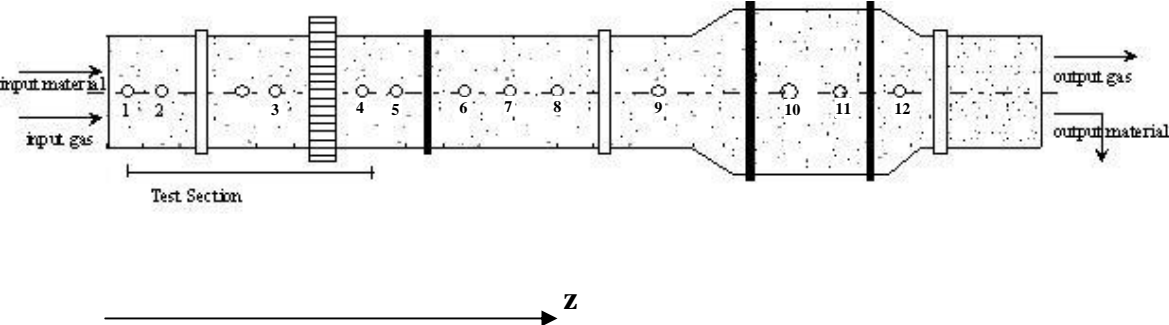


Figure 5-2. Axial locations of kiln thermocouples



Figure 5-3. Measuring device with five thermocouples

In addition, an infrared thermocamera was used to measure the outside wall temperature, and the measurements were corroborated by measurements with a contact thermocouple. A steel container was used for the collection of the outlet hot sand in regular time intervals. As depicted in the temperature measuring system shown in Figure 5-4, the temperature signals are routed to the sender and then transmitted to a receiver via radio. The thermocouples which are attached in the sockets extend into the interior of the kiln with different distances to the kiln wall, measuring the temperature of the gas, the wall, and the temperatures of the solid bed at different depths (see Figure 5-4). The thermocouples rotate together with the kiln continuously, so it is possible to measure the temperatures in dependence on time. To measure the temperature along the circumference direction, a pendulum is mounted on the kiln with which the rotational angle can be measured in dependence on time. Thus, the allocation of the measured temperatures is possible. This new measuring system can measure up to 32 temperatures simultaneously. The temperature signals are converted and saved as excel data sheet in the computer. With a developed program the temperature profiles can be monitored in real time. The time from the start up till the steady state conditions was about 3 hours and the time required for the data collection around 2 hours.

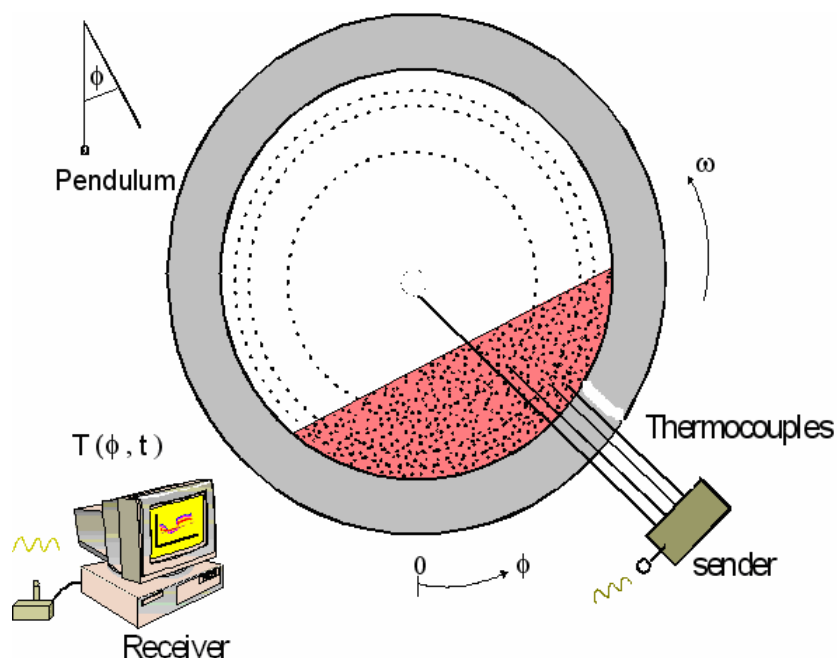


Figure 5-4. The temperature measuring system

Run	Inclination angle [°]	Feed rate [kg/h]	Filling degree [%]	Primary air [N, m3/h]	Natural gas [N, m3/h]	Max. temperature [°C]	Material
1	1.9	50	10	27.68	2.91	500	Sand
2	1.9	85	10	27.68	2.91	1000	Sand

Table 5-1. Summary of experimental conditions

Properties	SiO ₂
Density [kg/m ³]	1370
Heat Capacity [kJ/kg K]	0.76
Effective thermal Conductivity [W/m K]	1.4

Table 5-2. Physical properties of the experimental materials

5.2 Experimental work

Due to the inception of the experimental work, five thermocouples were installed at 4 axial positions along the kiln length. The thermocouples were inserted with different distance to the inner kiln wall. The locations of the thermocouples are summarized in

Sections Nr.	Axial distance (z) from the kiln head [m]	Radial distance (r) from the axis of the kiln [mm]					
		r1 (wall)	r2	r3	r4	r5	r6
1	0.5	0	5	20	40	-	125
2	0.8	0	5	20	40	65	-
3	1.39	0	5	20	40	65	-
4	1.795	0	5	20	40	-	125

Table 5-3. Distribution of thermocouples at the four sections of the kiln

The thermocouple r1 is attached and measured the kiln wall which due to the rotation touched the freeboard gas and immersed in the bed. Thermocouples r2, r3, r4, and r5 served to measure the temperatures within the solid bed. The thermo elements at the freeboard gas(r6) were shielded from the effect of radiation in the freeboard gas, so that the actual local temperature was recorded. The temperature of the freeboard gas was relative constant therefore at section 2 and 3 this part is abandoned.

The kiln was set at a rotation speed of 3.25 *rpm*, and the natural gas as fuel, was introduced from the end near the test section. The temperature of the gas is set to be constant at 1000°C for the first run and 500°C for the second run. The rotating kiln was then allowed to be preheated for about forty minutes, without solids. Having preheated the system for about forty minutes, the solid material –sand- was fed from the hopper, with the aid of a screw feeder which ensured a fixed feed rate of the sand into the rotating kiln, concurrently to the combustion gas. A cubic receiver was placed at the exit end of the kiln, and it became full at a typical feed rate within determined time intervals. It took around 30 minutes for the sand to be transported from the input section to the output section, after which the receiving sand was weighed continuously with time. The measured mass flow rate was observed to increase with time until after about two hours, when the flow remained steady at about 85 *kg/hr*, and the mass flow was considered to be at a steady state.

The temperatures at the respective sections were simultaneously being analyzed during the time when the kiln was rotating prior to the achievement of the steady state, and at steady state, the fluctuation of the inner wall temperature was observed to be minimal. The primary air feed rate was recorded to be 27.68 *m³/hr*, however, due to the influx of false air through the ends and the junctions of the kiln, as well as within the pores in the feed material from the hopper, the actual air utilized for the combustion reaction in the kiln was estimated to about 62 *m³/hr*, at an excess air number, λ , of about 2.16. The fuel -natural gas- feed rate, which was accompanied by the total air feed rate, was 2.9 *m³/hr*. The recorded experimental values are shown in appendix A. The recorded temperatures were plotted against the angles of rotation by the computer for each section.

5.3 Results and discussion

As mentioned previously, experiments were performed to measure the temperature distribution within a rolling solid bed. The experiments were carried out with inert solids (Sand) in order to exclude the influence of the chemical reaction. The kiln was heated up to desirable gas temperature ($T_G = 500^\circ\text{C}$ for the first run and $T_G = 1000^\circ\text{C}$ for the second run), the solids discharged at different intervals of time and the monitoring of several wall surface thermocouples began and continued for about 2 hours to ensure the steady-state condition was achieved.

Figure 3-4 and Figure 3-6 show the temperature distribution in dependence of the rotational angle, measured at two axial positions of the pilot kiln (First trial), respectively. At position 1 (Fig. 3-4), the wall temperature was constant with a value of 120°C . At position 2 (Fig. 3-5), the wall temperature increased to 150°C . Fluctuation of the wall temperatures were shown by the two thermocouples as it immersed into the solid bed and touched the gas region. Therefore, it was difficult to analyze the results since there was no thermocouple which measured only the gas temperature.

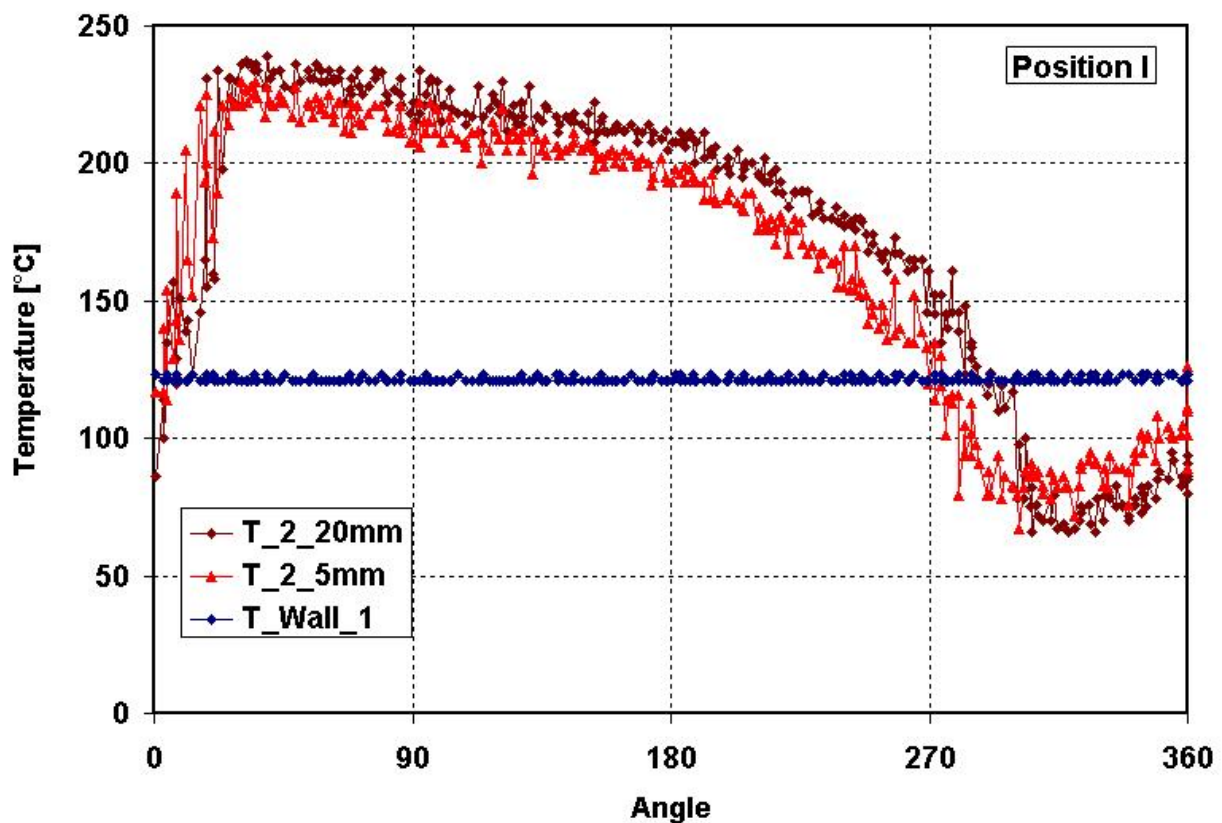


Figure 5-5. The temperature profile at section 1 trial 1 ($z = 0.5\text{ m}$)

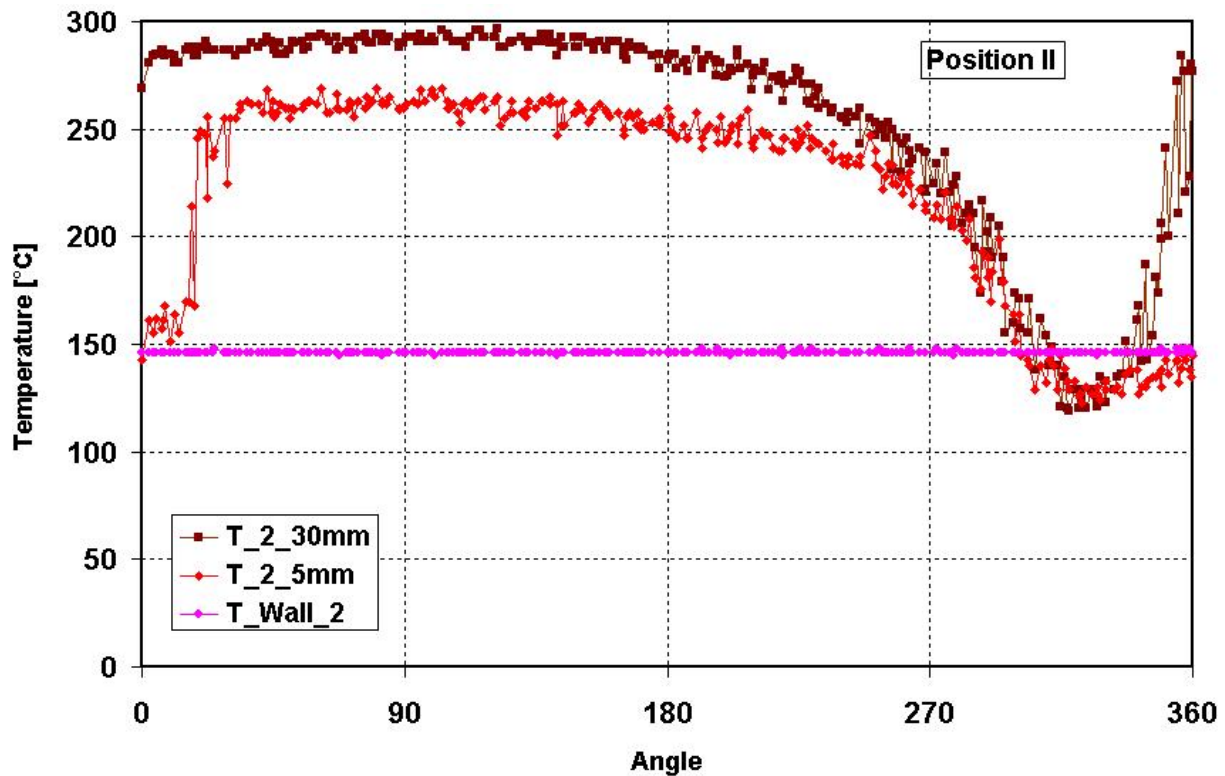


Figure 5-6. The temperature profile at section 2 trial 1 ($z = 0.8 \text{ m}$)

Figure 5-6 to Figure 5-9 show the temperatures of the thermocouples at different length in dependence to the rotation angle, measured at four section of the pilot kiln, respectively (Second trial). In this investigation, the gas temperature was measured with a thermocouple installed at the middle of the kiln (r6). At section 1 (Figure 5-6) the axial distance to the kiln head is $z = 0.5 \text{ m}$, the gas temperature and wall temperature were recorded to be constant at 970°C and 370°C , respectively. The gas thermocouple (125 mm) was installed at the center of the kiln, thus it does not touch the solid cold bed. The other three thermocouples varying with the kiln rotation, the temperature drops instantly as they immersed in the cold solid bed. During the way passing through the solid bed, the temperatures are approximately constant. Thermocouple r1 was installed near the kiln wall ($r = 5 \text{ mm}$), therefore the recorded temperature was higher due to the contact with the hot kiln wall than the other thermocouple (r1-r4). As the thermocouples came out of the solid bed into the hot gas side, the temperatures instantly increased toward the gas temperature. The cyclic of the temperature recorded (r1- r4) show a mixture of the hot gas and the cold solid bed due to the influence of the radiation of the kiln wall and the solid bed. Similar profiles are shown at the other measured section (Figures 5-6, 5-7, and 5-8). Within the profiles, in the solid bed

at section 1, there exist a ‘cold core’ due to the bad mixing of the solid. However, at a certain distance from the input load, the temperature differences of the thermocouples in the solid bed are small (Figure 5-10). This figure indicates that the solid was well mixed; therefore, for latter calculation the assumption of a uniformity of the solid bed temperature was acceptable.

The gas temperature detected by the thermocouples r6 in section 4 was lower than the other gas temperature detected by thermocouples r4 and r3. This fact was because of the measurement point was not in the center of the gas volume. As shown on the figures, the fluctuation of the inner wall temperature (r1) was relatively low, almost flat. However, this temperature actually scattered but do to the high range of temperature difference the fluctuation of the temperature can not be seen clearly. The level of the wall temperature depends on the ratio of the heat transfer coefficients, thus the measurements of the kiln wall temperature helps to analyze it. The gas and solid temperatures are required to determine the heat transfer coefficient gas-wall from the experiment which later on capable for the validation with the prediction model which are explained in the next section.

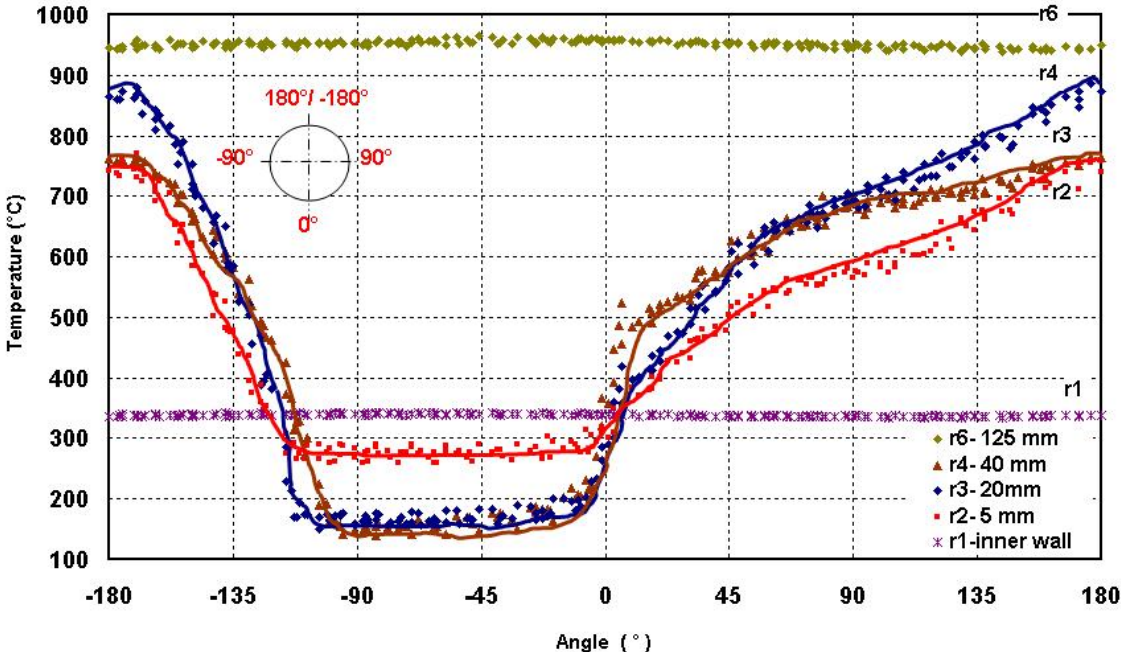


Figure 5-7. The temperature profile at section 1 ($z = 0.5 m$)

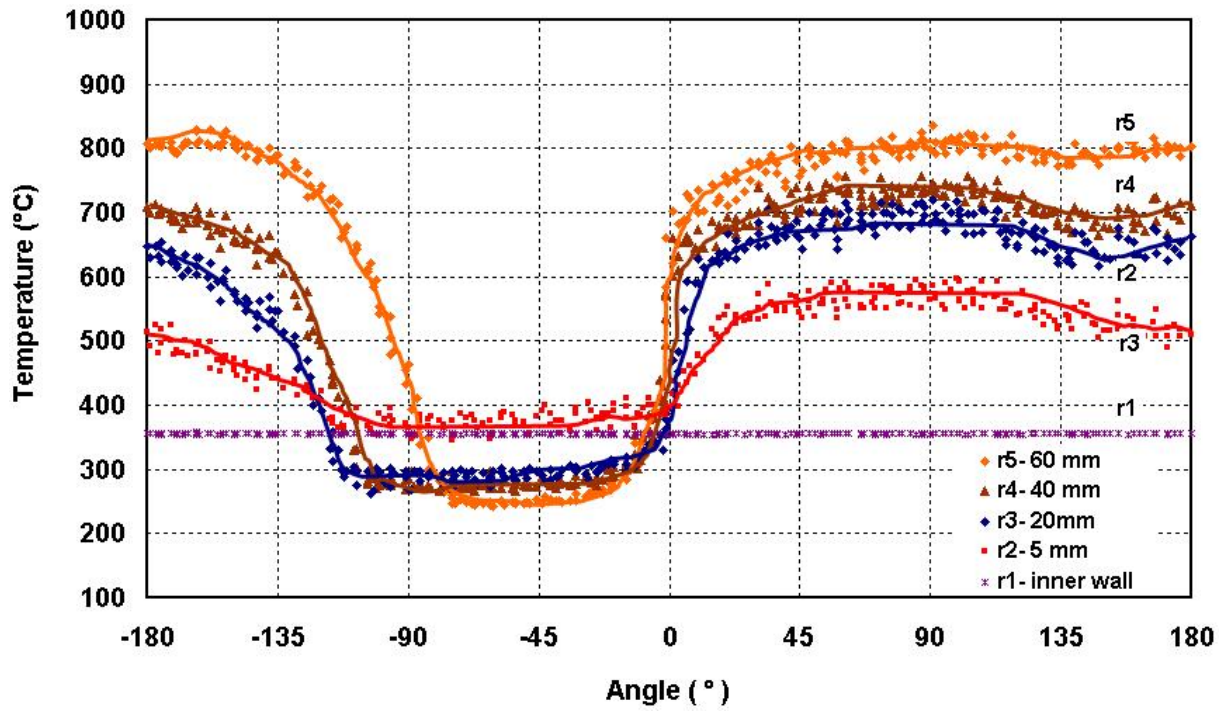


Figure 5-8. The temperature profile at section 2 ($z = 0.8\text{ m}$)

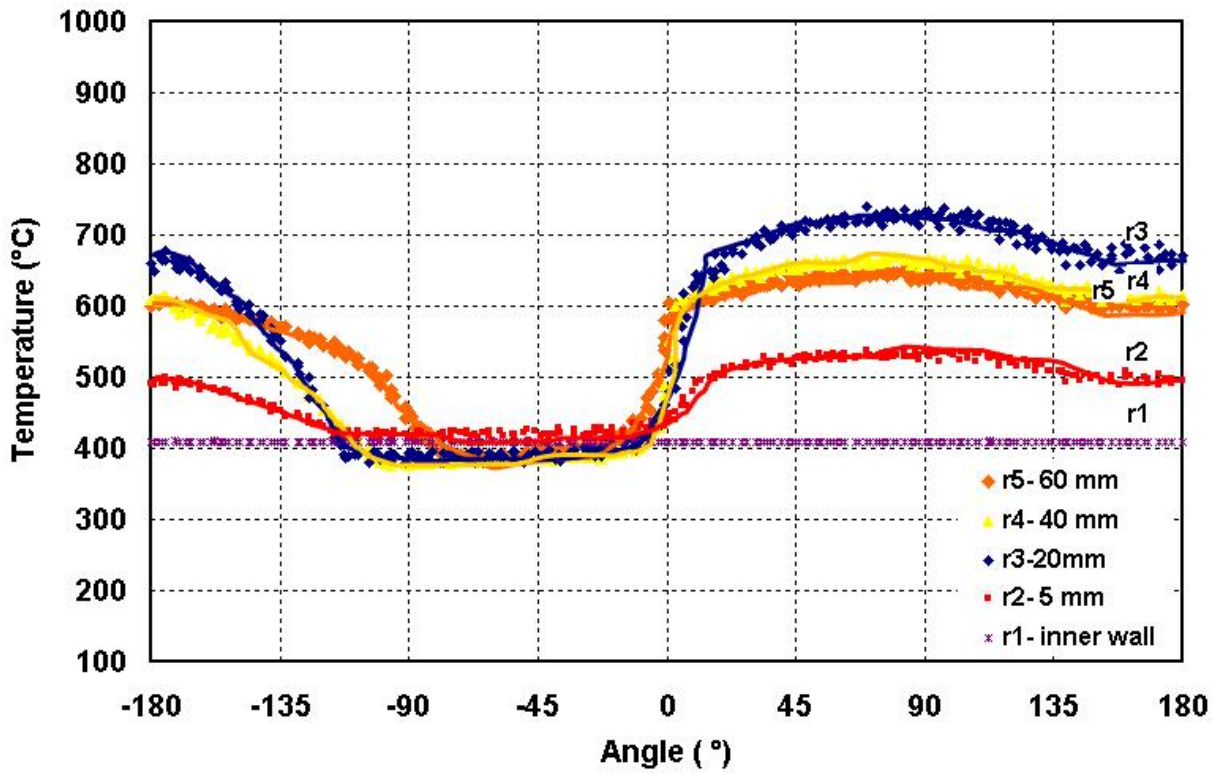


Figure 5-9. The temperature profile at section 3 ($z = 1.39\text{ m}$)

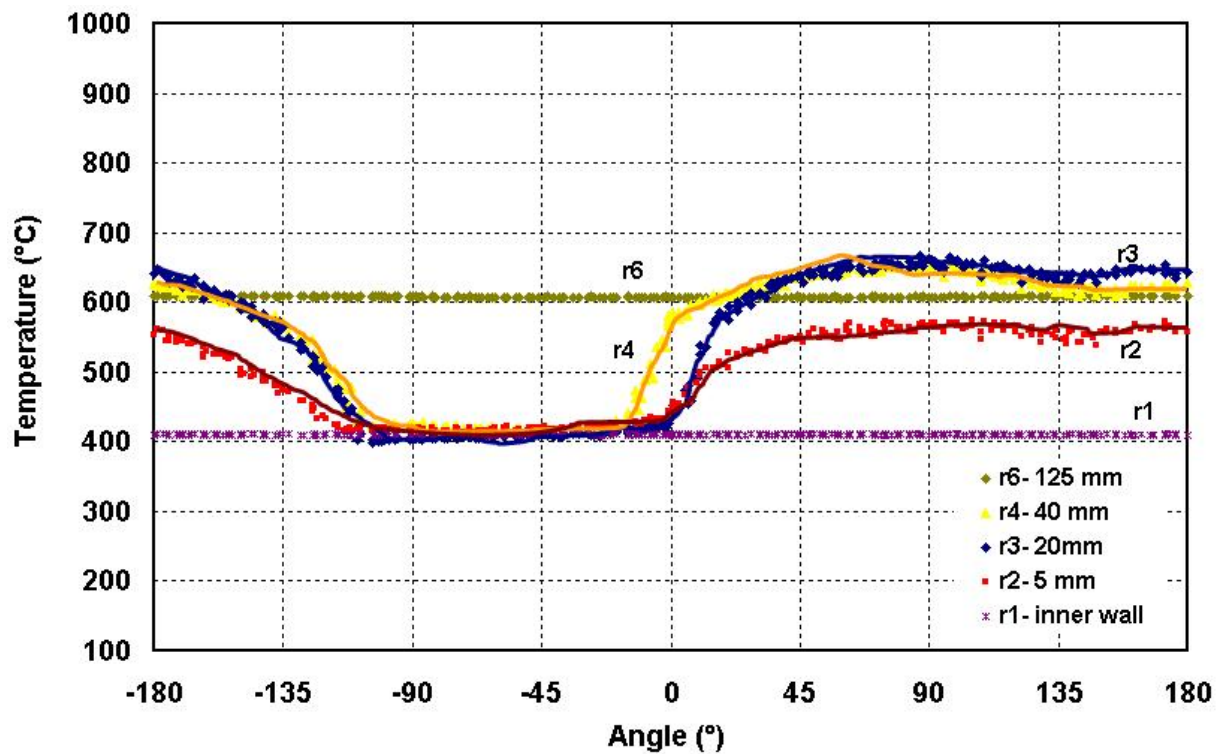


Figure 5-10. The temperature profile at section 4 ($z = 1.795 \text{ m}$)

5.4 Comparison of extended model with experimental results

5.4.1 Temperature distribution

In this section, analyzes are made between the experimental results, the extended model, and the literature study. The heat transfer coefficients ratio of the extended model based on Eqs. (3-18) and (3-19), and the heat transfer coefficients ratio based on the literature study (Chapter 2) are compared with the measurements data. It is difficult to predict the gas temperature for trial one, since there are no thermocouples which measured the gas temperature. As a consequence, the comparisons are made only for the second trial (gas temperature 1000°C). The level of the wall temperature from the experiment helps to analyze the ratio of heat transfer coefficients.

Figure 5-10 shows the temperature profile of the wall on position 1 is compared with the heat transfer ratio from the literature study and the extended model. The solid lines refer to the model prediction and the symbols represent the measurements data. The temperatures

of the wall were scattered and it seemed to be fluctuated along the rotational angle. The temperatures decreased at rotational angle 45° - 120° and then they tend to increase. The results improve the statements that the wall temperatures are fluctuated along the circumferential of the kiln. The level of the wall temperature from the measurements gives the heat transfer coefficient ratios for the extended model of 30. The fluctuation of the inner wall at this ratio is around 5%, which is relatively low. The heat transfer coefficients ratio from the literature study gives the same temperature level; the different is only of the mean temperature difference. Figure 5-11 shows the comparison of the wall temperature on position 4. The wall temperatures were scattered in the range of 409°C - 412°C along the rotational angle. The extended model agrees well with the experimental data which gives a heat transfer coefficient ratio of 40. The fluctuations of the inner wall temperature are around 2%, which is also very low.

Based on these results, it is clear that the regenerative action of the wall has a significant influence to the heat transfer mechanism in the rotary kiln. The direct heat transfer from the gas is lower than the indirect heat which is given from the wall. This is a typical fact in laboratory kilns with low gas temperature and low beam length. In industrial kilns, the direct heat transfer from gas to solid bed is higher than the indirect heat from the wall. Therefore, it is difficult to scale up the experiment result to the technical kilns. Thus, the analytical equations derived in this study can be used to solve the problem and for describing the regenerative heat transfer in complex process models.

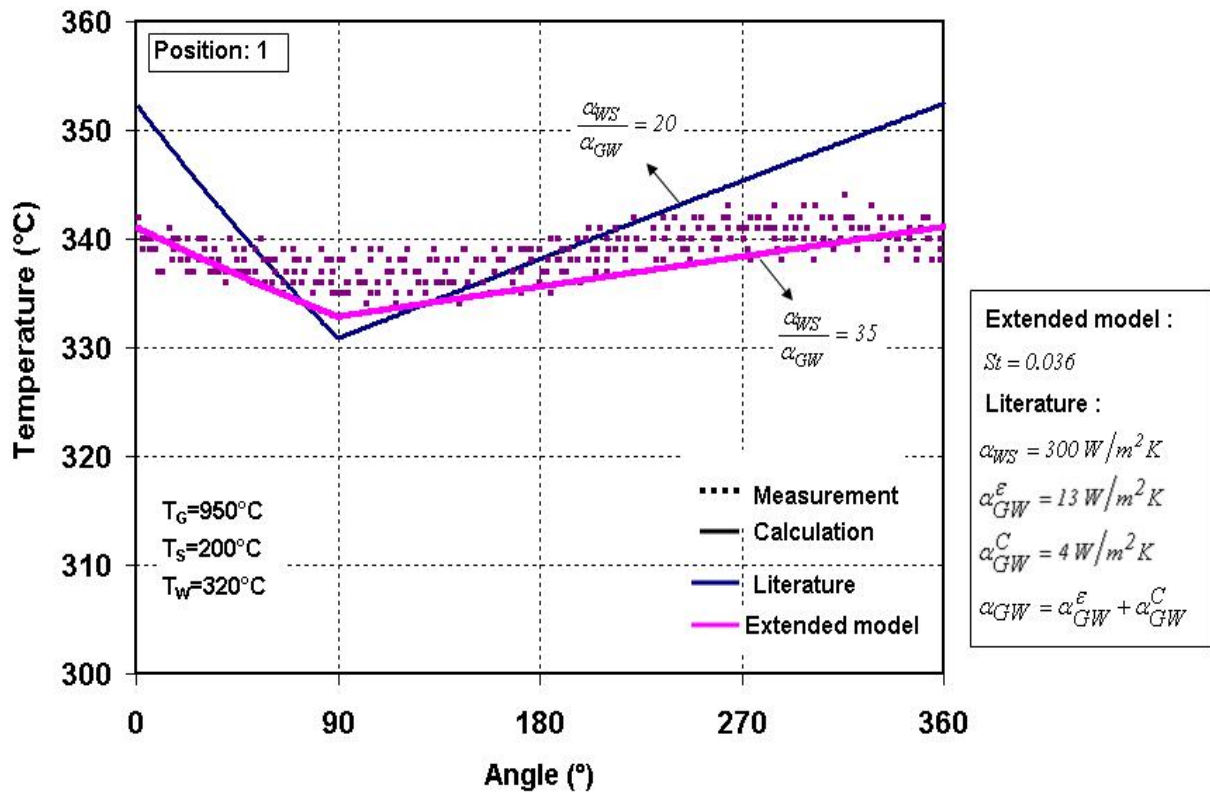


Figure 5-11. Measured and calculated inner wall temperature profiles for trial 1

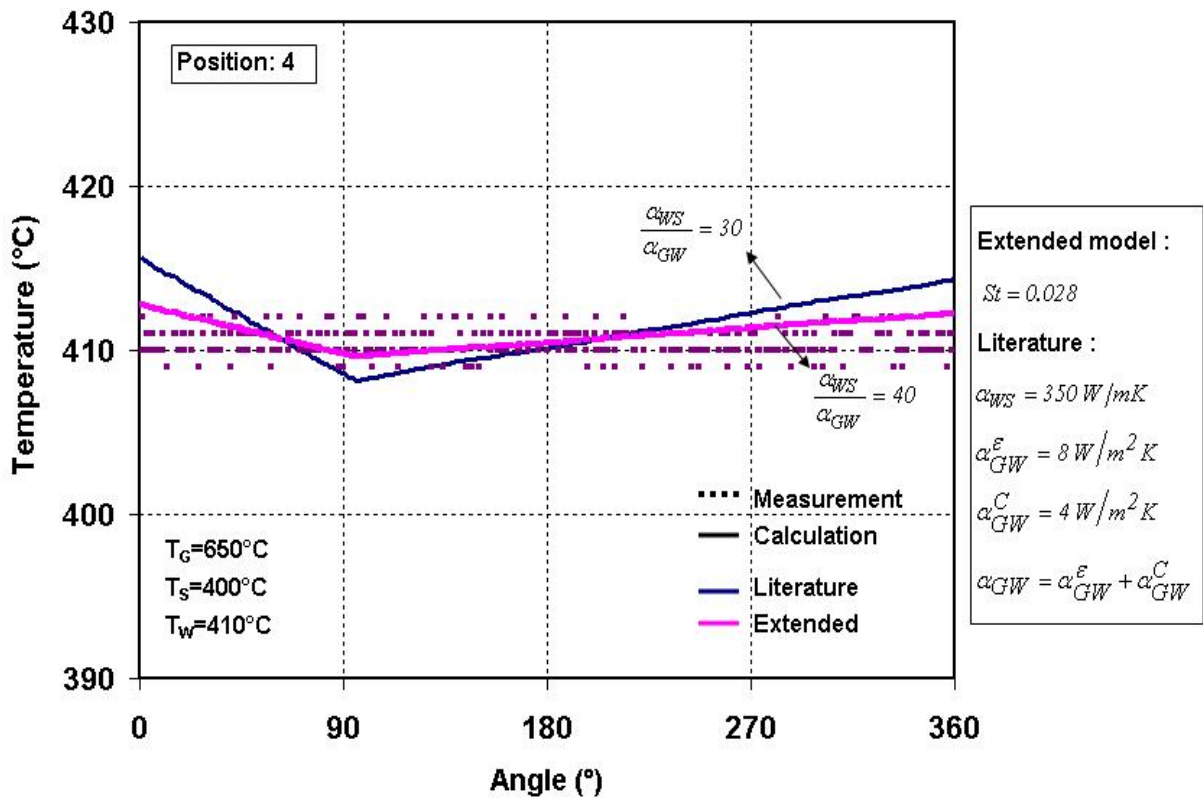


Figure 5-12. Measured and calculated inner wall temperature profiles for trial 2

5.4.2 Gas and solid mass flow

In this section, analyzes are made for solid mass flow from the experimental data Eq. 5-1 and the solid mass flow from the extended model Eq. 5-2 considering the overall regenerative heat transfer coefficient (α_R) from Eq. 3-44.

$$\dot{Q}_S = \dot{M}_S \cdot C_S \cdot \Delta T \quad (5-1)$$

$$\dot{Q}_S = (\alpha_R \cdot A_{WS} + \alpha_{GS} \cdot A_S) \cdot \Delta T_{lm} \quad (5-2)$$

Since the pilot plan kiln was operated at co-current flow, the log mean temperature difference can be used as shown in Figure 5-12.

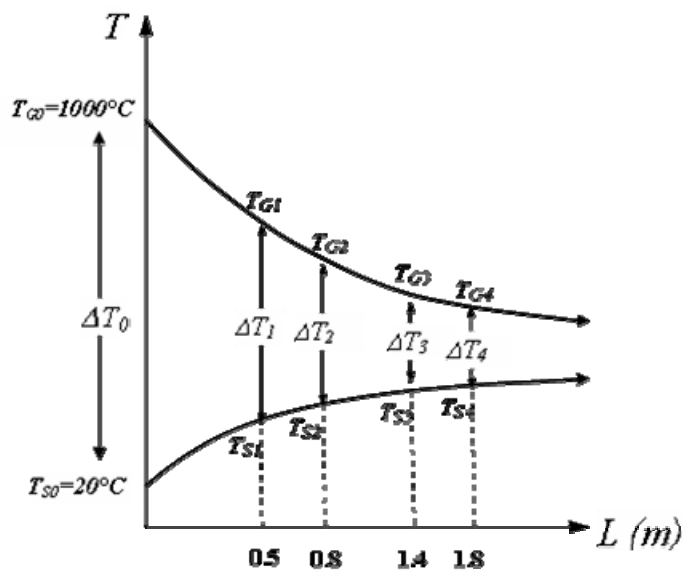


Figure 5-12. The temperature profiles in the pilot plan kiln

The temperature difference of gas and solid is summarized as follows

Sections	TG (°C)	TS (°C)
I (0.5 m)	950	200
II (0.8 m)	850	320
III (1.4 m)	710	400
IV (1.8 m)	620	420

Table 5-5. Measurements of gas and solid temperatures

The mean temperature difference between solid and gas is described here

$$\Delta T_{lm} = \frac{(\Delta T_{in}) - (\Delta T_{out})}{\ln \frac{(\Delta T_{in})}{(\Delta T_{out})}} \quad (5-3)$$

The results of every section is summarized in Table 5.6

Section	Experiment (kW)	Extended model (kW)	Overall regenerative heat transfer coefficient (α_R)
1	5	5.2	43
2	2.7	2.8	27
3	3.7	3.8	39
4	2.7	2.8	26

Table 5-6. Comparison between experiments with extended model solid mass flow

Based on these results, the experimental results are in accordance with the extended model in this study. The solid mass flow can be predict using a simple correlation of α_R . This simple correlation is important at an industrial level since the effort to solve the 2-dimensional problem can be omitted.

6 Conclusion

The following are conclusions concerning regenerative action of the kiln wall in directly and indirectly heated rotary kiln from this study

1. The regenerative heat flow of the wall in a direct heated rotary kiln can be calculated with a simplified one-dimensional model which has an analytical solution. The fundamental issue of this analytical model is the introduction of a lumped capacity layer characterized by an infinite conductivity in radial direction. Thus, the temperature profiles in the angular direction can be calculated using Newton's lumped capacity model. The thickness of the lumped capacity layer is determined from the heat penetration model in a semi-infinite body. The deviations from the two-dimensional numerical results are less than $\pm 5\%$.
2. From the analytical model a new heat transfer coefficient for the heat transportation of the wall could be achieved $\alpha_T = \pi \cdot \sqrt{\lambda \cdot \rho \cdot c \cdot n}$, where n is the rotational speed.
3. The overall regenerative heat transfer coefficient (α_R) can be approximated by three heat transportation resistances in series. This includes the heat transfer coefficient gas-to-wall (α_{GW}), the heat transportation coefficient (α_T), and the heat transfer coefficient wall-to-solid (α_{WS}) i.e. $\frac{1}{\alpha_R} = \frac{1}{\alpha_{GW}} + \frac{1}{\alpha_T} + \frac{1}{\alpha_{WS}}$. An advantageous of this analytical solution is its implementation in complex simulation models of processes without the necessity to solve numerically the two-dimensional Fourier equation for the regenerative heat flow.
4. The heat transportation coefficient α_T has relatively high values than the other heat transfer coefficients. Therefore, it has a low influence on the overall regenerative heat transfer. However, the heat transportation coefficient influences the fluctuation of the inner wall temperature.
5. The kiln diameter exerts no influence either on the regenerative heat transfer or on the ratio of the regenerative and the direct heat transfer.

6. The ratio between the regenerative and the direct heat flow is determined only by three parameters : heat transfer coefficient gas-to-wall (α_{GW}), heat transfer coefficient wall-to-solid (α_{WS}), and filling angle (ε).
7. In technical rotary kilns, the gas temperature is estimated to be 1500°C-2000°C. This high temperature results in a high gas-to-wall heat transfer coefficient and a low ratio of α_{WS}/α_{GW} . In this case the regenerative heat flow is small in comparison to the direct heat flow from the gas. In the flue gas region of technical rotary kilns or in laboratory kilns the maximum combustion gas temperature is around 1200°C or lower. Moreover, the diameter of the laboratory kilns is small and therefore the beam length is also small. Thus, the gas-to-wall heat transfer coefficient is small and the ratio α_{WS}/α_{GW} is high. In this case the regenerative heat flow by the wall can be in the range of 20%-40%.
8. The measurement of the pilot kiln shows that the fluctuation of the inner kiln wall temperature at the circumferential direction is low. This result is in accordance with the analytical model. The inner wall temperature level depends on the ratio of the heat transfer coefficients, thus the measurements of the wall temperature helps to analyze the heat transfer mechanism.
9. In indirectly heated rotary kilns, a one dimensional model is established again to predict the temperature distribution of the kiln wall and the heat flows to the solid bed. A heat transportation coefficient was derived again from the model but in other definition ($\alpha_n = \rho \cdot c \cdot n \cdot s$) where s is the thickness of the kiln wall.
10. The model is determined only by three parameters : heat transfer coefficient gas-to-wall (α_{GW}), heat transfer coefficient wall-to-solid (α_{WS}), and convective outer wall heat transfer coefficient (α_{G0}). The kiln diameter has again no influence on the heat transfer mechanisms.
11. The analytical model could be reduced by introducing the resistance network of Fig. 4-28. The error associated with this approach is less than 1%.

REFERENCES

- Androutsopoulos, G.P., and Hatzilyberis, K.S., Gasification of Greek Lignite in an Indirect Heat Rotary Kiln Gasifier, *Chem. Eng. Comm.*, vol 190, pp. 1200-1232, 2003.
- Agustini, S., and Specht, E., Influence of the regenerative heat of the wall on the overall heat transfer in rotary kilns, *Cement International*, No. 5, p. 60-74, 2005
- Barr, P.V., Brimacombe, J.K., and Watkinson, A.P., A Heat Transfer Model for the Rotary Kiln Part I. Pilot Kiln Trials. *Metallurgical Transactions B*, vol. 20B, pp. 391-402, 1989.
- Barr, P.V., Brimacombe, J.K., and Watkinson, A.P., A Heat Transfer Model for the Rotary Kiln Part II. Development of the Cross Section Model, *Metallurgical Transactions B*, vol. 20B, pp. 403-419, 1989.
- Barr, P.V., Heat Transfer Processes in Rotary Kilns, PhD Thesis, University of British Columbia, Vancouver, BC, 1986.
- Baukal, C.E., Heat Transfer in Industrial Combustion, CRC Press, Oklahoma, 2000.
- Brimacombe, J.K., Watkinson, A.P., Heat transfer in a direct-fired rotary kiln: 1. Pilot plant and experimentation. *Metallurgical Transactions B*, 9B, 201-219, 1978.
- Bui, R.T., Perron, J., and Read, M., Model-Based Optimization of the Operation of the Coke Calcining Kiln, *Carbon*, vol. 31, no. 7, pp. 1139-1147, 1993.
- Bui, R.T., Simard, G., Charette, A., Kocaefe, Y., and Perron, J., Mathematical Modeling of the Rotary Coke Calcining Kiln, *The Canadian Journal of Chemical Engineering*, vol. 73, pp. 534-545, 1995.
- Canales, E.R., Borquez, R.M., and Melo, D.L., Steady State Modeling and Simulation of an Indirect Rotary Dryer, *Food Control*, vol. 12, pp. 77-83, 2001.

Carslaw, H. S., Jaeger, J.C., *Conduction of Heat in Solids*, 2nd edition, Oxford Clarendon Press, London, 1959.

Cross, M., and Young, R.M., *Mathematical Model of Rotary Kilns used in the Production of Iron Ore Pellets, Ironmaking and Steelmaking*, no. 3, pp. 129-137, 1976.

Cundy, V., Cook, C.A., *A Comprehensive Heat Transfer Model for Rotary Desorbers*, *The Canadian Journal of Chemical Eng.*, vol. 74, pp. 63-76, 1996.

Cundy, V., Cook, C.A., *A Study of Parameters Influencing Wall-to-Bed Heat Transfer in Low-Temperature Rotary Desorber*, *J. Energy Resources Technology*, vol. 117, no. 1, pp. 50-57, 1995.

Dhanjal, S.K., Barr, P.V. and Watkinson, A.P., *The Rotary Kiln: An Investigation of Bed Heat Transfer in the Transverse Plane*, *Metallurgical and Materials Transactions B*, vol. 35B, pp. 1059-1070, 2004.

Frankenberger, R., *Beitrag zur Berechnung des Wärmeübergangs in Zementdrehrohröfen, Zement-Kalk-Gips*, no. 4, pp. 31-35, 1971.

Friedman, S.J., and Marshall, W.R.J., *Studies in Rotary Drying, Part II. Heat and Mass Transfer*, *Chemical Engineering Progress*, vol. 45, no. 9, pp. 573, 1949.

Frisch, V., and Jeschar, R., *Deriving Effective Heat Transport Quantities using the Rotary Kiln as an Example*, *Metallurgical Transactions B*, vol. 10B, pp. 55-64, 1978.

Gardeik, H.O. and Jeschar, R., *Simplified Mathematical Models for Calculating the Heat Transfer in Internally Heated Adiabatic Rotary Kiln (convection models) Part I. Idealized Rotary Kiln with Infinitely Large Thermal Conductivity Coefficient of the Wall*, *Cement-Lime-Gypsum International*, vol. 7, pp. 201-210, 1979.

Gardeik, H.O. and Jeschar, R., Simplified Mathematical Models for Calculating the Heat Transfer in Internally Heated Adiabatic Rotary Kiln (convection models) Part II. Rotating Tube with Finite Value of the Thermal Conductivity of the Wall, Cement-Lime-Gypsum International, vol. 7, pp. 434-441, 1979.

Gardeik, H.O. and Ludwig, H., Calculation of Heat Loss through the Wall of Rotary Kilns and Mills, Part I. Fundamental, Cement-Lime-Gypsum International, vol. 4, pp. 53-62, 1980; and Part II. Approximation Equations and Application, Cement-Lime-Gypsum International, vol. 4, pp. 144-149, 1980.

Georgallis, M., Mathematical Modeling of Lime Kilns, PhD Thesis, The University of British Columbia, Vancouver, BC, 2004.

Ghoshdastidar, P.S., Rhodes, C.A., Orloff, D.I., Heat transfer in a rotary kiln during incineration of solid waste, ASME-Papers, vol. 8, no. 85-HT-86, pp. 1-6, 1986.

Gorog, J.P., Adams, T.N., Brimacombe, J.K., Radiative Heat Transfer in Rotary Kilns, Metallurgical Transactions B, vol.12B, pp. 55-64, 1981.

Gorog, J.P., Adams, T.N., Brimacombe, T.N., Regenerative Heat Transfer in Rotary Kilns, Metallurgical Transactions B, vol. 13B, pp. 153-160, 1982.

Goshdastidar, P.S. and Anandan Unni, V.K., Heat Transfer in the Non-Reacting Zone of a Cement Rotary Kiln, J. Eng. Industry, vol. 118, pp. 169-172, 1996.

Gygi, H., The Thermal Efficiency of the Rotary Cement Kiln, Cement and lime Manufacture, pp. 82, 1938.

Holmann, J.P., Heat Transfer, sixth edition, chapter 2, McGraw-Hill Book Company, New York, 1986.

Hottel, H.C., and Sarofim, A.F., Radiative Transfer, McGraw-Hill, Inc., 1967.

Ikuo, A., Development of a high density carbonaceous adsorbent from compressed wood,

Carbon, vol. 39, no. 10, pp. 1485-1490, 2001.

Imber, M., and Paschkis, V., Mathematical Analysis of the Rotary Kiln Heat Exchanger Part 1. The Well-Mixed Condition, Radex-Rundschau, no. 4, pp. 183-197, 1960.

Kaplan, W., Advanced Calculus, Addison-Wesley Publishing Company, Inc. 1957.

Klose, W., and Wiest, W., Experiments and Mathematical Modeling of Maize Pyrolysis in a Rotary Kiln, Fuel, vol 78, pp. 65-72, 1999.

Kolenko, T. and Glogovac, B., An Analysis of a Heat Transfer Model for Situations Involving Gas and Surface Radiative Heat Transfer, Commun. Numer. Math. Eng. vol.15, pp. 349-365, 1999.

Lemberg, J., Untersuchungen zum Wärmeübergang Zwischen der Wand und der Feststoffschicht eines Drehrohrofens, PhD Thesis, TU Hannover, Germany, 1975.

Li, A.M., Li, X.D., Li, S.Q., Ren, Y., and Shang, Y., Experimental Studies on Municipal Solid Waste Pyrolysis in a Laboratory-Scale Rotary Kiln, Energy, vol. 24, pp. 209-218, 1999.

Li, S.Q., Ma, L.B., Wan, W., and Yao, Q., A Mathematical Model of Heat Transfer in a Rotary Kiln Thermo- Reactor, Chem. Eng. Tech., vol. 28, no. 12, pp. 1480-1489, 2005.

Liu, X., Mellmann, J. and Specht, A., Prediction of Rolling Bed Motion in Rotating Cylinders, AIChE Journal, vol. 50, no. 11, pp. 2783-2793, 2004.

Manitius, A., Kursyusz, E., and Kawecki, W., Mathematical Model of the Aluminium Oxide Rotary Kiln, Ind. Eng. Chem. Process Des. Develop., vol. 13, no. 2, pp. 132-142, 1974

Marias, F., Roustan, H., and Pichat. A., Modeling of a Rotary Kiln for the Pyrolysis of Aluminium Waste, Chemical Engineering Science, vol. 60, pp. 4609-4622, 2005.

Martins M.A., Oliveira, L.S., Franca, A.S., Modeling and Simulation of Petroleum Coke Calcination in Rotary Kilns, Fuel, vol. 20, pp. 1611-1622, 2001.

Martins, M.A., Oliveira, L.S., & Franca, A.S. (2002). Modelling and simulation of limestone calcination in rotary kilns (part2: industrial rotary kiln). *Zement-Kalk-Gips International*, 55, 74-83.

Mellmann, J. and Specht, E., Mathematical Modelling of the Transition Behaviour between the various Forms of Transverse Motion of Bulk Materials in Rotating Cylinders, *Cement-Lime-Gypsum International*, vol. 54, pp. 281-296 & 380-402, 2001.

Mills, K.C., Recommended values of thermophysical properties for selected commercial alloys, Cambridge : Woodhead, 2002.

Mollekopf, N., Wärmeübertragung an Mechanisch Durchmischtes Schüttgut mit Wärmesenken in Kontaktapparaten, PhD Thesis, Uni Karlsruhe, 1983.

Murty, C.V.S., Evaluation of Radiation Reception Factors in a Rotary Kiln using a Modified Monte-Carlo scheme, *Int. J. Heat Mass Transfer*, vol. 36, no. 1, pp. 119-133, 1993.

Onissi, T.R., Some Considerations on the Heat Transfer in the Cement Rotary Kiln, *ZKG*, no. 12, pp. 639-647, 1980.

Ortiz, O.A., Suarze, G.I., and Nelson, A., Dynamic simulation of a Pilot Rotary Kiln for Charcoal Activation, *Computers & Chemical Engineering*, vol. 29, pp. 1837-1848, 2005.

Pearce, K.W., A Heat Transfer Model for Rotary Kilns, *J. of the Institute of Fuel*, no. 7, pp. 363-371, 1973.

Peray, K.E., Waddell, J.J., *The Rotary Cement Kiln*, Chemical Publishing Co., New York, 1972.

Pierson, Hugh O., *Handbook of carbon, graphite, diamond and fullerenes : properties, processing and applications*, Park Ridge, NJ : Noyes Publ., 1993

Queck, A., Investigation of the Heat Transfer into the Bed from the Gas Side and the Wall Side of Rotary Kilns, PhD Thesis, Otto-von-Guericke University of Magdeburg, Germany, 2002.

Rensch, T., Beitrag zum Prozeß der thermischen Bodendekontamination im Drehrohrofen, PhD Thesis, Uni Magdeburg, 2001.

Rovaglio, M., Manca, D., and Biardi, D., Dynamic modeling of waste incineration plants with rotary kilns: Comparisons between experimental and simulation data, Chemical Engineering Science, vol. 53, no. 15, pp. 2727-2742, 1998.

San Miguel, G., Fowler, G.F., Dall'Orso, M., and Sollars, C.J., Porosity and Surface Characteristics of Activated Carbons produced from Waste Tyre Rubber, J. Chemical Tech. Biotech., vol. 77, pp. 1-8, 2001.

Sass, A., Simulation of the Heat Transfer Phenomena in a Rotary Kiln, I & EC Process Design and Development, vol. 6, no. 4, pp. 532-535, 1967.

Schlünder, E.U., Heat Transfer to Packed and Stirred Beds from the Surface of Immersed Bodies, Chem. -Ing. Tech., vol. 6, pp. 71-78, 1971.

Schnabel, W., Zur Wärmeübertragung bei der Direktreduktion im Drehrohrofen, PhD Thesis, TH Aachen, 1977.

Schulz, D., Brentrup, L., Kupper, D., Thermal Treatment of Raw and Waste Materials in a Rotary Kiln with Indirect Heating, Aufbereitungstechnik, vol. 34, no. 6, pp. 287-295, 1993.

Siegel, R., Howell, J., Thermal Radiation Heat Transfer, 4th edition, Taylor and Francis, New York, 2002.

APPENDIX

DATA GRAPHS AND TABLES OF THE EXPERIMENTS

1. Data at Steady State for composition of combustion gas and, flow of sand, primary air and natural gas.

data at steady state

material: sand

primary air: 27.98 m³/h at 0°C

natural gas: 2.91 m³/h at 0°C

time	length from kiln head [mm]	N2O [ppm]	NO [ppm]	NO2 [ppm]	SO2 [ppm]	CO [ppm]	CO [Vol%]	CO2 [Vol%]	O2 [Vol%]	H2O [Vol%]	CH4 [ppm]
11:49:55	2565	62	5	52	0	62	0,19	4,91	11,68	9,65	0
11:37:07	2565	62	5	55	0	65	0,19	4,84	11,87	9,22	0
average value	2565	62	5	53,5	0	63,5	0,19	4,875	11,775	9,435	0

time	primary air [°C]	secondary air [°C]	flue gas [°C]	solid discharge [°C]	primary air [Pa]	secondary air [Pa]	kiln head [Pa]	kiln discharge [Pa]	primary air [m ³ /h]	secondary air [m ³ /h]	natural gas [m ³ /h]	flue gas [m ³ /h]
11:43:17	34	20	150	70	11088	-1409	-49	-65	27,68	0	2,91	159,62
11:49:27	34	20	151	71	11108	-1400	-49	-65	27,68	0	2,91	159,44
average value	34	20	150,5	70,5	11098	-1404,5	-49	-65	27,68	0	2,91	159,53

2. Table of temperatures of sand, gas and wall at specific sections.

solid / Wand Temperature		Solid Temperature [°C]						wall temperature [°C]	
measuring position	distance from kiln head [mm]	thermoelement 20 mm	5 mm	40 mm	60 mm	125 mm	average value	inner wall	outer wall
S1	500	170	276	161		952	193	339	86
S2	800	291	374	278	248		300	356	103
S4	1390	390	420	383	392		397	409	86
S5	1795	408	418	420		607	416	410	99

gas- Temperature

Sections	Dist. of Sect. From kiln end [mm]	gas Temperature [°C]						average value
		thermoelement 20 mm	5 mm	40 mm	60 mm	125 mm		
S1	500	672	573	652	810	952	710	
S2	800	636	523	693	738	872	676	
S4	1390	668	504	619	594	715	612	
S5	1795	618	537	620	496	607	569	

3. Programme for determination of properties of the gas and the fuel with the aid of the excess air number.

erdgas97(1)

Verbrennungsrechnung für gasförmige Brennstoffe									Stoffwerte	
Brenngas: Erdgas 97										
Bestandteil		$V_{O_2,n}$	$V_{L,n}$	$V_{CO_2,n}$	$V_{H_2O,n}$	$V_{SO_2,n}$	$V_{NO_2,n}$	$V_{N_2,n}$	ρ_n	$H_{u,n}$
Komponente	Vol.-Anteil m^3/m^3	m^3/m^3	m^3/m^3	m^3/m^3	m^3/m^3	m^3/m^3	m^3/m^3	m^3/m^3	kg/m^3	kJ/m^3
CH ₄	0,8922	1,7844	8,4971	0,8922	1,7844			6,7093	0,71740	35824
C ₂ H ₂	0	0,0000	0,0000	0,0000	0,0000			0,0000	1,17500	56984
C ₂ H ₄	0	0,0000	0,0000	0,0000	0,0000			0,0000	1,26110	60001
C ₂ H ₆	0,0544	0,1904	0,9067	0,1088	0,1632			0,7159	1,35660	64400
C ₃ H ₆	0	0,0000	0,0000	0,0000	0,0000			0,0000	1,91490	88283
C ₃ H ₈	0,012	0,0600	0,2857	0,0360	0,0480			0,2256	2,00960	93646
C ₄ H ₈	0	0,0000	0,0000	0,0000	0,0000			0,0000	2,58200	113926
C ₄ H ₁₀	0,0028	0,0182	0,0867	0,0112	0,0140			0,0684	2,73200	123647
C ₆ H ₆	0,0003	0,0023	0,0107	0,0018	0,0009			0,0085	3,49000	140449
H ₂ S	0	0,0000	0,0000		0,0000	0,0000		0,0000	1,53620	23715
CO	0	0,0000	0,0000	0,0000				0,0000	1,25000	12654
NH ₃	0	0,0000	0,0000		0,0000		0,0000	0,0000	0,77140	
H ₂	0	0,0000	0,0000		0,0000			0,0000	0,08990	10768
CO ₂	0,0119			0,0119					1,97690	
N ₂	0,0259							0,0259	1,25050	
O ₂	0	0,0000	0,0000					0,0000	1,42895	
SUMME=	0,9995	2,0553	9,7869	1,0619	2,0105	0,0000	0,0000	7,7536	0,80259	36978
$V_{L,min} =$		9,7869 m^3/m^3		$V_{AG,u,min} =$		8,8155 m^3/m^3		$H_{u,n} =$		36978 kJ/m^3
				$V_{AG,l,min} =$		10,8260 m^3/m^3		$\rho_{EG,n} =$		0,80259 kg/m^3

Stoffwerte		Oxidizer		Abgasbestandteile					Literatur
		O ₂	Luft	CO ₂	H ₂ O	SO ₂	NO ₂	N ₂	
Mol. Masse	M [kg/kmol]	31,99900	28,95000	44,00800	18,01500	64,06500	46,00500	28,01300	Blanke
Mol. Volumen	V _n [m ³ (N)/kmol]	22,39000	22,40000	22,26000	22,40000	21,89000	22,40000	22,41000	Meyer/Schiffner
Normdichte	ρ_n [kg/m ³ (N)]	1,42895	1,29230	1,97690	0,80424	2,92630	2,05379	1,25050	Blanke

Luftbedarf	Luftzahl	Spezifische Luftmenge
minimal (stöch.)	$\lambda = 1,0$	$V_{L,min} = 9,7869 \text{ m}^3/m^3$
technisch	$\lambda = 2,15$	$V_{L,tech} = 21,0418 \text{ m}^3/m^3$
Luftüberschuß	$\lambda - 1 = 1,2$	$V_{L,Ü} = 11,2549 \text{ m}^3/m^3$

Abgaszusammensetzung, trocken						
minimal (stöch.)			technisch			
$\lambda =$	m^3/m^3	m^3/m^3	m^3/m^3	Vol-%	ppm	mg/m ³
1,0	1,0619		1,0619	5,2909	52909	104595
	0,0000		0,0000	0,0000		0
	0,0000		0,0000	0,0000	0	0
	7,7536	8,8914	16,6451	82,9330	829330	1037077
		2,3635	2,3635	11,7762	117762	168276
Summe:	8,8155		20,0705	100,0000	1000000	1309947
				$\rho_{AG,t,n} = 1,3099 \text{ kg/m}^3(N)$		
				$V_{AG,t,min} = 8,8155 \text{ m}^3/m^3$		
				$V_{AG,t,tech} = 20,0705 \text{ m}^3/m^3$		
				$Y_{CO_2,max} = 12,0458 \text{ Vol.-%}$		

Abgaszusammensetzung, feucht						
minimal (stöch.)			technisch			
$\lambda =$	m^3/m^3	m^3/m^3	m^3/m^3	Vol-%	ppm	mg/m ³
1,0	1,0619		1,0619	4,8091	48091	95071
	2,0105		2,0105	9,1051	91051	73227
	0,0000		0,0000	0,0000	0	0
	0,0000		0,0000	0,0000	0	0
	7,7536	8,8914	16,6451	75,3818	753818	942650
		2,3635	2,3635	10,7039	107039	152954
Summe	10,8260		22,0810	100,0000	1000000	1263902
				$\rho_{AG,f,n} = 1,2639 \text{ kg/m}^3(N)$		
				$V_{AG,f,min} = 10,8260 \text{ m}^3/m^3$		
				$V_{AG,f,tech} = 22,0810 \text{ m}^3/m^3$		

Curriculum vitae

Name : Sri Silvia Agustini
Nationality : Indonesian
Religion : Islam
Place, Date of Birth : Medan, 17 August 1975
Marital status : Married

School:

1980 – 1986 : Primary school in Rangoon, Myanmar
1986 – 1989 : Secondary school in Rangoon, Myanmar
1989 – 1992 : High school in Medan, Indonesia

Study:

1992 – 1997 : Bachelor of Engineering (S.T) in Chemical Engineering at University of North Sumatera (USU), Medan – Indonesia.
1998 – 2000 : Master degree (M.Sc.) majoring in Chemical and Process Engineering at Otto-von-Guericke Universität Magdeburg in co-operation with Bandung Institute of Technology (ITB).
2001 – 2006 : Doctorial degree (Phd.) majoring in Chemical and Process Engineering at Otto-von-Guericke Universität Magdeburg

Working Experience:

1994 - 1995 : Laboratory assistant in analysis chemistry laboratory
01.10.'99 – 31.06.'00 : Working Student (HiWi) at a Project at Institute of Environment Engineering at Otto-von-Guericke Universität Magdeburg : measurement of particle diameter
01.07.'00 – 31.10.'00 : Working Student (HiWi) at Institute of Chemical Engineering at Max Plank Magdeburg during my Master study working with the reactive distillation column
01.11.'00 – 31.12.'00 : Working Student (HiWi) at Institute of Fluid and Thermodynamic

01.01.'01 – 31.07.'06 : Working as a staff academic member at Insitute of Fluid and Thermodynamic during my PhD study. Experimental study with a pilot plan rotary kiln and modelling the heat transfer in the kiln.

Publications:

1. M.Sc. S. Agustini, Prof. Dr.-Ing. E. Specht, Einfluss der regenerativen Wärme der Wand auf den gesamten Wärmeübergang in Drehrohröfen , Cement International, 05/2005 S. 60-73.
2. M.Sc. S. Agustini, Dr.-Ing. A. Queck, Prof. Dr.-Ing. E. Specht, Modeling of the Regenerative Heat Flow of the Wall in Direct Fired Rotary Kilns, Heat transfer engineering, 08/2007.